UNIVERSITA' DEGLI STUDI DI GENOVA

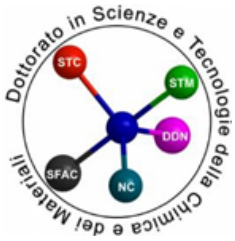

DOCTORATE SCHOOL IN SCIENCES AND TECHNOLOGIES OF CHEMISTRY AND MATERIALS

CURRICULUM IN PHARMACEUTICAL, FOOD AND COSMETIC SCIENCES

XXXIII CYCLE

PhD THESIS

Computational approaches guiding for the design and optimization of novel chemo-types endowed with F508del-CFTR modulator ability

Giada Righetti

Advisor: Dr. Elena Cichero

Summary

AIM OF THESIS

To date, monotherapy with VX-809 (Lumacaftor) or VX-770 (Ivacaftor) has not resulted in obvious clinical benefits for CF patients, while their combination regimen has provided positive results, stabilizing disease progress. Consequently, therapy combined with dual modulators or triple combination represents today the most promising prospect for developing new therapies. In this context, the research group in which I have been carrying out this thesis has dealt with rational design and computational studies of CFTR modulators during the past few years. The information obtained from our previous studies allowed us to proceed with the rational design and to predict the possible corrective activity of a new series of compounds with an aminoarylthiazole structure (AAT)[1,,165]. The previously proposed studies' reliability was supported by biological studies carried out on the newly synthesized molecules in collaboration with the research group led by Dr. Nicoletta Pedemonte (Istituto Giannina Gaslini, Genoa) verifying the corrective activity for F508del-CFTR of the newly designed derivatives. About the computational approaches so far applied, a QSAR model has been developed on the correctors available in literature guiding the following design and synthesis of hybrids compounds. This ligand-based method was used to overcome the paucity of information regarding a single and specific mechanism of action responsible for the corrective activity of VX-809. Indeed, as described in the literature, several hypotheses suggest multiple sites on the CFTR protein to which VX-809 could bind, first of all, the NBD1 domain. This thesis deepened the structure-based approach concerning various correctors described in the literature, including the hybrids developed by the present research group. In this context, experimental but partial data of the NBD1 domain of F508del-CFTR (PDB code: 4WZ6) were considered to perform molecular docking simulations of the compounds mentioned above. This research has been completed by molecular docking calculations performed on a whole model of the F508del-CFTR protein, which has been built *in silico* by our research group. Unlike what occurs for CFTR correctors, applying structure-based methods in the rational design of potentiators appears to be a more straightforward strategy since the experimental data concerning the binding mode of the VX-770 potentiator has recently become available (PDB code = 6O2P) and GLP1837 (PDB code = 6O1V). Starting from these assumptions, in this thesis, several libraries of compounds, described in the literature as CFTR potentiators, such as indoles, pyrazolquinolines, thienopyranes, cyanoquinolines, and AAT, have been studied to perform molecular docking

studies and QSAR analysis activities. These approaches allowed us to obtain information to guide the rational design and future synthesis of new CFTR modulators.

The research activity's further goal was to apply - in parallel to the studies just mentioned - ligand-based drug design analysis, using classical QSAR type analysis. This approach made it possible to overcome any limitation related to uniquely examining a single possible target for CFTR modulators and focusing on chemical scaffolds known today as correctors or potentiators.

CHAPTER 1

INTRODUCTION

Cystic fibrosis (CF) is an autosomal recessive disorder caused by mutations in the gene that encodes the cystic fibrosis transmembrane conductance regulator protein (CFTR)[2]. Around 2500 mutations were discovered that could cause the disease, but the most common is the F508 deletion. This mutation leads to the instability of the protein that is being formed and its structural modification. Furthermore, F508del-CFTR is unstable on the cell surface by losing its anion channel function, so that it is rapidly degraded by lysosomes [3]. The primary cause of death is respiratory problems caused by the lack of functional CFTR in membrane[4], which determines a reduction of anionic permeability in the respiratory tract cells and leads to a succession of related problems. In particular, dehydration of the pulmonary epithelium increases mucus, making it difficult to eliminate through ciliary movement. Therefore, this results in airway obstructions and inflammation, favoring colonization of the airways by pathogens, such as *Pseudomonas Aeruginosa*[5].

Another problem that affects people with cystic fibrosis is salt loss syndrome. It consists of compromised reabsorption of chloride ions and other small ions in the sweat glands, and consequently, their elimination. For this reason, the iontophoretic sweat test is one of the most important diagnostic tools for the diagnosis of CF, along with the genetic test. [6]

Cystic fibrosis occurs with the respiratory system's symptoms and at the level of other tissues, being a multiorgan disease. Among the organs affected is the digestive one, with clinical manifestations expressed above all with pancreatic insufficiency. Other symptoms include cirrhosis, diabetes, bone disease, and infertility; the latter mainly affects male patients [7].

The first treatments for cystic fibrosis approved in the 1960s to the present day are based on a holistic approach [8]. Scientific advances of the past few years have enabled us to expand the knowledge about the disease; this was the main reason for the increased CF patients' life expectancy that has changed and improved over the years. CF was initially considered a fatal disease in the first years of life. Today statistics suggest a life expectancy of around 40 years, while for the newborn, it is expected an increase in life expectancy up to 50 years[9].

1.1 Cystic Fibrosis: A brief history

Cystic fibrosis (CF) is an autosomal recessive disease that occurs mainly in childhood. The first description of CF was found in a medieval text dating back to 1595, which described a correlation between infant death and pancreatic damage and salty skin. Furthermore, there was a saying in this text which states: "*Woe to that child which when kissed on the forehead tastes salty. He is bewitched and soon must die'*[9]. The first documented cases of CF date back to the 1930s. In 1936, Dr. Guido Fanconi, a pediatrician at the University of Zurich, published the disease's first description. During an autopsy, he noticed on two children the presence of pancreatic fibrosis and bronchiectasis, typical of the disease.

Nevertheless, on that occasion, he was unable to recognize the genetic basis of the disease. For a more detailed description of this pathology, it is necessary to wait two years when Dr. Dorothy published her data collected. Up to that period, the diagnosis was performed only on autopsy subjects; the American pathologist was able to study many cases of children who died prematurely and went to highlight in all these subjects severe alterations of the pancreas, finding the formation of abnormal cysts. These were due to the dilation of the secretory ducts drenched in fibrous tissue, justifying the pathology as "cystic fibrosis of the pancreas." She was also the first to theorize that a lack of vitamin A could cause C.F [10]. Starting from this hypothesis, in *vivo tests* were performed through the duodenal incubation tried to demonstrate the abnormal digestion of vitamin A which was then found in the blood.

In 1949, CF was described by Dr. Sidney Farber as a multiorgan disorder with an excess of mucus, leading to a secondary staphylococcal infection [11]. Since then, numerous studies have been carried out to discover the etiology of the disease. In 1944, Dr. Howard realized a survey of two families with high mortality due to CF suggesting possible heterozygous inheritance [12]. Two years later, a study guided by Drs Andersen and Hodges on 113 families led to the conclusion that "the disease, although hereditary, requires more than one factor for the expression" [13].

A great discovery for CF diagnosis occurred in the 1950s during a heatwave in New York, when Dr. Paul Di Sant 'Agnese observed an increase in the salt content in the sweat of CF patients, establishing the basis for the sweat chloride test still used in the diagnosis of CF [14]. In 1955, modern treatment for CF was developed by Schwachman, consisting of diagnosis, early treatment, and adequate nutrition. In 1955, CF's first organization was founded; the US National CF Research Foundation, organizations specialized in diagnosis and therapy, began to emerge. The first

specialized clinics started to occur, the early prenatal diagnoses were defined, and a register was drawn up to enter all patients affected by this pathology. These records are still maintained today and find great use in the creation of guidelines in the treatment of CF, and at the same time, they are used by the same researchers to design new trials.

During the 1980s, Paul Quinton realized research on the chloride (Cl^-) impermeability in the sweat duct cells. This study has identified the primary defect in the apical membrane of epithelial cells with a decrease in chloride flow across the cells and an increase in sodium (Na^+) transport [15]. In the mid-1980s, using the analysis of restriction fragment length polymorphism (RFLP) was identified the Cystic Fibrosis Transmembrane Conductance Regulator (CFTR) gene. Finally, in 1989, several researchers' joint efforts as Lap Chee Tsui, Francis Collins, and Jack Riordan [16] have led to the cloning of the CFTR gene. The research resulting from positional cloning combined with identifying mutations in patients led to identifying a mutation in about 70% of the alleles of patients with CF [14]. This mutation consists of a three bp deletion in exon 10 (NBD1), which results in the deletion of the phenylalanine amino acid at position 508 (F508del) [17].

1.1.2 Aetiology

CF is caused by a mutation in the gene that encodes the CFTR gene. The CFTR gene is located on the long arm of chromosome 7 [18]. Cystic fibrosis is an *autosomal recessive disease*, so the CF gene is not located on the sex chromosome, which means that both males and females can contract CF. CF occurs in people with two mutated CFTR genes located in trans, a mutation on each allele. Healthy carriers of the CFTR gene are widespread worldwide, with a ratio of 1:25. These people have only altered one pair of the CFTR gene, which means that they do not present the disease or its manifestations. The healthy gene compensates for the defective one (www.cff.org Cystic Fibrosis Foundation) [19]. Therefore, when both parents are carriers and transmit a CF-related mutation to the child, none of the genes works appropriately, and the child will have CF.

When both parents carry a CF gene mutation, each baby has a:

- One in four (25 %) chances of not being a carrier and not having CF.
- Two in four (50%) chances of being a carrier but not having CF.
- One in four (25 %) chances of having CF.

To date, the only way to identify a healthy carrier is to perform a DNA test. However, it is a complex analysis since there are numerous rare mutations and others still unknown. Several genetic tests identify CFTR gene mutations on the DNA. The more straightforward tests identify the most frequent mutations and are called "first-level tests." The more complex ones identify the rarer mutations and are called "second and third level tests."

1.2 DIAGNOSIS

The enormous clinical variability and symptom diversity make the diagnosis of infant CF a complicated problem. Therefore, providing prenatal diagnosis and voluntary termination of pregnancy for couples with previously ill children or relatives is another strategy to control CF in the community [20].

1.2.1 Prenatal test

The first step in prenatal screening is to test the mother for CFTR gene mutations through a blood test. If the infant presents a non-mutated CFTR gene, the child will not have CF, but it can still inherit a mutated CFTR gene from the father, who may be a healthy carrier. If the mother is a carrier of a mutated-CFTR gene, the father should also perform the test. In this latter case, if the father also has a CFTR mutation, the child will have a 25% (1 in 4) chance of having CF. Once confirmed that both parents carry the mutated-CFTR gene, amniocentesis or chorionic villus sampling is performed.

1.2.2 Newborn screening

Newborn screening has been recommended for the initial diagnosis of CF. All babies are screened for CF soon after birth. Newborn screening is performed on blood samples collected from the heel. These blood samples are stored as blood "stains" on a special filter paper. Dried blood stains are tested for a variety of diseases, including CF.

In this case, various screening algorithms are used that usually involve two tiers, starting by measuring the IRT on dried blood spots. Immunoreactive trypsinogen is a precursor of pancreatic enzymes found in the blood and is generally elevated in CF. In CF, its abnormal secretion in the pancreatic duct seems to enhance its release into the circulation. Therefore, regardless of the predicted or actual pancreatic adequate state, the serum IRT level of CF newborns increase. The second level of screening includes a second IRT analysis about 1-2 weeks after the initial measurement (IRT / IRT) or a CFTR mutation analysis for newborns with a higher initial IRT

concentration more remarkable than the predefined threshold (IRT / DNA). Then, the babies whose newborn screening results positive are referred to a diagnostic test, specifically to sweat chloride test or molecular genetic test of the CFTR gene[21],[22],[23].

1.2.3 Sweat chloride test

CFTR regulates chloride flux in the sweat ducts. In the presence of CFTR dysregulation, Cl^- concentration is very low, as well as its reabsorption. As a consequence, the levels of NaCl in the sweat of CF patients are increased [24]. Current strategies used to collect the sweat, using filter paper, gauze, or the Macroduct ® system put on to an extremity to gather sweat. QPIT is the preferred technique for sweat testing and also the sole legitimate practice recognized by CFF. The sweat test is often used as the primary CF diagnostic tool [14].

The sweat test is based on Darhling's observation that CF patient's sweat is very salty under certain stimuli. There are four primary steps to sweat testing: pilocarpine iontophoresis to induce sweat production, sweat collection, quantification of the sweat gathered up by volume or weight, and the sweat chloride concentration [25],[26]. In the usual tests, pilocarpine applied through the skin can stimulate sweating, causing a potential gradient to the sweat glands. Collected sweat produced lead to determine the Cl^- concentration and sometimes the Na^+ one [20]. The aim of the test should be reduced to patients showing any clinical symptoms other than respiratory dysfunction.

In this context, The Clinical Laboratory Standards Association has published guidelines on the adequate performance of the QPIT. To ensure a sweat rate of 1 g per square meter per minute within a collection time of 30 minutes, when using gauze or filter paper, the minimum sweat weight required by the QPIT is 75 ml, or the minimum volume of sweat using a microporous tube is 15 µl. However, for the latter, if the sweat volume is less than 50 µL, the analytical system must be validated. The chloride concentration in sweat> 60 mEq/L in two different cases can be led to diagnosed CF. This test is positive for 98% of individuals tested with CF. Sweat chloride concentrations in newborns <30 mEq/L or older children and adults <40 mEq/L are considered within the normal range (average population value ≤3 SD). Current newborn screening guidelines indicate that 30-59 mEq/L is a marginal result, and the test should be repeated in the future [27].

There are many possible reasons for false-positive sweat tests, despite that these people are generally distinguished from those with CF [28] [29]. Other potential sources of error in sweat testing usually include insufficient sweat collection or mistakes in sweat electrolyte analysis[30].

1.2.4 Transepithelial nasal potential difference

In addition to measuring the NaCl concentration in sweat, a second diagnostic test can also be performed: measuring the potential difference in the nasal mucosa cells (NPD), particularly useful when sweat tests give uncertain results [31]. Respiratory tract epithelial cells regulate ion transport and control the airways' fluid surface content through the active transport mechanism. Non-functional CFTR on the apical membrane surface leads to changes in chloride efflux and sodium transport, resulting in an abnormal potential difference across the epithelial surface. The procedure for measuring NPD in people over six years of age is well described, standardized, and safely performed in many professional CF centers[32]. This potential difference can be measured by placing an electrode on the surface of the nose. After the electrode is positioned on the nose's surface is bathed in a series of solutions that contain different salts. These solutions are projected to change the flow of ions across the cell surface in a predictable way. These solutions contain (1) a Ringer's saline solution (a particular salt solution used to obtain the baseline NPD), (2) amiloride, which blocks sodium channels, (3) a chloride-free solution, and (4) isoproterenol, which stimulates CFTR.

The solutions are always administered in the same order during the NPD testing. Individuals with CF after the NPD tests have specific results. First of all, the basal NPD is higher (more negative), reflecting greater sodium absorption through a relatively chloride-impermeable membrane. There is a significant NPD change during the nasal mucosa's perfusion with amiloride, an epithelial sodium channel inhibitor. Finally, in response to perfusion with amiloride / low chloride / beta-agonist, the NPD change is minimal as a measure of defective cAMP-mediated chloride transport by CFTR [27].

1.2.5 Genetic test

Several mutation detection techniques are handy in genetic counseling, prenatal diagnosis, and carrier screening, especially in complex clinical cases. As the number of mutations identified in the CFTR gene continues to increase, this analysis is usually limited to the most common mutations present in a specific region or country. Consensus diagnostic criteria presume that patients should have one or more characteristic clinical features. These include a sibling history of CF or a positive neonatal screening result followed by laboratory evidence of CFTR dysfunction [33]. Moreover, clinical applications of CFTR molecular genetic testing include diagnosing symptomatic individuals and the search for carriers of at-risk individuals and their reproductive partners.

Prenatal genetic diagnosis is suitable for pregnancy with an increased risk of CF. In some symptomatic individuals, only one or both pathogenic mutations are detected; in some carriers, the pathogenic mutation cannot be identified [27].

Currently, this analysis is performed by sequencing the complete coding sequence of the CFTR gene. This test can identify two variants; however, as most mutations are infrequent, the mere discovery of two variants in the CFTR gene alone cannot be considered a confirmed diagnosis.

1.3 CYSTIC FIBROSIS TRANSMEMBRANE CONDUCTANCE REGULATOR: CFTR STRUCTURE AND FUNCTION

1.3.1 CFTR structure

CFTR belongs to the C subfamily of the ABC transporter superfamily of membrane proteins, and for this reason, it is known as ABCC7 [34 35]. Among the ABC transporters, CFTR is unique in that it functions at low conductance (6-10 pS). Other ABC transporters utilize the energy derived from ATP hydrolysis to transport substrates across the plasma membrane actively. Instead, CFTR is an ATP-regulated anion-selective channel with channel gating regulated by ATP binding at the NBD domains and through phosphorylation of consensus phosphorylation sites located within the R domain [36 37]. CFTR regulates fluid flux across epithelial membranes, mainly by regulation of Cl^- secretion, which creates adequate electrochemical and osmotic driving forces for the movement of ions and molecules such as Na^+ and H_2O[38].

Furthermore, CFTR facilitates HCO_3^- secretion, which plays an essential role at this level. It has an antibacterial role and participates in the physiochemical properties of the mucosal layer [39 40]. In the airways, CFTR interacts with the Na^+ epithelial channel (ENaC). The abnormal function of CFTR can affect the lung's innate immune response.

CFTR has many structural similarities to other members of the ABC transporter family. CFTR forms a highly symmetric protein with two transmembrane domains (TMD1 and 2); each domain consists of six transmembrane helices (TM1-12). Together they constitute the transmembrane pore of the protein and two cytoplasmic binding domains (NBDs) [41]. NBDs contain two ATP binding sites, each formed by the Walker A (WA) and Walker B (WB) sites on the 'head' of an NBD and the ABC specific signature sequence (LSGGQ) located on the tail of the opposite NBD [37].

The regulatory domain (RD) is unique for CFTR in the ABC transporter family and consists of a ~ 200 a.a. and a region that connects the C terminal of NBD1 with the N terminal of TMD2. RD contains consensus protein kinase A (PKA) phosphorylation sites, as well as sites for phosphorylation by protein kinase C (PKC) and activated protein kinase 5 'adenosine monophosphate (AMPK) [16 42 43] (Fig.1).

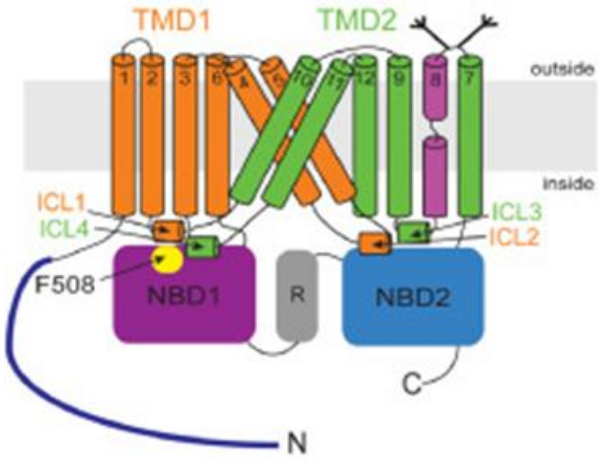

Fig.1. Schematic representation of CFTR structure. Two cytoplasmatic domains NBD1 (purple) and NBD2 (light blue); two transmembrane domains: TMD1 (orange), TMD2 (green), and one regulatory domain R (grey)[44]. *Picture from Kleizen, B. et al. J Cyst Fibros.* ***2020****;19 Suppl 1:S19-S24.*

The CFTR gene has approximately 180,000 base pairs and can be found on the long arm of chromosome 7. This gene encodes 1,480 amino acids that form the CFTR protein. To CFTR functions correctly should be synthesized, folded, and transported to the apical membrane of the cells. The pathway from the nucleus to the plasma membrane requires many other proteins that sit in various compartments on this path. During this process, the CFTR protein must pass rigorous quality control checking to eliminate any misfolded proteins[2].

The first step to form a fully functional CFTR protein starts at the nucleus level, where the CFTR gene is transcribed into the mRNA. When the transcription is completed, the mRNA leaves the nucleus, and once achieved, the ribosome binds to the ER, and then the translation continues until the CFTR protein is translated. As CFTR is a membrane protein, its process folding is complicated because the membrane domains and the cytoplasmic domains should be adequately assembled for the protein's correct functioning. The entire folding process follows two standard folding rules. The first rule is based on a hydrophobic interaction, while the second rule requires that the CFTR protein folded into a double-layered structure in the ER [45].

The folding process also requires help from other proteins called chaperones that are important for the correct folding and aggregation prevention. One of the essential cytoplasmic chaperone belongs to the heat shock protein families; Hsp70 guides CFTR to bend correctly [46].

A co-chaperone called HDJ-2 reduces the aggregation in the early stages of the folding of CFTR recruiting Hsc70 [47]. Another important co-chaperone is calnexin[48]. It is present in the ER and possesses two regions that allow it to interact with the immature CFTR allowing its correct folding[49]. When the protein is misfolded, it is targeted for degradation, and in this case, the ubiquitin plays a crucial role bind covalently to the lysine residues on CFTR. The ubiquitilination process requires three enzymes: the ubiquitin E1 activates the enzyme, ubiquitin E2-binding enzymes, and the ubiquitin E3 ligases. The ubiquitilination process begins with the activation of E1 by the hydrolysis of ATP. In this way, the ubiquitin is activated and then transferred to an active E2 site. Hence, the E3 ligase covalently binds the activated ubiquitin to a lysine on the protein. Once the misfolded CFTR is polyubiquitinated, it is removed from the ER membrane and sent in the cytoplasm for degradation [50].

Two separate systems detect the CFTR misfolded during the folding process. One system acts at the cytoplasmic level, while the other system works at the ER membrane. In this context, ERAD (endoplasmic reticulum-associated degradation) is a further complex that represents a rigorous system to detect malfunctioning CFTR channels and avoid them reaching the plasma membrane even if they can still function. The CFTR protein folded properly inside the ER reaches the Golgi apparatus. This transfer requires the Coating Protein Complex II (COPII) presence at the level of the membrane of the endoplasmic reticulum. COPII helps to maintain the correct structure of the CFTR. At the Golgi apparatus level, the mannose-enriched side chain of CFTR is replaced with the mature complex oligosaccharide's sidechain. So, the protein's maturation process is completed, and it is transferred to the apical membrane through clathrin-coated vesicles.

The half-life of CFTR in the plasma membrane is approximately 12-24 hours, and then it is internalized by the clathrin-coated endosomes. The last quality control system is at the plasma membrane level that can detect the defective CFTRs. The recognized defective proteins are finally polyubiquitinylated and degraded in the lysosome [2].

1.4 CLASSES OF MUTATIONS

Over a thousand different mutations of the CFTR gene have been discovered that can lead to the cystic fibrosis phenotype. These mutations have been found in various locations, such as the CFTR and mRNA splice signals' coding sequence. CF-causing mutations have traditionally been classified into six groups according to their effect on channel production, processing, function, and membrane stability [51].

The purpose of this classification system (Fig. 1.1) was to group CF-causing mutations according to potential therapeutic strategies to develop mutation-specific personalized therapies [52]. Some mutations can be well classified into only one of these classes; however, other mutations can cause multiple defects and belong to more than one group. For this reason, it may be more appropriate to consider mutations according to their phenotype when developing therapeutic strategies [53].

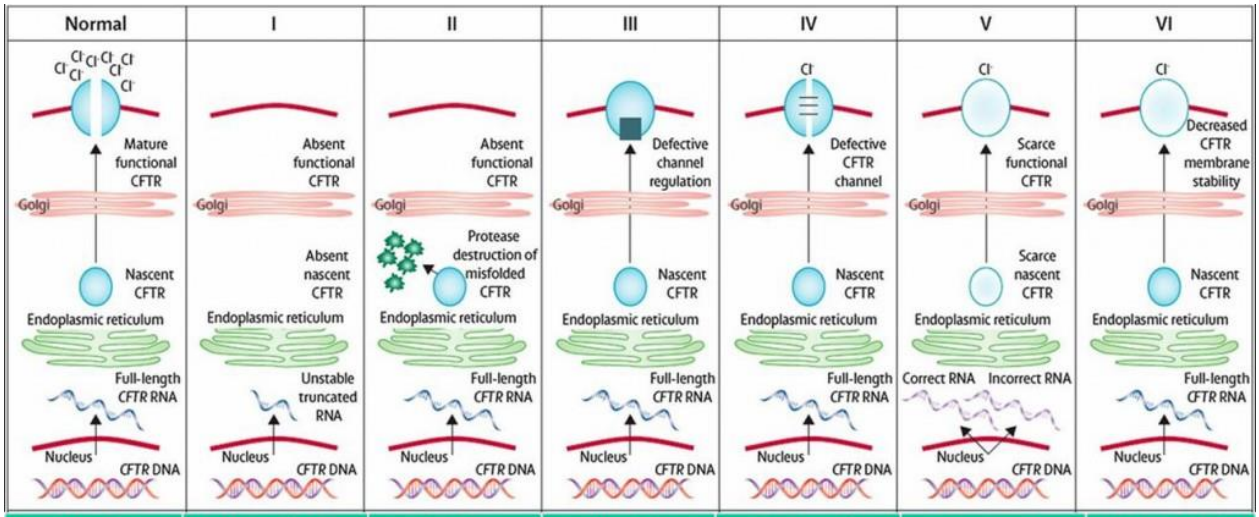

Molecular defect	No synthesis	Block in processing	Block in regulation	Reduced conductance	Reduced synthesis	Reduced half-life
Functional abnormality	Protein is not synthesized	Folding defect	Channel opening defect	Ion transport defect	Decreased protein synthesis	Decreased half-life of the protein
Type of mutations	Nonsense; frameshift; canonical splice	Missense; Aminoacid deletion	Missense; Aminoacid change	Missense; Aminoacid change	Splicing defect; Missense	Missense; Aminoacid change
Main mutations	Gly542X Trp128X Arg553X 621+1G→T	Phe508del Asn1303Lys Ile507del Arg560Thr	Gly551Asp Gly178Arg Gly551Ser Ser549Asn	Arg117His Arg347Pro Arg117Cys Arg334Trp	3849+10kbC→T 2789+5G→A 3120+1G→A 5T	4326delTC Gln1412X 4279insA

Fig. 1.1. Classification of CFTR mutations into six classes based on CFTR-structure functions [54].

Class I mutations are caused by deletions, frameshifts, and nonsense mutations leading to a prematurely truncated CFTR. Class I mutations result in defective channel production leading to a complete absence or severe reduction in the amount of CFTR proteins produced [55] [53]. R553X and G542X are the most relevant mutations within class I.

Class II mutation includes changes that result in defective channel processing and biogenesis. A most common example of class II mutation is F508del, which results in protein misfolding and premature degradation through the endoplasmic reticulum quality control system (ERQC). Class II mutation results in a reduction in mature CFTR availability, leading to a deficit in the amount of active CFTR expressed at the cell membrane [55] [53].

Class III mutations lead to a defective channel regulation, primarily affecting channel gating and typically resulting in reduced channel activity by producing channel closures and decreasing the percentage time that channels occupy the stable open conformation [55] [53].

Class IV mutations affect the ion permeability pathway through the CFTR protein, resulting in decreased channel conductance and a reduction in the overall rate of cellular anion efflux [56] [57].

Class V mutations reduce CFTR expression levels, for example, by affecting promoter sequences or splice mutations. Class V mutations reduce CFTR expression levels, for example, by affecting promoter sequences or splice mutations.

Class VI mutations lead to a destabilization of CFTR in the post-ER compartments or at the PM by decreasing conformational stability [71].

Mutant classes I, II and III, lead to the most severe phenotypes because there is little or no channel activity associated with these mutations [50]. Also known as a residual function (RF) or minimal function (MF), classes IV-VI causes less severe CF. Some proteins are usually able to survive and maintain some level of homeostasis.

1.4.1 The two most common CF-causing mutations: F508del and G551D

The most common CF-causing mutation is F508del-CFTR, and it has been estimated that 90-95% of patients have at least one allele with this mutation [59]. Furthermore, it is also responsible for two-thirds of diagnosed CF cases [60]. F508del results from the deletion of a phenylalanine at position 508 in the NBD1 domain. It was found that cells with F508del failed to produce fully glycosylated CFTR proteins; the CFTR is not fully processed and is degraded

by the UPS before it reaches the apical membrane. A small amount of F508del-CFTR proteins can bypass the ERAD system and reach the membrane; however, the proteins are unstable and malfunctioning due to endocytosis and degradation by the UPS [49]. The F508del-CFTR occurs within the NBD1 domain of CFTR. It has been found that the backbone structure and thermodynamic stability of F508del-CFTR are similar to those of wild-type CFTR [61]**.** However, the F508del can cause kinetic and thermodynamic folding defects within NBD1.

During the folding process, CFTR employs a cooperative folding mechanism. This process implies that NBD1 wild-type folding energy is stabilized by a coupled domain folding, but this coupled domain folding is impaired in the F508del-NBD1. Due to this impairment, the interface assembly between NBD1 and MSDs is impaired, which destabilizes the conformations of MSD1 and MSD2 [62].

The second most common CF mutation is G551D, which is found in the population at a frequency of about three percent [63]. This mutation is caused by a substitution of aspartic acid (D) for glycine (G) at position 551 within NBD1[64]. As a result, the NBD1 domain is unable to bind and hydrolyze ATP. The protein folds appropriately go to the plasma membrane, and the R region is correctly phosphorylated, but the NBD1 domain cannot dimerize with NBD2 because it cannot hydrolyze ATP[65]. Therefore, the protein rarely opens because it cannot bind to the energy source it needs to open the gate, making this mutation a class III mutation.

These two mutations are just a sample of the many mutations responsible for CF. Currently, about 2000 different mutations in the CFTR have been discovered that can cause the disease phenotype. Compared to the F508del mutation, the other mutations are infrequent and not widely discussed [63]. Currently, only 22 mutations have been classified as occurring with a frequency of over 0.1%. The other mutations are typically seen in only one or a few individuals [66].

The classification mentioned above has become well established over the past decades. However, these classifications have some limitations, mainly because many of the most common and severe mutations that cause CF, including F508del, can cause defects that apply to multiple classes. As such, the system is frequently under review, and a more combined approach may need to be taken as a potential therapeutic target for the treatment of such mutations[53].

1.5. THERAPIES IN CYSTIC FIBROSIS

1.5.1 Treatment of cystic fibrosis: an overview

Current treatments for cystic fibrosis, particularly those used for F508del-CFTR, can treat the symptoms but not CFTR's aetiological defects. These therapies include antibiotics, mucolytics (such as DNAse), anti-inflammatory drugs, hypertonic saline spray, and lung transplantation. Compounds that restore normal CFTR function in the apical epithelium of cell membranes to chlorine permeability are very promising. In this context, many theories attempt to explain the correlation between dysfunction in CFTR and cystic fibrosis.

One theory is that cystic fibrosis lung defect decreases the secretion of chloride, bicarbonate, and fluid in the airways' submucosal glands. This process forms an acidic liquid airway surface (ASL), promoting bacterial colonization, damaging the mucociliary clearance and bactericidal capability. Another theory is that cystic fibrosis's primary defect is the overactivity of the epithelial sodium channel (ENaC), which involves the CFTR-ENaC interaction, in which excessive absorption of sodium on the airway surface can lead to ASL dehydration. For this reason, some studies regarding ENaC inhibitors are in development.

Up to now, the treatments for CF can be divided into three main categories:

- Symptomatic treatment: The first is the downstream treatment. These efforts treat the symptoms of CF. A high-calorie, high-fat diet can compensate for malabsorption. It can be combined with the appropriate use of pancreatic enzymes and gastro protectors to combat pancreatic insufficiency. The goal is to remove sputum (also known as mucus) from the lungs through airway clearing techniques to control and prevent bacterial infections with antibiotics and reduce lung inflammation. Together, these therapies can improve lung function, but they are not without drawbacks. For many years, these downstream therapies have been the only option to help CF patients, and each new advancement and discovery has added years to CF patients' lives. It should be a complete and thorough treatment plan to treat CF's damages, whose purpose is to treat all clinical symptoms related to the disease. Besides, respiratory physiotherapy is the primary method to eliminate respiratory secretions and allowing for better ventilation. Using osmotic compounds can be helpful in hydrating mucus. These compounds recall water from the inside of the cell to the outside, allowing the mucus' hydration and favoring a better respiratory tract's clearance. Antibiotic treatment of

lung infections is almost always inevitable due to multiple infections. In many cases, lung transplantation is required if the respiratory system is severely damaged

- Gene therapy: After cloning the CFTR gene in 1989, gene therapy was developed to treat cystic fibrosis. More than 25 gene therapy studies have been conducted using various viral and non-viral gene transfer reagents. Several vector systems have been tested in human studies, including adenovirus vectors, adeno-associated viruses, and cationic lipids. However, even if the in vitro studies have obtained good results, various experimental projects conducted in vivo have not confirmed these results. [67] [68] [69].

- Therapies directed to the primary genetic defect: this approach includes small molecules, called modulators directed to correct or improve the CFTR protein function. These modulators are grouped into five classes: amplifiers, stabilizers, readthrough agents, correctors, and potentiators [70].

1.5.2 Symptomatic therapies

Current therapies treat disease symptoms and include antibiotics, anti-inflammatory agents, mucolytics, hypertonic nebulized saline formulations, pancreatic enzymes, and lung transplantation[71] [72].

Nutrition and maintenance of body weight are essential in CF, establishing an epidemiological link between good nutritional status and improved lung function and survival [73]. Optimizing body weight through proper nutrition, mineral and vitamin supplementation, and replacing digestive enzymes, and controlling CF-related diabetes (CFRD) is essential. In CF patients, the energy requirement is more significant due to lung infections and decreased intestinal absorption, even when there is an adequate intake of pancreatic enzymes. The diet must be high calorie (equal to 120-150% more than the levels usually recommended for subjects of the same sex and age), hyperlipidic and hyperproteic. The proportion of carbohydrates must facilitate the intake of starches with a percentage of carbohydrates for rapid absorption not higher than 10%. It is necessary to ensure an adequate supply of mineral salts and sodium (particularly in the summer season or during gastroenteritis), fat-soluble vitamins, and vitamin B12 in subjects who have had extensive intestinal resections. There is evidence that there is a correlation between optimal

nutrition/body mass index (BMI) (defined as the ratio of weight in kilograms to the square of height in meters) and decreased lung function [74] [75]. A decrease in blood glucose is also associated with poor lung function, a longer duration of lung disease [76] [77], and lung function improvement after insulin therapy initiation.

Use of gastro-protected pancreatic enzymes: the administration of digestive enzymes is aimed at patients with pancreatic insufficiency. Doses are calculated to allow adequate absorption of ingested fats and are based on the subject's degree of pancreatic insufficiency.

Respiratory physiotherapy: aims to keep the lungs free of secretions. Removing thick, viscous mucus from the airways reduces the chance of infections; moreover, keeping the bronchi and lungs clear of secretions improves breathing and helps drugs perform their activities in the best possible way. Respiratory physiotherapy is recommended 1 to 4 times a day. After each lung segment has been drained, the patient is encouraged to cough, blow, and make force expirations. Voluntary coughing and repeated forced expiratory maneuvers with positive expiratory pressure (PEP-mask) can also help eliminate mucus.

rhDNase: Bioengineering product Dornase alfa (Pulmozyme®) is a recombinant human deoxyribonuclease (rhDNase) administered by a nebulizer that works by decomposing extracellular DNA released by neutrophils in sputum, making it thinner and more comfortable to spit. There is evidence that its use in CF can significantly improve long-term lung function and reduce lung deterioration. Short-term use (24 weeks) can improve FEV1 by 5.8% and reduce the risk of aggravation[78]. Long-term use for 12 months can improve FEV1 by up to 7% [79]. It has also been shown to reduce airway inflammation progression, and the ICL improves in young children, [80]. rhDNase is now the standard of care in CF.

Antibiotic therapy: is aimed at eradicating the first infection. It is indicated in the prophylaxis for the treatment of exacerbations in patients presenting chronic infections and in the treatment of exacerbations. The drug treatment schedule varies from short intermittent courses with a single antibiotic to almost uninterrupted administration of one or more antibiotics. Some of them are often 2 to 3 times higher than the recommended dose for minor infections, as patients with CF have proportionally more lean mass and a faster clearance rate. Also, it is difficult for many antibiotics to obtain adequate drug levels in respiratory secretions. These can be applied directly to the airways' surface (nebulized or inhaled) or taken systemically (oral and intravenous antibiotics). Antibiotics used in "maintenance"

therapy are designed to inhibit or prevent infection, maintain stable lung function, and reduce the frequency of pulmonary exacerbations[81].

Anti-inflammatory therapy: administering oral corticosteroids is indicated in infants who have protracted bronchiolitis forms or in patients with refractory bronchospasm, allergic bronchopulmonary aspergillosis, and complications due to multiple inflammations. Prolonged corticosteroid therapy can slow down lung function deterioration; it is not recommended as a routine treatment due to steroid complications. The use of non-steroidal anti-inflammatory drugs (NSAIDs) has been studied: researchers report that administration of regular high-dose of ibuprofen (with specific activity against neutrophil chemotaxis) can reduce the rate of decline in lung function, with the reduction of acute lung attacks [82]. Its characteristics side effects limit its use in clinical practice. Continued administration of ibuprofen appears to reduce the rate of deterioration of respiratory function.

Nocturnal oxygen therapy and support with Non-Invasive Ventilation (NIV): it is necessary for patients with advanced lung disease who undergo nocturnal hypoxemia and hypercapnia, especially during broncho pneumopathy exacerbations.

Airway surface osmotic agents: Both the nebulized hypertonic saline and the inhaled dry powder mannitol work by creating an osmotic gradient to pull water into the airway lumen, thereby replenishing mucus and improving defects in MCC. In a randomized controlled trial, after 48 weeks of HTS treatment, lung function FEV1 enhanced by 3.2% (not significant), and statistically, the exacerbation of lung disease was also reduced [83].

Maintenance of inhaled antibiotic therapy: The purpose of applying regular or cycling antibiotics directly to the airway surface through nebulization or inhalation is to inhibit the number of bacteria, and mainly for chronic airway infections caused by Pseudomonas aeruginosa. In this context are used in clinical practice, three main types of nebulized antibiotics: (i) colistimethate sodium (colistin), (ii) tobramycin, and (iii) aztreonam lysine. Recent advances in drug delivery have shown that the introduction of colistin and tobramycin dry powder inhalers reduces patient administration times and improves treatment compliance. Although it has been used as a first-line nebulized antibiotic, there is no evidence to demonstrate nebulized colistin's clinical benefit. In contrast, the aminoglycoside tobramycin has become the "standard" for new topical antibiotics. It is an administration in which continuous administration is alternated for one month and

suspension for the following month; after six months of treatment with nebulized tobramycin, FEV1 improved by approximately 7%, and the risk of hospitalization to pulmonary aggravation was also reduced [84]. In a head-to-head study, nebulized Aztreonam showed a better effect than tobramycin: FEV1 improved by 2.7% after alternate month cycles, and pulmonary deterioration was reduced [85].

1.5.3 Therapies aimed to correct the genetic basic defect

Currently used therapy for CF is mainly based on controlling the disease's symptoms without treating the underlying genetic defect; this approach reduces the disease's progression by improving the patient's quality of life. [86]

The discovery of CFTR modulators provides a breakthrough for CF treatment because these molecules can improve or potentially correct CFTR function by limiting the complications caused by this disease (Table. 1.1) [87]. The rapid development in drug discovery, with the help of high-throughput-screening (HTS), has made it possible to study the activity of thousands of small molecules simultaneously in a short period, thus accelerating the identification of compounds that can improve the function of defective CFTR proteins[88]. Some small molecules that control the CFTR malfunctioning are currently used in the clinical field, and many others are undergoing clinical trials. One of the potential strategies in treating CF is to act at the mRNA level or the CFTR protein to correct the gene dysfunction.

According to the mechanism of action, modulators are divided into five groups: amplifiers, readthrough agents, stabilizers, correctors, and potentiators. Briefly, the potentiators keep the CFTR channel open at the membrane surface [87]. Correctors can be used as molecular chaperones to prevent CFTR's misfolding in the ER and transport it to the plasma membrane [87]. The amplifiers increase the amount of CFTR protein produced by cells [89]. There are three ways to improve the CFTR activity: by increasing the number of CFTR channels on the plasma membrane, increasing the opening channel's time, or increasing the size or conductance of the channel[90]. Modulators can improve CFTR function in the cells by increasing any of these variables. There are currently four CF modulators therapies available to patients: Ivacaftor, Lumacaftor/Ivacaftor, Tezacaftor/Ivacaftor, and Elexacaftor/Tezacaftor/Ivacaftor. Ivacaftor was the first drug approved by the FDA to treat CF patients with the G551D mutation on January 31, 2012 (FDA, 2012). Ivacaftor is a potentiator that increases the time of CFTR opening and can be used for various mutations.

Lumacaftor, Tezacaftor, and Elexacaftor are all correctors, mainly used to correct the mutation F508del CFTR. When combined with Ivacaftor, these drugs form a combination therapy. The corrector is responsible for the folding of CFTR so that CFTR can be transported to the plasma membrane, and Ivacaftor increases the possibility of channel opening. The latest addition to these drug therapies is Trikafta (Elexacaftor / Tezacaftor / Ivacaftor), which the FDA approved on October 21, 2019, the first second-generation triple modulator therapy (FDA, 2019).

Table 1.1. The pipeline of current CF modulators in clinical trials and the market.

Name	Function	Development stage	Company
Ivacaftor	Potentiator	FDA-Approved 2012	Vertex Pharmaceuticals
Orkambi ® (lumacaftor + ivacaftor)	Corrector + potentiator	FDA-approved 2015	Vertex Pharmaceuticals
Symdeko ® (tezacaftor + ivacaftor)	Corrector + potentiator	FDA-approved 2018	Vertex Pharmaceuticals
Trikafta ® (ivacaftor + tezacaftor + elezacaftor)	Potentiator + corrector + corrector	FDA-approved 2019	Vertex- Pharmaceuticals
Ataluren (PTC124)	Read-through agents	Phase III (discontinued)	PTC-Therapeutics
PTI-801	Correctors	Phase III	Proteostasis Therapeutics
VX-659	Correctors	Phase III	Vertex Pharmaceuticals
PTI-808	Potentiators	Phase III	Proteostasis Therapeutics

PTI-428	Amplifiers	Phase III	Proteostasis Therapeutics
ELX-02	Read-through agents	Phase II	Eloxx Pharmaceuticals
ABBV-2222	Correctors	Phase II	Abbvie/Galapagos
ABBV-2737	Correctors	Phase II	Abbvie/Galapagos
FDL169	Correctors	Phase II	Flately Discovery Lab.
VX-121	Correctors	Phase II	Vertex-Pharmaceuticals
VX-152	Corrector	Phase II	Vertex. Pharmaceuticals
VX-440	Corrector	Phase II	Vertex Pharmaceutical
VX-561	Potentiator	Phase II	Vertex- Pharmaceuticals
ABBV-974	Potentiator	Phase II	Abbvie/Galapagos
ABBV-3067	Potentiator	Phase II	Abbvie/Galapagos
Cavosonstat	Stabilizers	Phase II (Discontinued)	Nivalis

1.5.4 CFTR structure and its role in the development of new modulators

For many years, the lack of a high-resolution CFTR structure has been a significant obstacle in CF research[91]. In the beginning, X-ray crystallography allowed the determination of the structure of NBDs at the atomic level [92] [93]. However, until progress was made in cryo-EM, TMD's resolutions and the R domain remained insufficient. Previously, the best structural approximations of CFTR were obtained via the high-resolution structures obtained for related ABC transporters, including the P-glycoprotein (Pgp) multiple resistance transporter [94], the bacterial transporter Sav1866[95], and bacterial lipid flippase MsbA [96]. These homologs pave the way for designing a series of CFTR *in-silico* models that could be used to investigate CFTR structure-function correlations [97] [98] [99] [100].

The first high-resolution structure of the entire CFTR protein was obtained using the zebrafish CFTR ortholog in the ATP-free, non-phosphorylated inactive (closed) state [101], followed shortly after that by the human CFTR structures (Fig. 1.2) [41]. Despite sharing only 55% amino acid identity, these two CFTR orthologs' resulting structures were mostly similar. These structures result in many unique features that homology models cannot predict. One such feature is the presence of an interface motif named the "lasso motif" that could be involved in the mediation of protein-protein interaction [102]. Furthermore, a secondary structure breakdown of TM8 was observed, which may allow primary chain residues to interact with ions and water within the channel pore [103]. Despite these important discoveries, the cryo-EM models did not show consistent structural features attributable to RD, which may be due to the domain's disorganization, which cannot be resolved in cryo-EM images [101].

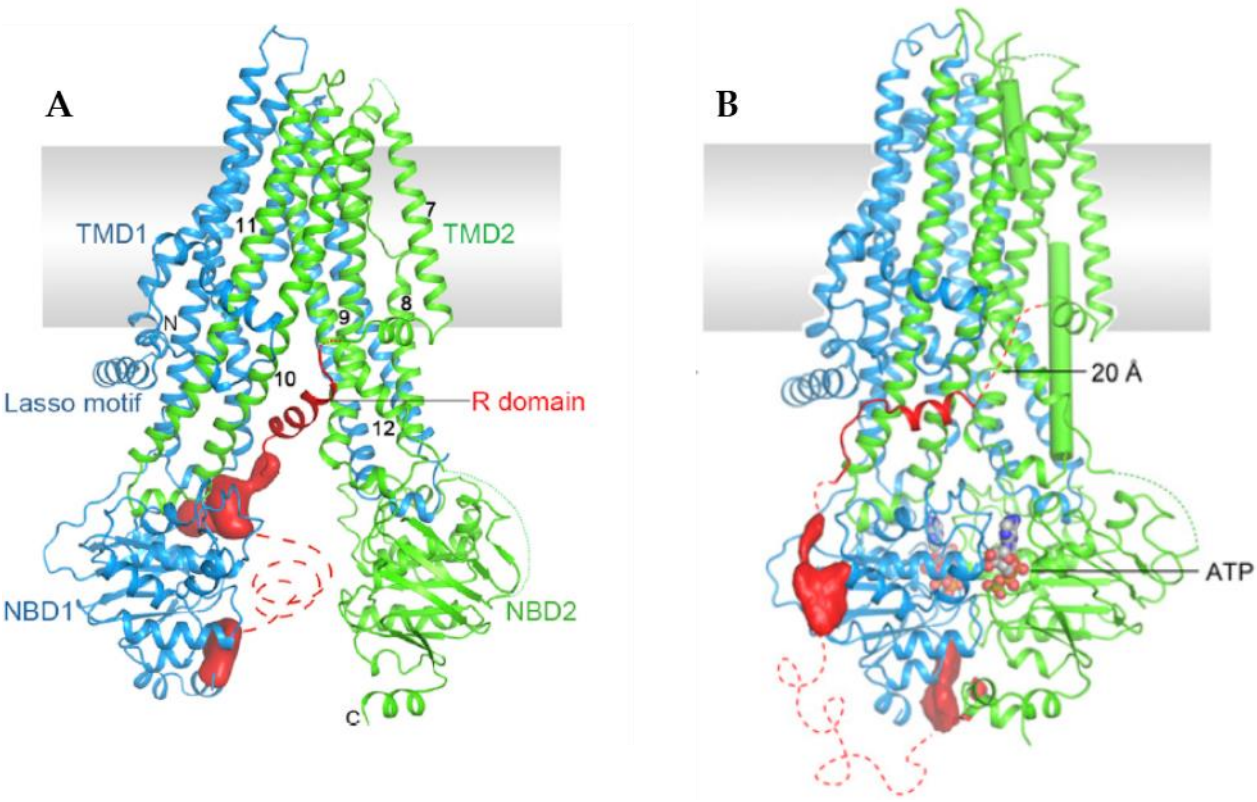

Fig.1.2. Structure of human CFTR. (**A**) hCFTR in dephosphorylated, ATP-free conformation (PDB: 5UAK). *Picture from Liu F. et al. Molecular structure of the human CFTR ion channel. Cell.* ***2017****, 169, 85-95.* (**B**) hCFTR in phosphorylated, ATP-bound conformation (PDB: 6MSM). *Picture from Zhang, Z. et al. Molecular structure of the ATP bound, phosphorylated human CFTR. Proc Natl Acad Sci U S A.* ***2018****, 115, 12757-12762.*

Recently, cryo-electron microscopy (cryo-EM) revealed structures formed by the N-terminal region of TMD1, called the lasso motif (LM), similar to a lasso that appears perpendicular to

the TM helix of TMD1 [101] [41]. This motif's functional importance is still unclear, although there is evidence that the interaction between LM and NBD1 is involved in the regulation of ATPase activity [104]. The TMD transmembrane helices are connected by four intra and six extracellular loops. Among these, the ICLs are more extensive and extend below the plasma membrane, enter the cytoplasm, forming coupling helices with NBDs. ECLs are much smaller than ICLs. However, ECL4 is larger than the others and undergoes co-translational N-glycosylation at two sites N894 and N900 [105].

An alpha-helix region within the channel pore's intracellular vestibule between the ICLs has been determined, and it seems to correspond to a part of the RD. Finally, another cryo-EM model of CFTR has been disclosed representing the protein in its closed-phosphorylation ATP-bound state and bounded with the potentiator Ivacaftor and the modulator GLPG1837. These findings paw the way to identify hotspots for drug-binding and the application of rational design for a new generation of modulators[58].

1.5.5 Correctors and potentiators

The CFTR corrector can correct abnormal folding and processing of class II (and possibly V) CFTR mutation channels (such as F508del), thereby increasing the number of successfully processed channels and then expressed on PM [107]. CFTR mRNA is translated in the ER, and most of the tertiary folds are co-translated at this stage [108]. Wild-type (WT) CFTR undergoes further post-translational folding and is transported to PM via the Golgi apparatus. Before expressing the mature channel, the glycans that were added to the CFTR channel were further modified[109] [110]. However, class II mutations (such as F508del) can misfold the protein during co-translational folding [111]. Therefore, CFTR corrective compounds can act through multiple mechanisms. They can primarily act as pharmacological chaperones by binding to the same developing CFTR protein because it translates in the ER and promotes proper folding, thus preventing targeting to ERAD. [112] [113]. Second, they can interact after translation with incorrectly folded CFTR to correct the folded structure. Alternatively, they can act as regulators of protein stability, interact with non-CFTR proteins belonging to the CFTR interaction group, and determine the correct protein folding and transport of CFTR to the Golgi proteasome [114].

Lumacaftor is a corrector that is thought to interact with residues in TMD1 to stabilize mutant CFTR and correct folding early in biogenesis [115] [7]. To date, F508del is the most common CF mutation, and about 70% of patients are homozygous for the disease variant [116]. Therefore, the development of small molecule therapies that prove useful for F508del patients is the key. In WT-CFTR, the F508 residue is located on NBD1 at the interface between NBD1 and ICL4 of TMD2 [98]. Although F508del affects the structural folding of NBD1, the correct folding of NBD2 also depends on the integrity of NBD1. Therefore, this mutation indirectly affects proper NBD2 folding, leading to misfolded CFTR recognition, which is subsequently degraded by ERQC [111]. WT-CFTR is a protein with a relatively low folding efficiency. Depending on the cell type, only about 30-50% of the protein successfully reaches the PM [112]. Since CF is an autosomal recessive genetic disorder and the heterozygous F508del mutation is asymptomatic, it is believed that a 50% recovery of CFTR expression should be sufficient to deliver enough CFTR protein to the PM for its normal functioning.

The relatively low information for adequately managing CF provides a strong reason for combining correctors and potentiators to treat patients with F508del-CFTR mutation. Orkambi, which the FDA approved in 2015, is one such combination therapy, the purpose of which is to combine ivacaftor and lumacaftor to achieve this [117]. It has been shown that only lumacaftor can correct F508del-CFTR processing to levels 14% of wild-type [118]. Theoretically, this level should be sufficient to restore the patient's near-normal CFTR function combined with potentiators.

However, for F508del homozygous patients, lumacaftor itself has no clinical benefit. Besides, the benefits of Orkambi shown by FDA approval are relatively limited for F508del homozygous CF patients [90].

In 2018, the FDA approved Vertex Pharmaceuticals Symdeko's dual combination therapy, which combines ivacaftor with the corrector tezacaftor (VX-661) combined with an additional dose of ivacaftor [119]. Compared with Orkambi, the combination of ivacaftor with tezacaftor instead of lumacaftor resulted in a similar recovery level of FEV1 but an increased level of tolerance[119].

However, using multiple corrector compounds with different mechanisms of action or binding sites, the relatively low level of improvement in FEV1 caused by these dual therapy

strategies can be improved using a triple combination of MCG1516A, RDR1, and VX- 809. These three corrector compounds interact with different sites on NBD1 [120].

Additionally, results from two recent Phase II clinical trials for this type of therapy (involving the combination of VX-659 or VX-445 with ivacaftor and tezacaftor) showed that FEV1 increased by 13.3%. (VX-659) and 13.8% (VX-445). For G551D patients, this level of response exceeds ivacaftor's level, and it is hoped that the level of tolerance of these therapies is comparable to that of Symdeko[121].

Abbvie/Galapagos has developed novel classes of correctors, including the molecules GLPG-2222, GLPG-2737, GLPG-2851, GLPG-3221, and GLPG-3748 are the most promising. GLPG-2222 has a similar structure to the Tezacaftor and Lumacaftor (Fig. 1.3). A phase IIa clinical trial demonstrates improving the sweat chloride concentrations but did not ameliorate ppFEV1 in F508del-homozygous patients. Up to now, there are other clinical trials to test the safety and efficacy of GLPG-2222 in combination with other modulators.

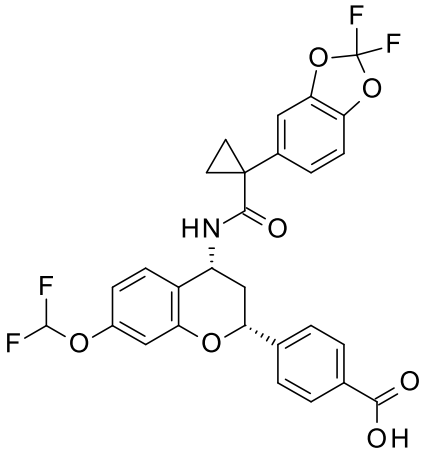

Fig. 1.3. Chemical structure of GLPG-2222.

CFTR potentiators enhance the CFTR activity present in PM by promoting the stable open state of the channel and are targeted for the treatment of class III and class IV mutations [52]. The CFTR potentiator ivacaftor (VX-770; Kalydeco® from Vertex Pharmaceuticals) is the first CFTR small molecule modulator approved by the FDA [122] [123]. Ivacaftor was initially approved to treat the third most common type III mutation (G551D) that causes CF, causing severe gating defects [124]. However, its use has expanded to cover more than 38 mutations, including S549R and G1349D and the class IV mutation R117H [125].

The CFTR potentiators rely on the existing pool of CFTR proteins that already exist on PM. Therefore, unless used combined with other compounds, they are not suitable for patients with mutations affecting CFTR expression (including F508del). So far, although many patients have benefited from it, combination therapies (such as Orkambi and Symdeko) have not successfully demonstrated the efficacy of ivacaftor for class III mutations (such as G551D).

Therefore, it is still necessary to develop CFTR potentiators with greater efficacy. So far, there are many drug candidates in clinical trials, including QBW251 (Novartis), CTP-656 (Concert Pharmaceuticals), and GLPG1837(AbbVie / Galapagos) [107]. The obstacle to developing such compounds is that there is currently little understanding of existing potentiators' mechanisms (including ivacaftor).

A better understanding of existing CFTR potentiators' mechanisms may help develop new potentiators compounds with greater efficacy against a broader range of mutations. When these modulators are used in combination with other compounds (such as correctors), they may also be more effective. Identifying potentiators that act through different CFTR protein regions (e.g., through TMDs rather than NBDs) can improve efficacy. Additionally, identifying multiple CFTR potentiators with different sites of action can help develop combinations that can be used in conjunction with correctors for mutations such as F508del.

1.5.5.1 Ivacaftor

Ivacaftor, also known as Kalydeco ® or VX-770 (Fig.1.4), was initially approved for patients with at least one G551D allele. Since its first FDA approval, Ivacaftor has been approved for more than 33 mutations, including gated mutations. Ivacaftor, developed by Vertex Pharmaceuticals, is a small organic molecule initially discovered via High-throughput-screening (HTS) studies.

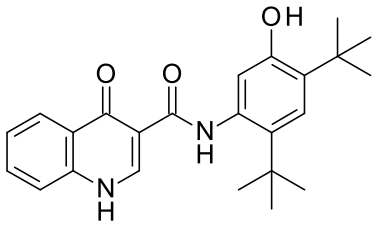

Fig. 1.4. Chemical structure of VX-770 (Ivacaftor ®).

Ivacaftor's effect was tested using human bronchial epithelial cells (HBE) from CF patients with the G551D mutation, F508del mutation, and non-CF cells' control. Studies have shown that ivacaftor increases the possibility of CFTR channel opening and in wtCFTR cells increases chloride secretion to approximately 50% of normal chloride secretion[122].

Furthermore, Ivacaftor can prevent ASL dehydration and increase cilia beating. After this promising result, Ivacaftor proceeded for human clinical trials. For individuals with at least one G551D allele, ivacaftor produced significant results in both changes in ppFEV1 and changes in sweat chloride levels. Ivacaftor acts by binding directly to the CFTR protein and causes the spontaneous opening of the ATP-dependent channel [126] [127].

When Ivacaftor binds to the protein, phosphorylation of the CFTR regulatory region is required, but ATP is not needed to dimerize the NBD1 and NBD2 domains. This problem can correct the G551D mutation, which does not respond to ATP and is therefore rarely activated. Ivacaftor has little effect on the homologous F508del because Ivacaftor only increases the possibility of opening existing CFTR channels on the plasma membrane, while F508del CFTR never reaches the plasma membrane [128].

Since Ivacaftor also increases the possibility of opening the wtCFTR channel, it has been approved for 33 different mutations, including gating, residual function, splicing, and conduction mutation. Although Ivacaftor can only cause clinical changes in some mutations representing a small percentage of total CF patients, Ivacaftor is the gold standard for modulating therapy (FDA, 2017).

1.5.5.2 Lumacaftor

Lumacaftor (VX-809) (Fig.1.5) was the second modulator developed by Vertex Pharmaceuticals. It has been designed to prevent the misfolding of F508del-CFTR. Concerning this function, it falls within the class of corrector-type modulators. Lumacaftor acts cotranslationally. It alters the protein conformation of the MSD1 domain, which allows the establishment of a more stable connection between the MSD1 and NBD1 domains, only partially correcting the F508del mutation[129]. As for the clinical studies conducted on Lumacaftor, the first study was carried out using only the Lumacaftor corrector in patients with CF, homologous for the F508del mutation. This study showed that Lumacaftor used alone has no clinically relevant effects on ppFEV1 or sweat chloride levels. These results could be explained by the fact that the F508del-.CFTR mutation also has gating defects as well

as misfolding [130]. From these studies' data, Lumacaftor was combined with Ivacaftor to create a dual modulator therapy that led to the re-establishment of a specific function of CFTR. Lumacaftor would facilitate the correct bending of the CFTR canal. At the same time, the Ivacaftor would increase the opening time of the channel.

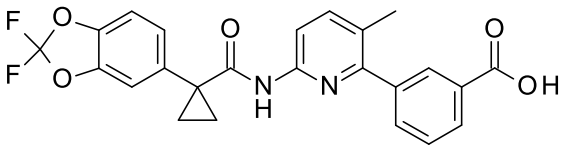

Fig.1.5. Chemical structure of VX-809 (Lumacaftor ®).

The Lumacaftor / Ivacaftor combination, also known by the trade name of Orkambi, has some clinical benefits for homozygous F508del patients but does have an effect on F508del heterozygous patients[131]. Compared to the impact that Ivacaftor has on the G551D mutation, the Lumacaftor / Ivacaftor combination therapy results in a much more modest lung function improvement. However, Lumacaftor / Ivacaftor significantly reduces the decline rate of FEV1, allowing for stabilization of ppFEV1 [132]. For this reason and the proven improvement in lung function, albeit modest, the combination therapy with Lumacaftor / Ivacaftor was approved by the FDA in 2015 (FDA, 2015)

1.5.5.3 Tezacaftor

Tezacaftor (VX-661) (Fig. 1.6) has a similar structure to that of the previous corrector. Tezacaftor is a CFTR corrector with a broader action than Lumacaftor, enabling cell production and facilitating the trafficking of many mutated forms of CFTR, including F508del-CFTR [133]. Since Tezacaftor does not induce CYP3A4 enzymes, there are fewer drug-drug interactions than those found using Lumacaftor. It follows that Tezacaftor, from a clinical point of view, has a better safety profile. Clinical studies conducted combining Tezacaftor with Ivacaftor have shown that this combination results in changes in ppFEV1 and sweat chloride levels similar to those produced with treatment with the Lumacaftor / Ivacaftor combination modulator therapy. Based on these clinical trials, the therapy Symdeko (Tezacaftor / Ivacaftor) was derived, which was approved by the FDA in February 2018 for patients with one allele of F508del and a residual function allele that responds to Ivacaftor (FDA, 2018). For homologous F508del patients, similar clinical benefits were found with both

Lumacaftor / Ivacaftor and Tezacaftor / Ivacaftor treatment, but the latter dual combination has been shown to have fewer side effects [134].

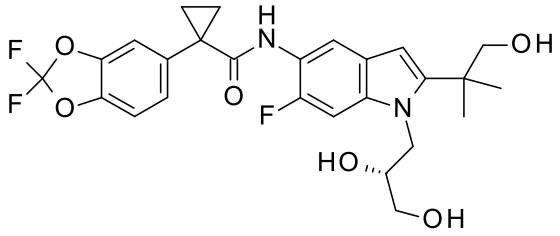

Fig.1.6. Chemical structure of VX-661 (Tezacaftor ®).

1.5.5.4 Trikafta

The next step in modulator development was to design a triple combination of modulators known as second-generation modulators. Heijerman and colleagues theorized that adding a second corrector with a complementary mechanism of action to the Tezacaftor / Ivacaftor combination would better restore CFTR function [135]. Furthermore, the goal was to develop a modulator capable of providing therapy to patients with CF who are heterozygous for F508del and a minimal function mutation. Minimal functional mutations include nonsense, insertion/deletion, splicing, and several severe protein misfolding mutations[121]. Therefore, the final aim was to correct the CFTR function by restoring the only F508del allele regardless of the mutation carrying the second allele. In this context, Vertex Pharmaceuticals had initially identified two very similar modulators to combine with Tezacaftor / Ivacaftor. The drug candidates in this study were VX-659 and VX-445 (Fig. 1.7). Separate phase 2 and phase 3 studies were carried out on these two compounds. Both were found to have a corrective function as they reduce CFTR misfolding by promoting CFTR trafficking from the ER to the plasma membrane. They also have an additive effect on Tezacaftor. Clinical studies have shown that both VX-659 and VX-445 triple combination therapy provide dramatic lung improvement in homozygous and heterozygous patients [121].

After conducting parallel phase 3 clinical trials on both VX-659 and VX-445, Vertex Pharmaceuticals decreed that compound VX-445 (Elexacaftor) was the most effective drug of the two candidates. Both parallel clinical trials included 24-week tests for heterozygous patients carrying one F508del mutation and one MF mutation and 4-week tests for F508del homozygous patients. Both programs met their primary and secondary endpoints, and both

triple combinations were generally well tolerated with a low amount of adverse effects [136]. Based on the data collected, Vertex submitted Elexacaftor in combination with Tezacaftor / Ivacaftor for FDA approval. On October 21, 2019, Trikafta (Elexacaftor / Ivacaftor / Tezacaftor) was approved by the FDA for patients with at least one F508del mutation [137]. This drug is a significant step forward in the search for modulators for CF. It is available to patients who previously could not access previous modulatory therapies, demonstrating a noticeable improvement in lung efficiency over the modulators mentioned above. It is important to note that Trikafta is not the definitive cure for CF. If a patient cannot continue therapy, they return to their previous treatments [138].

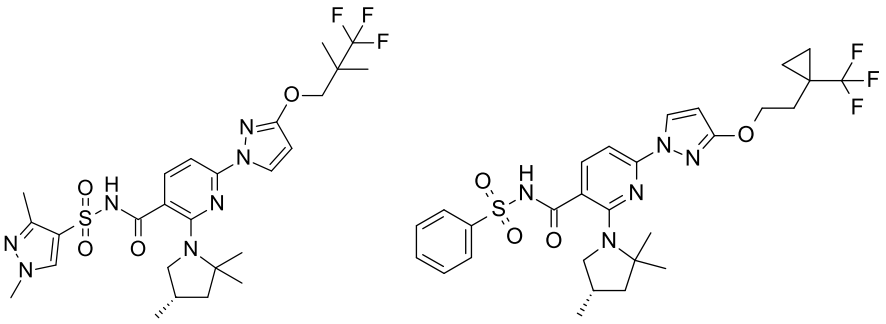

Fig. 1.7. Chemical structures of VX-445 (Elezacaftor) (*left*) and VX-659 (Bamocaftor) (*right*).

1.5.5.5 Stabilizers

Stabilizers are compounds that anchor CFTR at the PM, so avoiding its degradation by lysosomes [139].

Despite Lumacaftor demonstrated to bail out the functional expression of F508del-CFTR in cells, it does not provide long-term stability at the PM surface (He et al., 2013). For this reason, new treatments are explored to extend the residence time of CFTR at the PM. In this scenario, the Hepatocyte growth factor (HGF) was proved to abet CFTR at the PM in F508del-expressing cells as it induces the CFTR interaction with Na+/H+ exchanger regulatory factor 1 (NHERF1) [140]. Other adopted strategies involved administering vasoactive intestinal peptide (VIP) [141] or the use of S-nitrosoglutathione reductase inhibitors [142].

The first stabilizer tested in a clinical trial was Cavosonstat (N91115; Nivalis) (Fig. 1.8). A phase I clinical trial showed reduced sweat chloride concentration in F508del-CFTR homozygous patients but not showing any further improvement in lung function and sweat

chloride levels in phase II clinical trial [140]. For this reason, the clinical development of Cavosonstat has been terminated for CF.

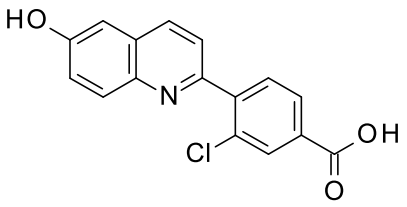

Fig.1.8. Chemical structure of N91115 (Cavosonstat).

1.5.5.6 Readthrough agents

A significant portion of CF-related mutations is in-frame nonsense, frameshift, and splice variants introducing a premature stop codon (PTC) into CFTR mRNA, eliminating CFTR protein synthesis, or producing shortened or truncated forms of CFTR.

Readthrough agents are compounds that perform a ribosomal over-reading of a premature stop codon and allow the insertion of an amino acid at that point allowing translation to continue until a standard final transcript is produced[144]. The so-called readthrough effects were first found in aminoglycoside antibiotics, such as gentamicin. This drug is used in CF patients to eradicate P. aeruginosa infections. Although in numerous studies conducted on cell lines, these compounds have been shown to increase full-length CFTR expression, they cannot be used in clinical practice since their use over long periods causes nephrotoxicity and ototoxicity [145].

In this context, Ataluren (Fig. 1.9) (also known as PTC124; PTC Therapeutics) identified by HTS studies has shown that it can restore the expression and function of CFTR transgenic mice. Despite the results observed in phase II clinical trials, treatment with Ataluren did not demonstrate a significant trend in improving the ppFEV1 of CF patients. against this, its clinical development as a CF drug has been halted. However, it has been approved to treat patients with Duchenne muscular dystrophy with the trade name Translarna® (PTC Therapeutics).

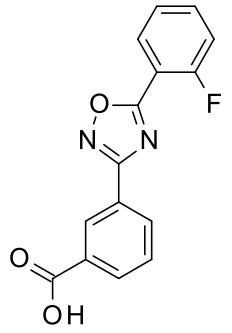

Fig.1.9. Chemical structure of PTC124 (Ataluren).

1.5.5.7 Amplifiers

CFTR amplifiers are modulators that increase immature CFTR protein expression. These compounds act synergistically with correctors and potentiators, increasing therapeutic benefit [146]. Up to now, there are known two types of amplifiers devised both by Proteostasis Therapeutics. These drugs, named PTI-428 (fig. 1.10) and PTI-CH, passed the pre-clinical and clinical studies with promising results [147].

In vitro studies conducted on PTI-428 demonstrated double CFTR activity when used in combination with other modulators. in these latter cases, a clinical trial supported by Proteostasis Therapeutics showed that the patients who received PTI-428 in co-treatment with Orkambi improved lung function. However, there are no changes in the levels of sweat chloride.

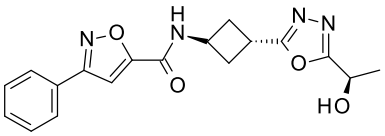

Fig. 1.10. Chemical structure of PTI-428.

CHAPTER 2

STRUCTURE-BASED DRUG DESIGN

2.1 Molecular docking studies of correctors as modulators of F508del-CFTR

During my Ph.D., I performed docking studies of a library of F508del-correctors, such as the *in-house* series VX-809-AAT hybrids and modulators described in the literature (Fig.2.1). All the compounds possess variable chemical features (see Appendix A1-A3)[148].

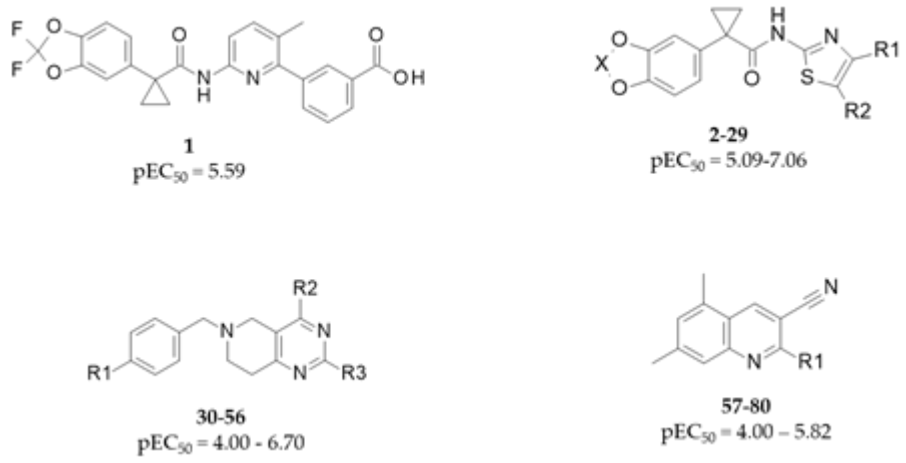

Fig.2.1. Chemical structures and biological activity of the examined F508del-CFTR correctors.

Firstly, these calculations have been performed on the human F508del-CFTR NBD1 (PDB code:4WZ6) domain starting from the several experimental efforts described in the literature that affirmed that the NBD1 domain plays a key role for the corrector's activity at this domain of channel [149],[150],[151],[152]. Since the data derived from calculations performed only on the NBD1 domain are partial, our research group decides to perform molecular docking studies on the whole protein. Given the absence of crystallographic data of the CFTR mutant protein, our research group modeled the whole protein superimposing the cryoelectron microscopy available data of the wild type protein (PDB code: 6MSM) [153] and that of the mutant NBD1 domain (PDB code: 4WZ6) (Fig.2.1.2). Furthermore, I align our *in-house* model of F508del-CFTR onto the cryoelectron microscopy data of the wild-type protein (PDB code: 6MSM) to evaluate the conserved regions. (Fig.2.1.3)[154].

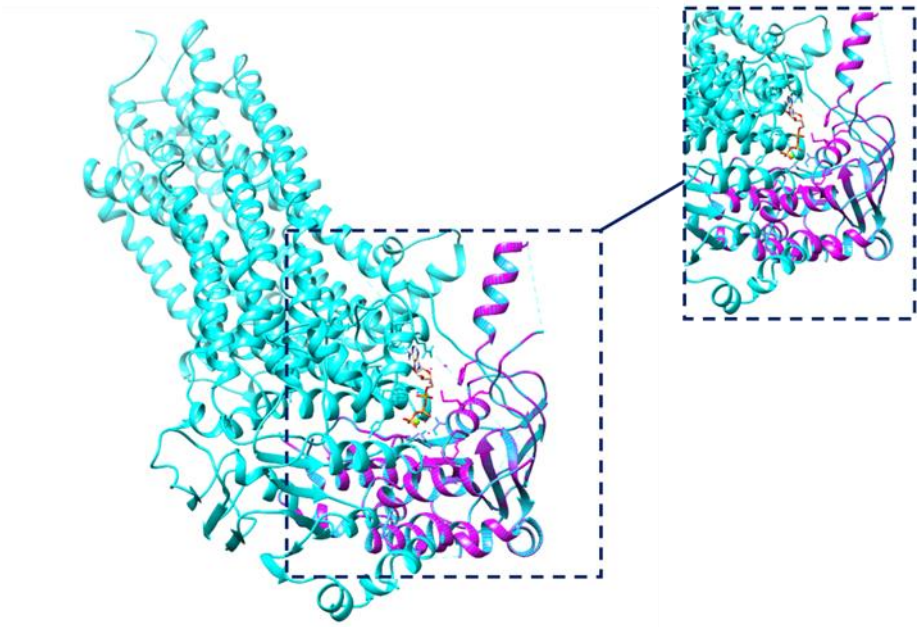

Fig.2.1.2. Superimposition of the modeled F508del-CFTR (cyan) onto the mutant NBD1 domain (PDB code:4WZ6) (magenta). At the right, a focus on the zone that contains ATP (C carbon orange) and Mg^{2+} (green).

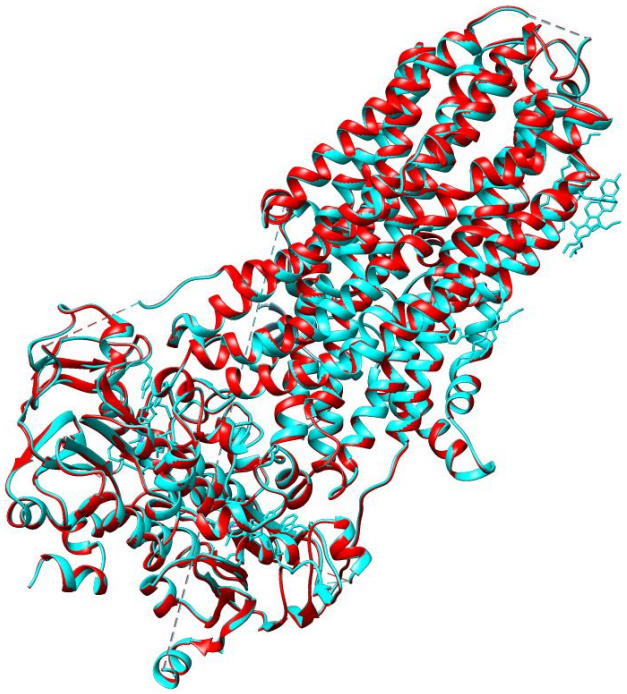

Fig.2.1.3. Superimposition of the modeled F508del-CFTR (cyan) onto the WT-CFTR structure (PDB: 6MSM) (red). The two superimposed structures show a strong similarity.

Molecular docking studies on VX-809 and related analogs were performed considering the putative binding site proposed by the site finder module implemented in the MOE software. This software module identifies tight atomic packing regions to filter out sites that are "too exposed" to solvent. This approach allows removing protrusions that are unlikely to be good active sites. The derived preliminary sites are then classified based on their

hydrophobic or hydrophilic profile. The generation of alpha spheres on these sites is made by collecting sets of points using a modified Delaunay triangulation method to derive different spheres displaying different radii. All the collected sites are ranked according to their Propensity for Ligand Binding (PLB) score, which is based on the pocket's amino acid composition as described in the literature[160] (Table 2.1).

Table. 2.1. Top ten best-ranked scored sites identified with Site Finder at the modeled F508del-CFTR.

Site	Aminoacidic residues
1	L165 K166 S168 S169 R170 L172 D173 K174 S176 I177 G178 Q179 G253 S256 E257 V260 S263 E264 I266 E267 N268 I269 Q270 S271 A274 Q378 E379 Y380 K381 T382 L383 E384 Y385 N386 A399 F400 W401 E402 E403 G404 F405 E407 T438 V440 A457 G458 S459 T460 G461 A462 G463 K464 T465 S466 M469 M470 I471 M472 G473 E474 L475 E476 P477 S478 I482 K483 H484 S485 G486 R487 I488 F490 S492 Q493 N494 S465 W496 I497 M498 P499 G500 T501 E504 N505 I506 I507 G508 V509 S510 Y511 D512 R515 E527 D528 K531 F532 A533 E534 K535 V539 L540 G544 I545 T546 L547 S548 G549 G550 Q551 R552 A553 R554 R559 Y562 D564 D571 S572 P573 F574 G575 Y576 L577 L580 E582 L601 V602 T603 S604 K605 H608 A654 E655 R657 N658 L661 T662 V956 M961 L964 N965 T966L967 K968 A969 G970 I972 L973 P1050 T1053 H1054 V1056 T1057 L1059 K1060 G1061 L1062 W1063 T1064 L1065 R1066 A1067 F1068 G1069 R1070 Q1071 Y1073 F1074 L1077 K1080 A1081 L1084 K1218 Y1219 G1223 N1224 I1226 L1227 G1224 R1245 T1246 G1247 S1248 G1249 K1250 S1251 T1252 L1254 S1255 L1258 L1260 L1262 V1288 P1290 Q1291 K1292 V1293 F1294 I1295 F1296 S1297 G1323 L1324 S1326 V1327 Q1330 F1331 V1340 D1341 G1342 G1373 C1344 V1345 L1346 S1347 H1348 G1349 H1350 K1351 Q1352 L1353 D1370 Q1371 P1372 A1374 H1375 L1376 D1377 V1379 T1380 I1383 C1400 H1402 V1415 I1416 E1417 E1418 N1419 K1420 R1434 S1435 L1436 F1437 R1438
2	L88 E92 K95 Q98 P99 L102 F131 R134 L138 H139 I142 H146 I175 G178 Q179 L180 V181 S182 L183 S185 N186 N187 L188 N189 K190 F191 E193 G194 A196 L1987 F200 Q207 R242 M244 M245 K246 R248 D249

	R251 A252 G253 I255 S256 L259 R289 E292 T296 R303 N306 S307 F310 F311 F337 I340 S341 I344 V345 R347 M348 A349 R352 Q353 P355 W356 Q359 T360 Y362 D363 S364 G366 A367 L370 D373 F374 K377 Y913 V920 G921 V922 A923 D924 S977 K978 D979 A981 I982 D984 D985 L989 T990 F992 D993 L997 I100 V1001 A1004 K1041 S1045 R1048 W1092 L1093 L1096 R1097 F1099 Q1100 I1103 E1104 F1107 V1108 F1111 M1137 N1138 I1139 S1141 T1142 Q1144 W1145 N1148 S1149 I1151 D1152 S1155 L1156 R1158 S1159 R1162
3	A274 Y275 C276 W277 I1203 W1204 P1205 L1258 Q1281 R1283 A1285 F1286 G1287 V1288 L1304 D1305 P1306 Y1307 E1308 Q1309 W1310 E1314 K1317 V1318 E1321 R1358 S1359 V1360 L1361 S1362 K1363 A1364 K1365 I1366 L1367 A1391 F1392 A1393 D1394 C1395
4	F229 V232 L233 F236 L240 Y304 F305 S308 A309 F312 G930 F931
5	F994 L998 V1001 I1002 I1005 A1006 F1016 I1023 F1026 I1027 R1030 L1143 A1146 V1147 S1150
6	E282 I285 G286 R289 Q290 L293 S945 K946 I947 H949 H950 K951 L953 H954
7	I70 L73 R74 F77 F78 F81 M82 M152 F191 L195 W361 S364 I368
8	M1 L34 I37 L967 K968 G971 N974 R975 L1043 E1046 G1047 S1049 P1050 L1084 A1087 N1088 R1162 F1166
9	L6 V11K14 L15 F17 W19 V43 R80 Y84 P140 F143 G144 H147 I148 Q151
10	K273 C276 W277 E278 E279 A280 L957 Q958 T1171 E1172 G1173 L1279 Q1280 R1283 K1284 Y1307Q1309

Finally, I consider the best-ranked site by Site Finder for the following molecular docking calculations in these studies (Fig.2.1.4).

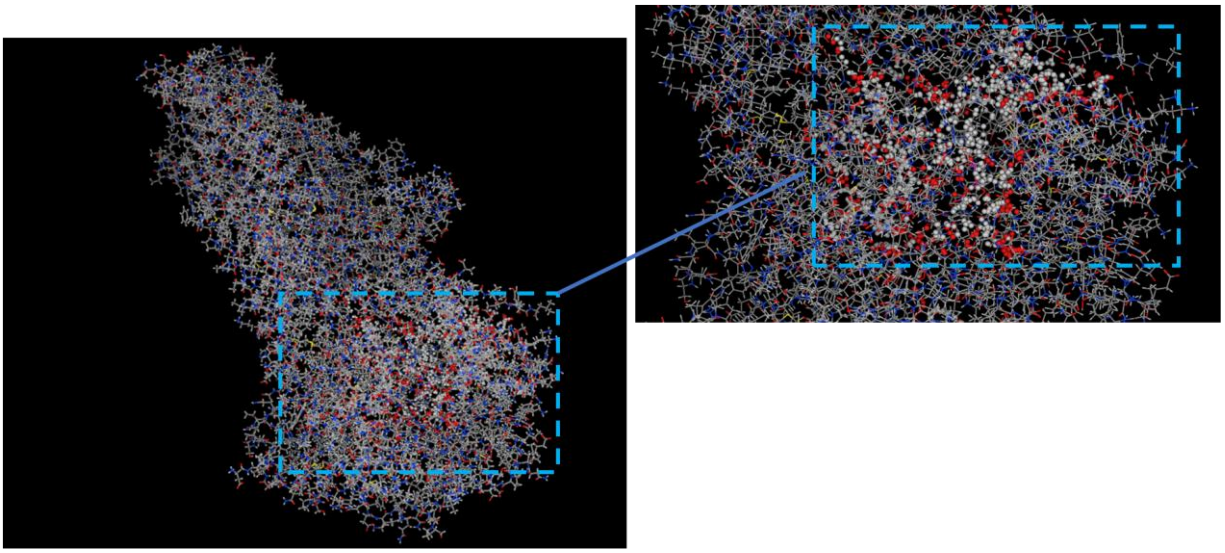

Fig.2.1.4. Representation of the first 'best-ranked binding site identified by Site Finder on the modeled F508del-CFTR.

The obtained scoring functions (see appendix A4-A5) proved to be in accordance with the experimental activity, supporting the docking protocol at the two putative binding sites. The most promising tetrahydropyridopyrimidines and cyanoquinolines (featuring $pEC_{50} > 5.5$) are supplemented by score values at the NBD1 domain lower than -20 kcal/mol. On the other hand, the most effective hybrids ($pEC_{50} > 6.0$) exhibited scoring values spanning from -20 to -25 kcal/mol. For all chemotypes investigated, the poorly activity correctors presented score values higher than -20 kcal/mol.

Regarding molecular docking at the modeled F508del-CFTR, the same promising hybrids experienced score values spanning from -22 to -30 kcal/mol, while the tetrahydropyridopyrimidines above and cyanoquinolines showed variable scores spanning from -20 to -30 kcal/mol.

Firstly, I investigated the putative docking mode of VX-809 and its related analogs ALK-809 and SUL-809, selected as reference compounds [149]. These two derivatives bore an amide and a sulfonamide function as a substitute for VX-809 carboxylic moiety, missing the possibility to display a negatively charged group[155].

Regarding VX-809, it demonstrates to assume two putative docking positioning within the NBD1 domain, namely POS1 and POS2 (Fig.2.1.5).

Notably, in POS1, the oxygen atom of the carboxamide group of VX-809 is H-bonded to the N659 sidechain. In contrast, the carboxylic group exhibits one salt-bridge with K464 and further H-bonds with T460 and G461 (Fig.2.1.5). The corrector's biaryl portion was enclosed by S573, G576, V603, and A655, presenting Van der Waals contacts. The benzodioxole ring is near Y577 and E656. Concerning POS2 (Fig. 2.1.5), the two oxygen atoms of the benzodioxole core detected two H-bonds with K464 and T465. At the same time, the negatively charged carboxylic group and the carbamide moiety of VX-809 are H-bonded to the backbone of E656 and N659, respectively.

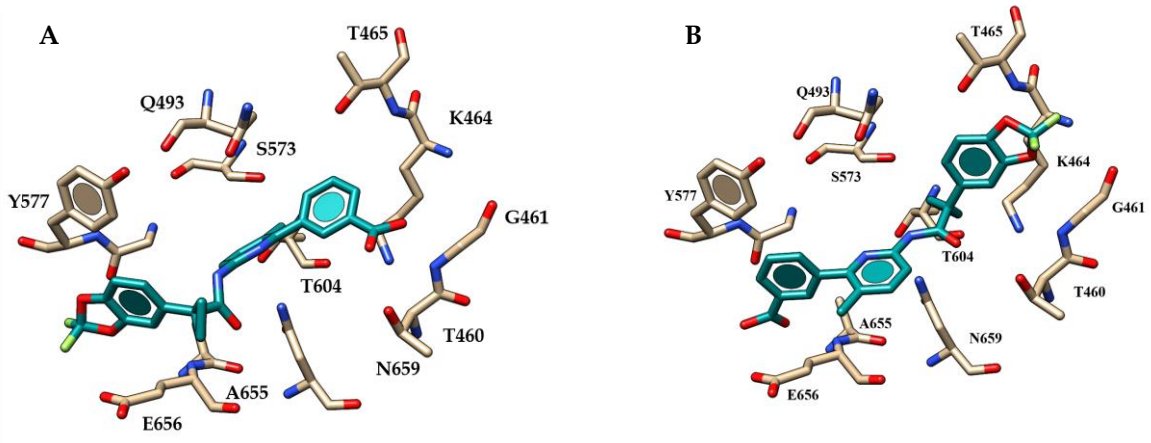

Fig.2.1.5. Selected docking pose of VX-809 within the hNBD1 domain as POS1 (A) and POS2 (B).

Molecular docking studies performed on the related analogs ALK-809 and SUL-809 revealed a unique positioning according to the POS2 of VX-809. The two analogs engage the (solfon)amide moiety in one H-bond with the E656 backbone, and the amide group positioned on their central core makes an H-bond with N659 (Fig.2.1.6). Again, as shown for VX-809, the benzodioxole ring of ALK-809 and SUL-809 featured polar contacts with K464 and T465 through its oxygen atoms. In this scenario, POS2 could be considered the possible bioactive conformation considering the comparable potency experienced by VX-809 and by the two congeners as CFTR correctors.

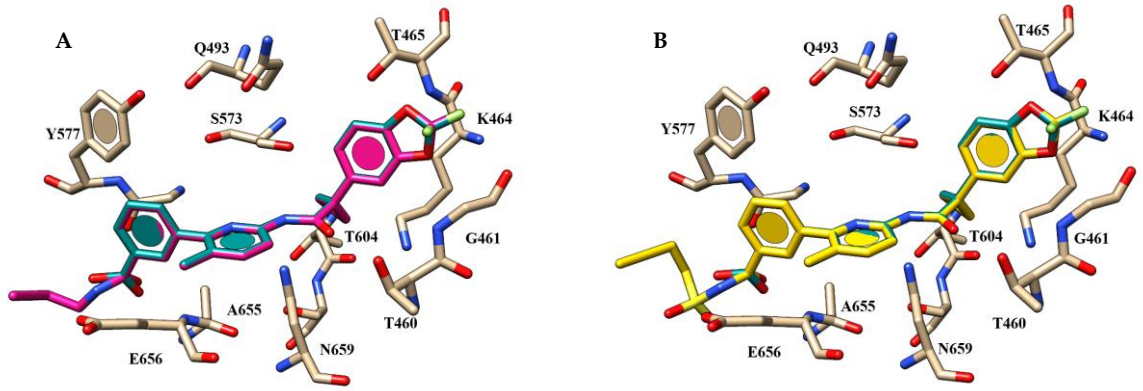

Fig.2.1.6. Selected docking pose of ALK-809 (A) (C atom; magenta) and SUL-809 (C atom; yellow) (B) within hNBD1 domain together with VX-809 (C atom; dark cyan).

The putative binding site herein identified is supported by other computational studies presented in the literature performed by Odolczyk[151].

Odolczyk and colleagues have identified four derivatives acting as F508del-CFTR correctors using molecular docking and virtual screening strategies. Thanks to these approaches, they disclose two different pockets within the NBD1 domain, describing the proposed compounds' corrector ability. Performing molecular dynamic simulations, they reported the NBD1 pocket1 and pocket2, including the first one, Q493, N659, and Y577. The research group conceived their work been aware that data reported in the literature highlighted NBD1 as a key anchoring point for CFTR modulators[156]. These findings suggested considering the related binding site as plausible even if an unwanted way to achieve corrector ability.

Proceeding, with molecular docking calculations performed at the mutant protein model, showed VX-809 highly stabilized within the protein crevice via polar contacts with R552, K1060, and K1292. The acid moiety displayed salt-bridges with R552 and K1292, while the two oxygen atoms of the benzodioxole were H-bonded to K1060. In this conformation, VX-809 exhibits a further H-bond with the carboxamide nitrogen atom and K1060. The terminal carboxy-substituted phenyl ring was projected to F494 and K1060, detecting cation-π and π–π stacking while the pyridine ring was in π–π contact with W496. Ultimately, the cyclopropyl moiety displayed van der Waals interactions with W1063 and C1344 (Fig.2.1.7).

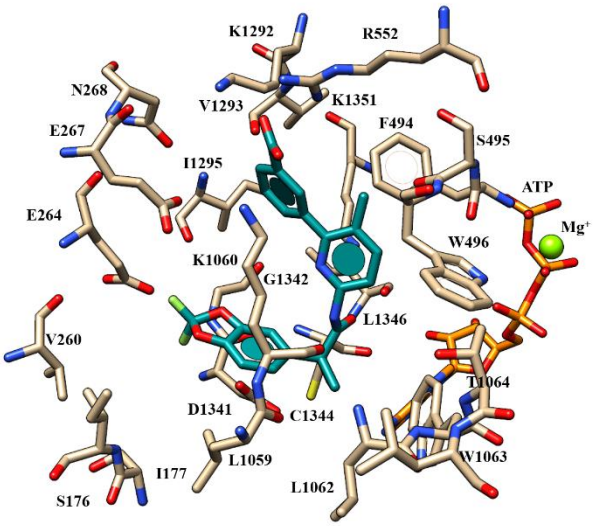

Fig.2.1.7. Selected docking pose of VX-809 (C atom; dark cyan) within the modeled F508del-CFTR.

The analogs ALK-809 and SUL-809 mentioned above show a comparable positioning (Fig 2.1.8). Their benzodioxole portion oriented towards a polar cavity delimited by E264, E267, N268, R552, K1292, V1293, and K1351, detects H-bonds with I1295 and V1293, respectively. The two correctors' central carboxamide moiety showed one H-bond with K1351 while the terminal one was H-bonded to L1062, W1063 and K1060, L1062, T1064, respectively. This positioning moved the bulkier and lipophilic groups of the modulators in the hydrophobic cavity, including W496, L1059, C1344, and L1346.

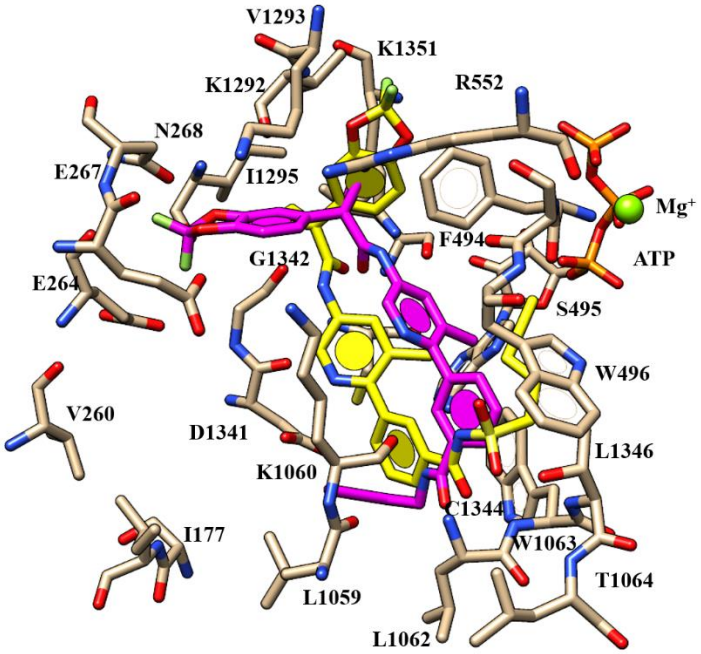

Fig.2.1.8. Selected docking posed of ALK-809 (C atom; magenta) and SUL-809 (C atom; yellow) within the modeled F508del-CFTR.

Subsequently, to in-depth investigate the *in-house* hybrids series and other chemical series like tetrahydropyridopyrimidines and cyanoquinolines and their positions at the F508del-CFTR NBD1 domain and both at the entire modeled protein, I performed molecular docking calculations (see Appendix A1-A3).

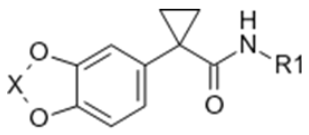

2-29
pEC50 = 5.09-7.06

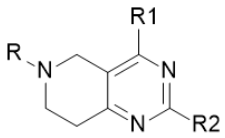

30-56
pEC50 = 4.00 – 6.70

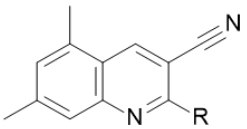

57-80
pEC50 = 4.00 – 5.82

Fig.2.1.9. Chemical structures and biological values of the examined series of F508del-CFTR correctors.

At the first observations, it is thought that all of them share a positioning highly related to that previously discussed for VX-809 and its related analogs. Regarding the hybrids that do not have a substitution in position 5 of the thiazole ring, the presence of a p- substituted

phenyl ring tethered to position 4 of the main thiazole ring was privileged to the m-substituted analogs, leading to compounds featuring higher potency values. On the other hand, the m-substitution was more effective when a methyl group or ester moieties decorate position 5 of the AAT. Furthermore, the concomitant substitution on positions 4 and 5 of the thiazole ring plays a beneficial role in terms of corrector activity[157].

Firstly, I analyze the binding mode of the *in-house* hybrid series on the NBD1 domain. Among the hybrids series, derivatives **2-4** proved to be the most potent; the derivatives **3**-**4** presented an ester moiety linked to position 5 of the thiazole, while the promising analog **2** (pEC_{50} = 7.06) displayed a benzoyl group at the same position.

In agreement with molecular docking calculations, all these compounds present the two oxygen atoms of the benzodioxole substituent H-bonded to K464 and T465, moving the carboxamide moiety to N659 detecting one H-bond.

The **2** docking mode was in good agreement with VX-809 (POS2) and SUL-809 binding mode. (Fig.2.1.10). Indeed, the carboxamide moiety was in proximity of N659 detecting H-bonds. Simultaneously, the corrector's benzodioxole ring proved to mimic the POS2 of the prototype VX-809, displaying the same interactions, being the two oxygen atoms of the benzodioxole ring H-bonded to K464 and T465. The benzoyl and the phenyl ring of **2** showed the same hydrophobic interactions showed by the benzoic group of VX-809, including π–π stacking with Y577, while the oxygen atom of the benzoyl group interacts with the E656 sidechain, as described for the two reference compounds.

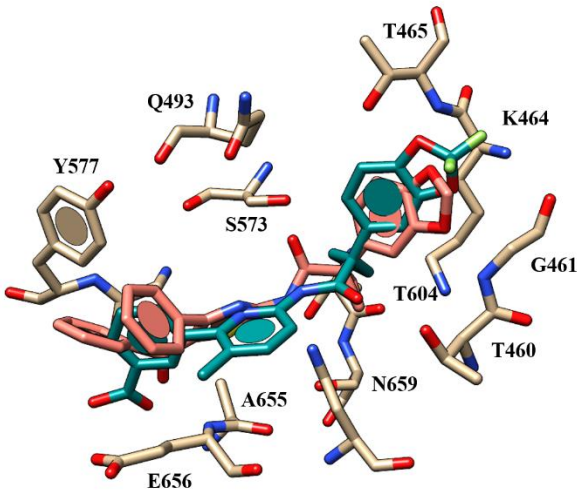

Fig.2.1.10. Selected docking pose of compound **2** (C atom; pink) within the hNBD1 domain with VX-809 (C atom; dark cyan).

The presence of the quite flexible ester group tethered to position 5 of the thiazole core, in the case of **3** (pEC_{50} = 6.52) and **4** (pEC_{50} = 6.25) derivatives, result in a different position within the NBD1 domain on the concomitant m- or p- substituted phenyl ring connected to the position 4 of AAT. Indeed, **3** and **4** present an H-bond with Y577 sidechain or the E656 backbone via the carbonyl group's oxygen atom, respectively. Based on the two correctors' high corrector ability, it is thought that H-bonding N659, K464, and T465 represents a critical anchor point for the correctors. At the same time, the interactions with E656 or Y577 residues could efficiently stabilize the compound at the protein domain.

Then I performed molecular docking calculations of the hybrid compounds on the F508del-CFTR model. The data derived from estimates highlighted important H-bonds between the oxygen atom of the benzodioxole group and K1060, the nitrogen atom of the carboxamide moiety and S495, and the ester oxygen atom and W1063 (Fig.2.1.11). In particular, the benzodioxole group interacts through cation-π contacts and π–π stacking with R552 and F494, while the phenyl ring at position 4 of the thiazole showed π–π contacts with W496 and W1063.

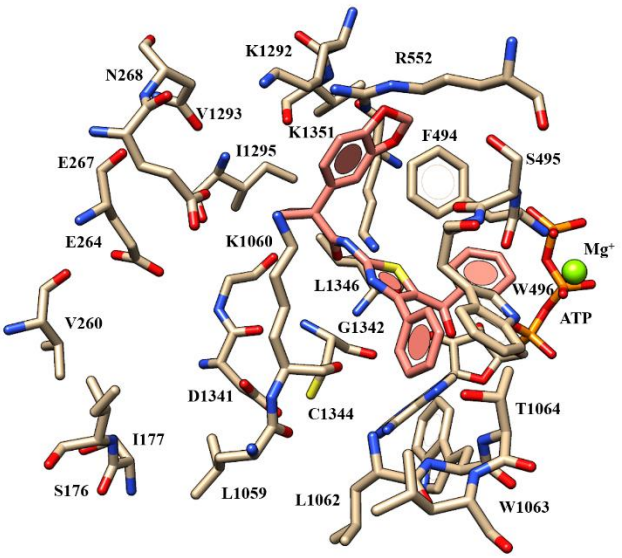

Fig.2.1.11. Selected docking pose of compound **2** (C atom; pink) within the modeled F508del-CFTR.

On the other hand, the ester group was projected towards C1344 and W1063, in agreement with the docking positioning described for the hydrophobic features of ALK-809 and SUL-809.

The introduction of a smaller group at position 5 of the thiazole, such as methyl group instead of the ester or carbonyl moiety, led to compounds **6-10** (pEC_{50} = 5.5-6.0) less potent than the previously cited analogs **2-5**.

Thus, they maintained the positioning previously described at the NBD1 domain, but they lost H-bonds with Y577. Within these less potent derivatives, compound 10 (pEC_{50} = 6.05) is the most interesting; it presents a p-F-phenyl ring and a methyl substituent at positions 4 and 5 of the thiazole, respectively. These substitutions increased its hydrophobicity and allowed it to make π–π stacking and hydrophobic interactions that improve its corrector ability. In this context, the benzodioxole moiety maintains the same interactions assumed by the prototype VX-809, featuring H-bonds with T465, K464, while the carboxamide moiety is H-bonded with the N659 side chain.

Regarding the binding mode assumed by the **6-10** derivatives within the entire CFTR model, they maintain the overall positioning so far discussed for the other derivatives but display different H-bonds involving I1295 and K1351 thanks to the benzodioxole and carboxamide oxygen atoms. In contrast, the main π–π stacking and van der Waals contacts were maintained. Indeed, the benzodioxole and the phenyl ring exhibited lipophilic contacts with F494, V1293, and W496, W1063, respectively. Notably, the overall positioning of **6** highly resembles ALK-809 but lacks H-bonds with L1062 and W1063.

Leaving unsubstituted the position 5 of the thiazole core diminished the compounds' corrector ability, as shown for **11-13** (pEC_{50} = 5.08-5.53), featuring lower pEC_{50} values than the methyl-substituted analogs **6-8** (pEC_{50} = 5.53-5.72).

Compound **11** was the most interesting because it shares a comparable position with its analog **6**. Despite this, the methyl group's presence is supposed to be related to the proper conformational and steric requirements that allow the corrector to bind NBD1, exhibiting the most effective overall shape. Conversely, the introduction of electron-withdrawing and hydrophobic substituents such as a halogen atom allowed the detection of hydrophobic interactions and π–π stacking with Y577 and several contacts with the surrounding residues S573, Q493, E656 at the NBD1 domain.

At the same time, at the level of the entire CFTR model, these introductions led the compounds to detect hydrophobic interactions with W496, for example, observing the docking position of compound **7** compared to **6**. This kind of substitution proved to be more

effective than halogens' replacement with other electron-withdrawing groups lacking hydrophobic properties, such as the carboxylic group of **20** (pEC_{50} = 5.30) and **21**, with the **21** the most promising (pEC_{50} = 5.53). Interestingly, the related docking pose was endowed with comparable contacts with those previously proposed for VX-809. Conversely, the presence of polar substituents with electron-donor properties such as the hydroxyl function improved the modulators' potency, as shown for **16-19** (pEC_{50} = 5.4-5.9).

In particular, at the NBD1 domain, compound **16** (pEC_{50} = 5.74) was more effective than **17** (pEC_{50} =5.64), thanks to additional H-bonds involving the hydroxyl group and E656.

Simultaneously, their congeners **18-19** (pEC_{50} = 5.92-5-40) bearing the methyl group at position 5 of the thiazole maintained a comparable docking mode. While pointing attention to these derivatives' binding mode on the model CFTR, compound **18** was H-bonded to K1060, keeping all the other contacts exhibited by compound **6**.

Another series investigated concerning the tetrahydropyridopyrimidines **30-56** (pEC_{50} = 4.00-6.70) that present variable substituents onto the positions 2 and 4 of the central core and at the nitrogen atom of the tetrahydropyrido portion.

The most effective compounds feature a 2-pyridine substituent at position 2, while substitution with a 3-pyridine or 4-pyridine groups led to less potent compounds.

In fact, the benzyl-6 substituted tetrahydropyridopyrimidines 31**-33** (R3 = 2-pyridine; pEC_{50} = 5.51-5.85) displayed higher potency than the related analogues **35-37** (R**3** = 3-pyridine;pEC_{50} = 4.00) and also then **39-40** (R3= 4-pyridine; pEC_{50} = 4.00).

The presence of benzyl group in R1 without any substitution was similar both with a secondary (**33**, pEC_{50} = 5.51) and a tertiary (**30**, **32-34**; pEC_{50}= 5.55-5.82) amine group directly tied to position 4 of the tetrahydropyridopyrimidine ring as R2.

On the contrary, in the presence of a 4-F or 4-methoxy-benzyl ring in R2, the presence of a secondary amine appears to be favored, as confirmed by the higher potency of **50,51** (R2= ethylamine-containing chain; pEC_{50} = 6.70) and **45** (pEC_{50} = 6.70), if equated to **42** (R2= piperazine-containing chain; pEC_{50}= 4.00) and **41** (pEC_{50} = 4.00), respectively.

Moreover, **41** and **42** were weakly active in relation to the unsubstituted analog **34** (pEC_{50} = 5.82). The unsubstituted- benzyl-based derivatives can be further effective than analogs, including H-bonding functions in the para position. Therefore, the isostere **52** (pEC_{50} = 6.70)

displaying a thiophene ring exhibited much-elevated potency than the analog **34**. With this, the introduction of branched or cyclic alkyl groups in R1, **53,54** (pEC_{50} = 6.52-6.70) supports hydrophobic groups' development tethering the position 6 of the tetrahydropyridopyrimidine core.

The docking calculations of the mentioned compounds, **50,51** (pEC_{50} = 6.70), showed a comparable binding position within the NBD1 domain. In detail, the pyridine nitrogen atom was involved in one H-bond with T465, as the protonated nitrogen atom of the tetrahydropyrido group established polar contacts with S573. Both the nitrogen atoms of the R2 substituent were H-bonded to Q493. Lastly, the 4-F benzyl ring was projected near F575, V603, T604, and A655, detecting hydrophobic interactions and π–π stackings. Regarding the 4-methoxy-benzyl derivatives, the most promising **45** (pEC_{50} = 6.70) presented two H-bonds with T604 and S505 via its methoxy group. Simultaneously, the nitrogen atom of the pyrimidine core was involved in polar contacts with T465 and K464. The imidazoyl group in R2 at the end of the aminoalkyl chain permitted to compound **45** to show additional H-bonds involving N659 (Fig.2.1.12).

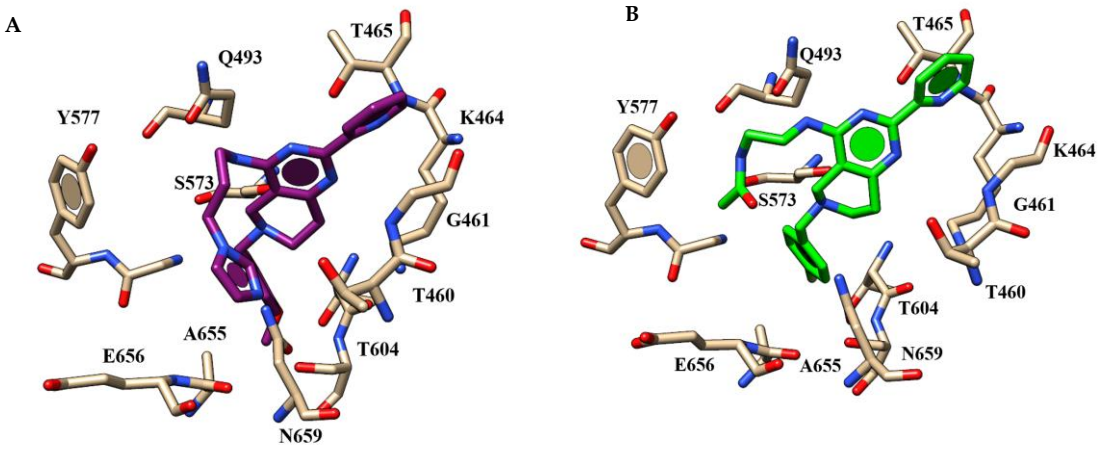

Fig.2.1.12. Selected docking poses of 45 (A) (C atom; purple) and **50** (B) (C atom; green) within the hNBD1 domain.

These discoveries sustain the compound's highest potency regarding the analogs, **41, 44, 46, 47** (pEC_{50} = 4.00-6.52), due to the amino-alkyl spacer, which showed the correct distance between the central core of the compound and the terminal H-bonding features. In contrast, the introduction of the strict linker in R2, for instance, a piperidine or piperazine-containing groups, guided to compounds **41, 43, 44, 46** (pEC_{50} = 4.00-6.40) that show a different docking mode at the NBD1 domain, if compared to the most active analog **45** previously described.

Among them, **43,46** detected several contacts inside the same channel cavity, involving interactions with G461 and K464 through their methoxy group, keeping modest F508del-CFTR corrector ability. Likewise, the two correctors formed via piperazine ring further interactions with S573. In compound **43,** the hydroxyl group on the piperazine ring made an H-bond with N659, while compound **46** was H-bonded to the T604 residue. Ultimately, for both compounds, the interactions of the piperidine moiety with the E656 sidechain remain stable. The only exception is characterized by compound **41** (pEC_{50} = 4.00) placed in a distinct crevice of the biological target, missing all the significant interactions so far discussed and preserving only one H-bond with N659.

The docking results obtained on the F508del-CFTR model show how the compound **43** was highly stabilized at the biological target due to salt-bridges, including the protonated piperazine and the hydroxyl moiety with D1341. The methoxy group's presence at the R1 substituents guided the corrector near to V1293, featuring one H-bond, while the pyridine ring was engaged in π−π stacking with W496 and W1063.

These findings support the highest potency of **45** and **50** bearing a flexible linker in R2, for most of the analogs designed with a rigid spacer, such as **41-44** and **46** and **47**, with **45** and **50** endowed with the proper distance between the main core of the compound and the terminal H-bonding features, which allowed us to interact with G1342 and V1293. The docking calculations on the F508del-CFTR model have been finding a common positioning for both **45** and **50**, as shown in Fig 2.1.13. In detail, the terminal amide and imidazoyl groups of **50** and **45** were involved in one H-bond with V1293, resembling the same contacts previously mentioned for SUL-809. The nitrogen atom of the secondary amine was H-bonded to G1342, while the protonated nitrogen atom of the tetrahydropyrido moiety was engaged in a salt-bridge with D1341. While the R1 substituent of both correctors was employed in polar contacts with E264, E267, and S176, the pyridine groups displayed one H-bond with K1351.

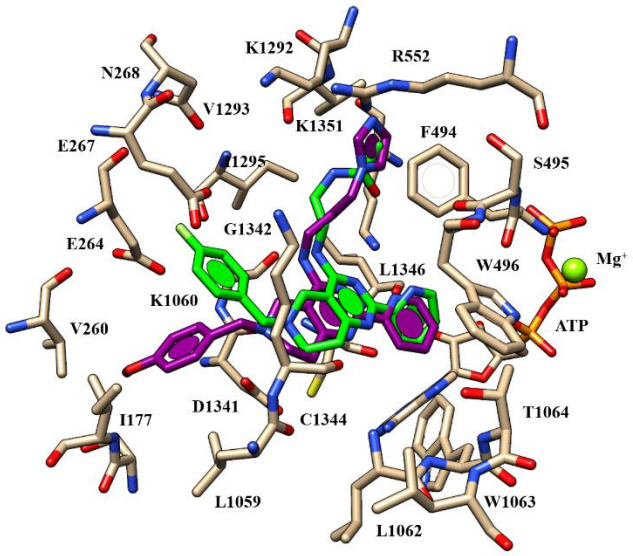

Fig.2.1.13. Selected docking poses of **45** (C atom; purple) and **50** (C atom; green) within the modeled F508del-CFTR.

Along with the unsubstituted benzyl-based derivatives, at the NBD1 domain, compound **31** (pEC_{50} = 5.85) was engaged in one H-bond between the nitrogen atom of the tetrahydropyrido moiety and the N659 sidechain. Simultaneously, the pyridine ring was involved in polar contacts with G461 and K464. The oxygen atom of the amide function experienced on H-bond with Y577 and the benzyl moiety was oriented to the F875, A655, S576, T604, and G576 residues, finding hydrophobic and π–π interactions. The same contacts were also held by compound **34** (pEC_{50} = 5.82). Introducing a more flexible linker in position 4 of the main bicyclic core reduced the corrector ability (**33**; pEC_{50}= 5.51). This substituent led the corrector's main core in a different region of the NBD1 domain, missing the aforementioned key contacts with the biological target.

Cyanoquinolines derivatives (**57-80**; pEC_{50} = 4.00-5.82) consist of different compounds containing the main bicyclic core tethered to a terminal (hetero)aryl-containing amide group by a flexible or rigid spacer. In particular, cyanoquinolines **57-68** (pEC_{50} = 4.00-5.82) and **69-74** (pEC_{50} = 4.00-5.52) show the diaminoethyl- and the diaminopropyl-chains, while cyanoquinolines **75-80** (pEC_{50} = 4.00) exhibited a piperazine linker. Within these compounds, the existence of an H-bonding function at the para position of the terminal (hetero)aryl ring led to several most active compounds (**59, 64, 65, 67**; pEC_{50} = 5.38-5.82). Though **59, 64,** and **65** exhibited a benzamide portion in R, compound **67** was characterized by the picolinamide group (pEC_{50} = 5.57).

According to our docking calculations at the NBD1 domain, these compounds preserved a comparable docking positioning, being the linker's carboxamide in H-bonds with S573 and N659. At the same time, the methoxy group on the terminal aromatic group shifted in proximity to T465, G461, and K464, detecting H-bonds. The docking positioning associated with compound **59** (pEC_{50} = 5.52) underlined several H-bonds, including the N659-side chain and G461 and K464, through the methoxy group. The flexible spacer permitted the compound to be well-suited in the domain pocket, finding hydrophobic contacts with the surrounding Y577 and A655. Compound **67** occupied the channel crevice placing the quinoline core towards Y577, A655, G576, being H-bonded to the backbone of E656 residue (Fig.2.1.14). In this way, the compound displayed a similar positioning to that previously reported for the reference compound VX809. Indeed, the amide group was involved in H-bond with S573 and N659, while the methoxy group behaves like a hydrogen acceptor function to T465. These conclusions were in good agreement with the higher potency trend noticed for the 4-substituted **59** and **67** compared to the unsubstituted **63** and **60** (pEC_{50} = 4.00), respectively.

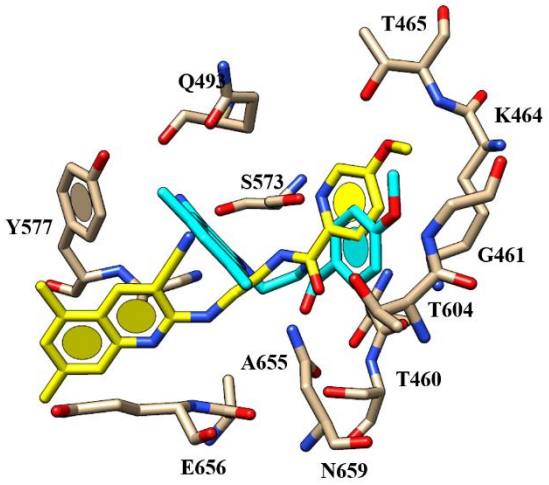

Fig.2.1.14. Selected docking poses of **59** (C atom; cyan) and **67** (C atom; yellow) within hNBD1.

While moving the 4-methoxy substituent onto the ortho position of the (hetero)aryl group led to the modest corrector **58** (pEC_{50} = 4.96), the 3,4-dimethoxy benzamide-based analog **65** (pEC_{50} = 5.82) proved to be the most potent within this series. Compound **65** was H-bonded to G461, K464, and T465 thanks to the dimethoxy-substituted phenyl ring, while the carboxamide moiety exhibited two H-bonds with S573 and N659. The cyanoquinoline main core was projected towards Y577, featuring π–π interactions. Therefore, the overall positioning of the derivative assures a comparable docking mode with that previously

discussed for the reference compound VX-809 as well as for the other chemotypes acting as CFTR correctors.

The unsubstituted pyridine-containing analogs **60-62** (pEC_{50} = 4.00-5.57) experienced a relatively similar positioning related to their previously described congeners but missing key interactions with N659 at the expense of corrector ability. The introduction of the 1,3-diamino propyl tether guided to the methoxy substituted benzamide-based compounds **49-51** (pEC_{50} = 4.0-5.37) pyridine-containing **52-54** (pEC_{50} = 4.00-5.52), which proved to be less potent than the previously mentioned analogs carrying the diaminoethyl chain. Indeed, **69-71** and **72-74** featured lower pEC_{50} values if compared to **57-59** (pEC_{50} = 4.96-5.66) and to **61-63** (pEC_{50} = 4.00-5.57). Among them, compound **73** (pEC_{50} = 5.52), featuring the nicotinamide portion as a terminal substituent, was placed within a specific crevice of the channel interacting with key residues involved in the corrector binding. The quinoline core's nitrogen atom was engaged in H-bonds with K464 and G461, while the cyano group detected polar contacts with N659. The nitrogen atom of the secondary amine group and the carboxamide function displayed contacts with S459 and T604.

Finally, the nicotinamide ring was correctly projected towards F575, S605, V603, N659, and A655. Choosing a rigid spacer tethering the bicyclic main core with the terminal aromatic ring deeply impaired the compounds' corrector ability, as shown by **75-80** (pEC_{50} = 4.00), being folded within the NBD1 domain and maintaining only interactions with E565 through the nitrile function.

At the whole protein, docking results highlighted the two derivatives' common positioning, with the CN-group H-bonded to L1062 and W1063, while the two nitrogen atoms of the linker were involved in H-bonds with K1060 and D1341. This type of positioning ensures the appropriately hydrophobic contacts and π–π stacking with C1344 and W1063, F494, W496. Remarkably, the methoxy group of the R substituent was engaged in contact with I177. These results are in good agreement with the higher potency trend observed for the 4-substituted **59** and **67** if compared to the unsubstituted **63** and **60** (pEC_{50} = 4.00), respectively. The 4-methoxy substituent's presence on the ortho-position led to modest corrector **58** (pEC_{50} = 4.96), while the 3,4-dimethoxy benzamide-based analog **65** (pEC_{50} = 5.82) is the most potent within this series. This last derivative maintains the key contacts described for analogs **59** and **67** (Fig.2.1.15).

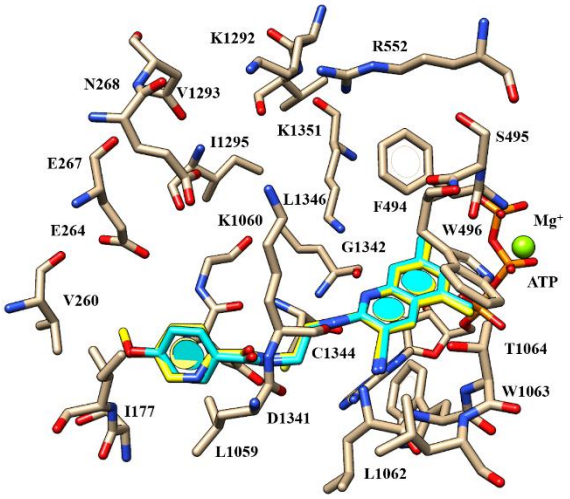

Fig.2.1.15. Selected docking poses of **59** (C atom; cyan) and **67** (C atom; yellow) within the modeled F508del-CFTR.

The most promising **73** (pEC_{50} = 5.52) highly imitated the docking mode of **65** with assured key contacts between the CN- and the spacer nitrogen atoms with L1062, W1063 with K1060, D1341, respectively. Also, the nicotinamide portion as terminal substituent was H-bonded to I177.

2.1.2 Discussion

In this study, I performed two series of molecular docking calculations regarding different chemotypes of F508del-CFTR correctors. Plausibly, based on the mean value of the docking scores (Score mean) derived by the two approaches, VX-809 and related analogues (**1-29**; NBD1 Score mean = -21.04; modelled CFTR Score mean = -23.54) tetrahydropyridopyrimidines (**30-56**; NBD1 Score mean = -17.60; modelled CFTR score mean = -26.67) and cyanoquinolines (**57-80**; NBD1 Score mean = -18.64; modelled CFTR Score mean = -25.56) were predicted to bind at the NBD1:ICL4 interface. These findings indicate that docking calculations at the modeled F508del-CFTR are more helpful in investigating the putative mechanism of action of CFTR correctors compared to visual examination centered at the only NBD1 domain.

Molecular docking results revealed a common positioning featured by the F508del-CFTR corrector VX-809, which is the most applied and investigated drug for treating cystic fibrosis. Regarding the molecular docking result of VX-809 at the modeled CFTR, two salt-bridges, including R552, K1292, and H-bonding to K1060, resulted in support of the mechanism of action of this corrector. The well-known corrector is further stabilized at the NBD1-ICL4

interface by π–π stacking and van der Waals contacts with F494, W496, and W1063. Moreover, calculations performed onto the analogs ALK-809 and SUL-809 revealed one H-bond with K1351 and further H-bonds to L1062, W1063 K1060, W1064, respectively. This kind of positioning allowed arranging the hydrophobic terminal chains of the two correctors in the hydrophobic cavity delimited by W496, L1059, L1063, C1344, and L1346.

Along with this, similar results were achieved for hybrids **2-29** (pEC_{50} = 5.08-7.06) and other chemotypes endowed with CFTR corrector ability, such as tetrahydropyridopyrimidines **30-56** (pEC_{50} = 4.00-6.70) and cyanoquinolines **57-80** (pEC_{50} = 4.00-5.82).

On the whole, mandatory interactions are experienced by all the correctors, suggesting a pivotal role played by proper polar features within the chemical structure of the molecule. Tetrahydropyridopyrimidines were able to detect most of the key contacts showed by SUL-809. Furthermore, these derivatives show additional contacts between the protonated nitrogen atom of the tetrahydropyrido moiety and D1341. The cyanoquinolines correctors experienced the aforementioned key contacts thanks to the main scaffold's CN- group, exhibiting H-bonds with L1062 and W1063. Simultaneously, the two nitrogen atoms of the spacer were engaged in H-bonds with K1060 and D1341.

2.1.3 Material and methods

The compounds **1–80** were manually built through the "MOE Builder" software and then were parameterized with AM1 partial charges as the calculation method. The energy minimization was made through the "Energy Minimize Program" using MMFF94x forcefield, and RMS (= root mean square) equal to 0.0001 Kcal/mol/A^2 of the MOE compute module to create a single low-energy conformation for every ligand. Molecular docking of all the analyzed compounds was performed on the crystallographic structures of the NBD1 domain of the F508del-CFTR (PDB code: 4WZ6)[154], which was prepared through the "Structure Preparation" program of the Molecular Operating Environment[158], and on the *in-house* model of F508del-CFTR protein. This model was "built" based on the superimposition of the whole protein (PDB code: 6MSM)[153] obtained by cryoelectron microscopy, with that of the mutated NBD1 domain (PDB code: 4WZ6)[154]. The modeled complete structure has been refined and minimized within MOE under the AMBER99 force field.

Molecular docking studies on VX-809 and related analogs were performed considering the putative binding site proposed by the site finder module implemented in the MOE software.

Site Finder aims to calculate possible active sites in a receptor from the receptor's 3D atomic coordinates. MOE's Site Finder falls into geometric methods, considering the relative positions and accessibility of the receptor atoms based on a rough classification of chemical type. The Site Finder methodology works on the Alpha Shapes represented by convex hulls developed and described in the literature [159]. This software module identifies tight atomic packing regions to filter out sites that are "too exposed" to solvent. This approach allows removing protrusions that are unlikely to be good active sites.

The derived preliminary sites are then classified based on their hydrophobic or hydrophilic profile. This primary classification of chemical type is used to split water sites from the more likely hydrophobic sites. The generation of alpha spheres on these sites is made by collecting sets of points using a modified Delaunay triangulation method to derive different spheres displaying different radii. The collection of alpha spheres is pruned by eliminating those that correspond to the receptor's inaccessible regions and those exposed to solvent. Additionally, only the small alpha spheres are retained since they correspond to tight atomic packing locations in the receptor.

Then, alpha spheres are classified as either "hydrophobic" or "hydrophilic," depending on whether the sphere is in the right hydrogen bonding spot in the receptor.

Clustering the alpha spheres using a double-linkage clustering algorithm leads to a collection of sites where each site consists of one or more alpha spheres, at least one of which is hydrophobic. All the collected sites are ranked according to their Propensity for Ligand Binding (PLB) score, which is based on the pocket's amino acid composition as described in the literature[160].

I consider the best-ranked site by Site Finder for the following molecular docking calculations in these studies. Then, I performed docking calculations using LeadIT 2.1.8 software suite (www.biosolveit.com) starting from the *h*NBD1-VX-809 complex previously derived from automatic docking with MOE software. The docking algorithm is a state-of-the-art fragment docker: Ligands are divided into fragments, and an initial fragment is

placed into several sites in the pocket and scored applying a rapid pre-scoring scheme. The ligand is built from the n solutions set, fragment by fragment, and the temporary solutions are scored against each other. The best scored passes the analysis and is delivered to the user. The preliminary idea correlates to the FlexX algorithm, but many advancements have been made over the years, such as the "Single Interaction Scan" (SIS) placement that discovers solutions when there are very few polar groups in a compound. The SIS algorithm utilizes virtual lines between protein and ligand interaction spots. It is trimmed for a high-speed rotation around these lines, generating solutions quickly for more hydrophobic character ligands. The final docking poses were highlighted by the score values of the lowest energy pose of the compounds docked to the protein structure. All ligands were refined and rescored by assessment with HYDE, included in the LeadIT 2.1.8 software. The HYDE module considers dehydration enthalpy and hydrogen bonding [161]. Briefly, HYDE was formulated to reflect the experimentally observed binding contributions due to hydrogen bonding and the hydrophobic effect in a very accurate way. HYDE works on new terms for the dehydration of idealized polar and nonpolar functional groups. It provides a simple explanation for inter-molecular interaction's main characteristics in aqueous solution, including the hydrophobic effect, dehydration penalties, and hydrogen bonding. Because the hydrophobic effects are quantitatively described as the free dehydration enthalpy of a nonpolar function, the noncovalent contributions to intermolecular interactions in aqueous solutions and $\Delta G_{binding}$ can be calculated by considering only two main terms: (i) the dehydration of the interacting molecular interfaces, $\Delta G_{dehydration}$, and (ii) the vacuum hydrogen bond energies between interacting hydrogen bond functions.

2.2 Molecular docking studies of potentiators as modulators of F508del-CFTR

For the studies of the binding mode of F508del-CFTR potentiators, I take into account different series of modulators, with variable chemotypes and potency, to explore the key features turning in more effective potentiators (A7-11)[162].

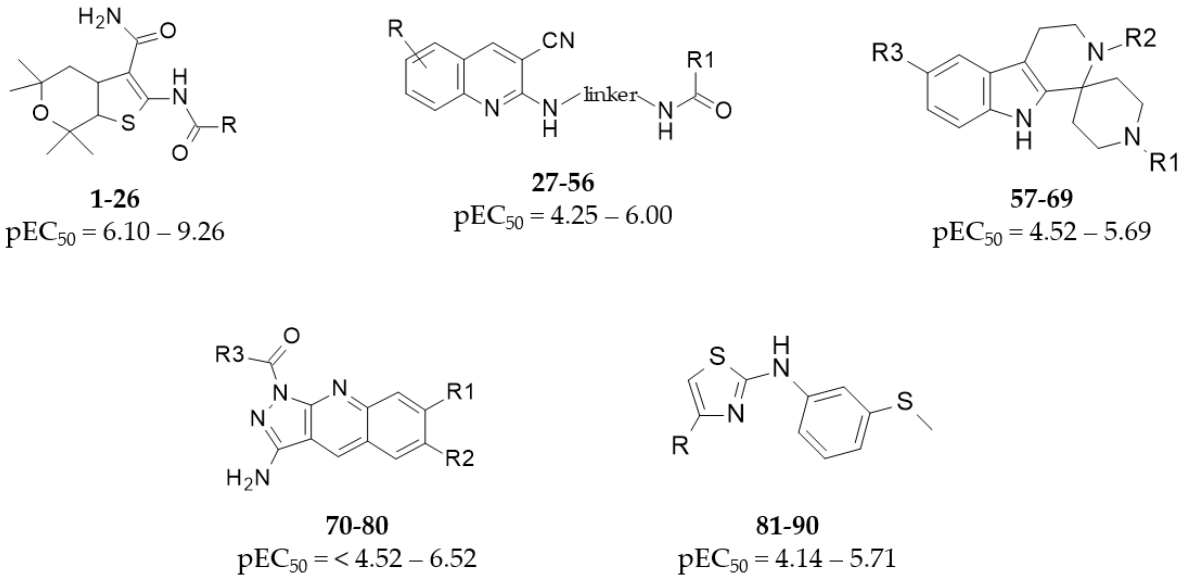

Fig.2.2.1. Chemical structures and biological values of the examined series of F508del-CFTR potentiators.

I considered the X-ray crystallographic structure of VX-770 in complex with CFTR (PDB code = 6O2P, resolution = 3.30 Å)[163] as well as of GLPG1837 (PDB code = 6O1V, resolution = 3.20 Å) [163].In particular, VX-770 was deeply investigated in the literature, enhancing the open probability (Po) of wild-type (WT) and mutant CFTRs in membrane patches, proteoliposomes planar lipid bilayers. Because the potentiation by VX-770 necessitates phosphorylation of CFTR by protein kinase A (PKA) being independent of ATP, it is believed that this potentiator might directly target CFTR. Not long ago, the new potentiator GLPG1837 has been discovered to display better efficacy than VX-770. Indeed, when the ATP concentration is saturated, the Po of phosphorylated WT- CFTR has risen from 0.23 to 0.54 upon the addition of 10 μM GLPG1837.

Therefore, I proceed to perform a re-docking of the co-crystallized ligands to evaluate the molecular docking protocol's reliability to be used in the subsequent modeling studies of the potentiators series. Both the two potentiators were adequately predicted within the CFTR channel, being the selected docking poses in good accordance with the experimental data (VX-770-RMSD = 0.8352 Å). Evaluating the two proteins, VX-770 and GLPG1837 occupied the

same channel crevice as the CFTR's backbone highly overlapped (RMSD = 0.182 Å) (Fig.2.2.2). The two potentiators were involved in π–π stacking with F931 and F312 through their main bicyclic core and their hydrophobic substituents; at the same time, the carboxamide moiety was H-bonded to Y304 and S308.

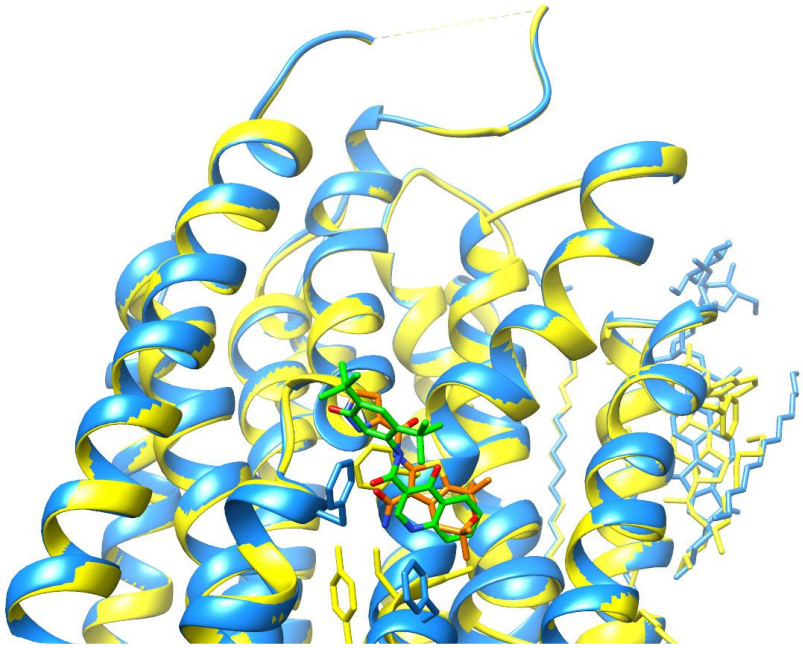

Fig.2.2.2. Superimposition of X-ray crystallographic data of hCFTR complexed with **VX-770** (PDB code = 6O2P) (C atom; green) (helix; blue) and hCFTR complexed with **GLPG1837** (PDB code = 6O1V)(C atom; orange) (helix; yellow).

These computational studies have been done contemplating the experimental data concerning VX-770, selected as a reference potentiator, being one of the CFTR modulators used in therapy. The obtained CFTR-VX-770 complex was refined by energy minimization within the MOE software's OPLs force field [158].

The quinoline ring of VX-770 is stabilized in a hydrophobic pocket surrounded by F236, Y304, F305, S308, A309, and F312, making numerous π–π stacking and van der Waals interactions. Furthermore, the potentiator's carboxamide moiety was H-bonded to F931. The potentiator's hydroxyl group displayed one H-bond with R933. At the same time, the *tert*-butyl substituents and the phenolic ring were projected in the direction of F931 and F932, forming hydrophobic contacts. The most relevant binding conditions discovered within the collected potentiator's database were suggested based on evaluating the obtained docking pose with the aforementioned VX-770 positioning (Fig.2.2.3).

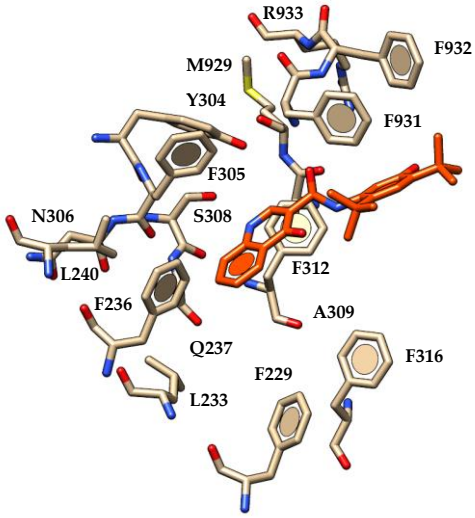

Fig.2.2.3. Selected docking pose of VX-770 (C atom; orange) within hCFTR.

Adopting this method, I investigated the most effective chemotypes that imitate the bioactive conformation and interactions experienced by the reference potentiators VX-770 (pEC_{50} = 6.63).

The GLPG1837 analogs (**1-26**; pEC_{50} = 6.10-9.26) involving thiophene-based compounds represent the most active potentiators within the CFTR modulators series examined.

Most of them assume the same docking positioning within the CFTR channel, featuring key contacts with F931, such as earlier described for VX770. Overall, compounds showing the 5,5,7,7-tetramethyl-4H-thieno[2,3-c] pyran scaffold (**6-26**; pEC_{50} = 6.33-9.26) displayed higher potency than the analogs with less hydrophobic bicyclic cores, as well as **1-4** (pEC_{50} = 6.10-7.88). Among the 5-carboxamide pyrazole-containing analogs **10-12, 22-26** (pEC_{50} = 6.86-8.69), compound **11** (pEC_{50} = 8.52) exhibited two H-bonds between the two oxygen atoms of the carbonyl moieties and the F931 backbone together with polar contacts with S308 and π–π stacking including the same residue F931 and F932 and the pyrazole substituent (fig 2.2.4). Additionally, the pyrazole substituent and the potentiator primary amide group were H-bonded to the R933 and Y304 sidechain. At the same time, the thienopyran-based core was projected towards F236, F305, and F312, detecting π–π stacking and van der Waals contacts, comparably to VX770. Therefore, whereas the thienopyrane ring was bioisosteres of the quinoline ring of VX-770, the presence of the carboxamide moieties and the pyrazole ring allowed **11** to improve the stability at the biological target, making **11** (pEC_{50} = 8.52) more potent than VX-770.

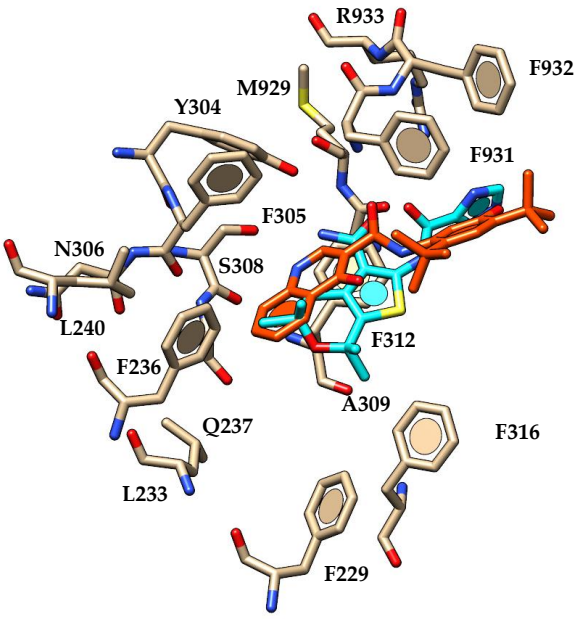

Fig.2.2.4. Selected docking poses of **11** (C atom; cyan) and VX-770 within hCFTR.

This type of positioning was well retained by most docking poses collected for those analogs featuring a CH_3 or a Cl^- substituent on position 3 of the pyrazole **22-23** (pEC_{50} = 8.69), then exhibiting comparable potency values to compound **11**. On the contrary, the docking poses analyzed for the 3-substituted pyrazole containing (**25-26**; pEC_{50} = 7.88-8.52) derivatives missing any H-bond with R933, generating lower pEC_{50} values than the 4-substituted analogs (**22-23**; pEC_{50} = 8.69). The introduction of a 4-carboxamide- as a substitute of a 5-carboxamide-pyrazole substituent tethered to the main bicyclic moiety, such as **10** (pEC_{50} = 6.90) compared to **11** (pEC_{50} = 8.52) or the introduction of methylene tethered to the pyrazole core to the amide moiety of the potentiator, (see **12** (pEC_{50} = 6.86)) reduced the potency profile of the derivatives. This decrease in potency was influenced by the absence of any H-bonds with R933 for all the related docking poses.

Selecting a triazole moiety as a replacement for the pyrazole led to compound **9** (pEC_{50} = 6.33), exhibiting two H-bonds via the carbonyl oxygen atoms to the F931 sidechain. At the same time, the primary amide group detected one H-bond with Y304. Remarkably, the triazole ring proved to simulate the hydroxyl group of the reference potentiator VX-770 but presents a limited number of hydrophobic interactions within the protein cavity. The triazole ring also proved to mimic the behavior of **10** and **12**, displaying comparable potency levels. Moving from the aforementioned five-membered ring derivatives (**9-14**; **22-26**; pEC_{50} = 6.33-8.69) to the six-membered ones (**4-8**; pEC50 = 6.72-8.39), permitted the conservation of the promising potency values as F508del-CFTR potentiators. Compounds **4-6** presented the two

key contacts with F931 and Y304. Even if they cannot interact with R933, these potentiators were effectively stabilized within the biological target thanks to cation-π contacts with the same residue.

On the contrary, the pyridine analog **7** (pEC_{50} = 6.72) or the sulfone amide-substituted benzoyl derivatives **8** (pEC_{50} = 6.83) were characterized by a lower potency than that of prototype **6** (pEC_{50} = 8.39), perhaps for the absence of any contacts with R933 as well as with F932.

The importance of an H-bond donor group decorating the benzoyl moiety linked to the carboxamide functions was determined by the adequate potentiator ability, as exhibited by those derivatives bearing an alcohol group **15-21** (pEC_{50} = 6.89-9.26), sometimes showing comparable interactions with those indicated for VX-770 and the analog **11**.

The compound **20** (*S* enantiomer) (pEC_{50} = 8.56) exhibited one H-bond between the hydroxyl group and the R933 side chain imitating the role played by the VX-770 hydroxyl group or by the pyrazole group of **11** (Fig.2.2.5**)**, while the **19** (*R* enantiomer) (pEC_{50} = 6.89) not show this contact. Concerning the compound **21** racemic mixture (pEC_{50} = 9.26), the *S* enantiomer was expected to be more effective than the *R* enantiomer, providing H-bonds with R933, S308, Y304, F932 via the alkoxy group and the two carboxamide moieties. The high number of interactions with the biological target guarantees a high potency level, **21** more effective than **11**.

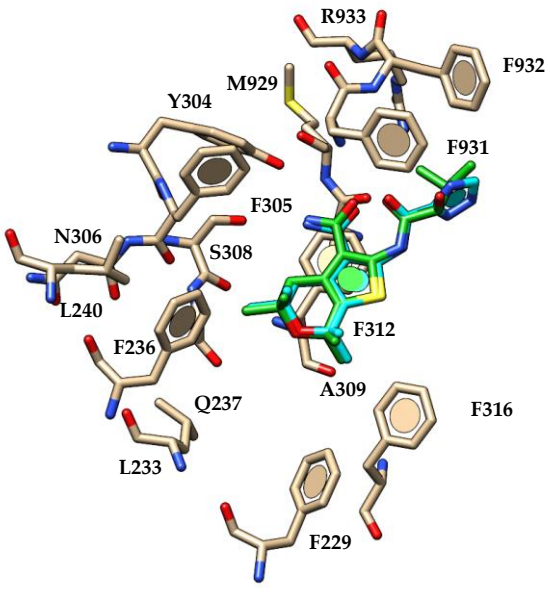

Fig.2.2.5 Selected docking poses of **11** (C atom; cyan) and **20** (C atom; green) within hCFTR.

The deletion of any H-bond donor group from the amide group tied to the main bicyclic core complemented by less hydrophobic R substituents led to compounds **1-3** (pEC_{50} = 6.10-6.18), displaying a thiophene ring with loss of potency as F508del-CFTR potentiator. Compound **3** only mimics the positioning of VX-770, is characterized by a limited number of hydrophobic contacts and H-bonds with F931 and F932.

The second class evaluated involves cyanoquinoline-containing derivatives.

All these compounds show a low potency profile as F508del-CFTR potentiator compared to the first-class discussed above. Specifically, compounds **27-56** (pEC_{50} = 4.25-5.92) include cyanoquinoline-containing derivatives, exhibiting a moderate potency as F508del-CFTR potentiators if compared to the above-mentioned series of thienopyran -based compounds (**1-26**; pEC_{50} = 6.10-9.26). Following the molecular docking calculations, this potency range might be clarified through the ability of cyanoquinolines to interact only with F931 and sometimes with R933, missing any contacts with S308 or Y304. Certainly, the most potent cyanoquinolines **29,33-56** (pEC_{50} = 4.25-5.92) bore a 5,7-dimehtylquinoline-3-carbonitrile main core, being more effective than the analogs characterized by a monomethyl-substituted quinoline ring, such as analogue **27** (pEC_{50} = 4.82) and the 6-methylquinoline-3-carbonitrile derivative **28** (pEC_{50} = 4.82). Nevertheless, the potentiator potency trend modestly improved with the 6-methoxyquinoline-3-carbonitrile ring, as shown by **30-32** (pEC_{50} = 4.95-5.33). The computational study derived that the compounds **30-32** displayed a relative positioning moving the benzoyl moiety towards L233, F236, and A309 and the main cyanoquinoline core near F305, F312 detecting π–π stacking. The **32** methoxy group's oxygen atom was H-bonded to F931 backbone nitrogen atom, while the piperazine tying the main core with the benzoyl substituent was involved in van der Waals contacts with F236.

The presence of a rigid linker between the bicyclic core and the terminal aromatic ring permitted to derive effective derivatives even within the 5,7-dimethylquinoline-3-carbonitrile-containing cyanoquinolines, as confirmed by the promising potency values of the methoxybenzoyl substituted **45-47** (pEC_{50} = 5.88-6.00).

The piperazine ring of the potentiator **45** moved the terminal benzoyl group in the proximity of R933, detecting H-bonds and cation-π contacts. The piperazine ring shows many hydrophobic contacts in agreement with that displayed for the reference compound VX-770. In contrast, the nitrogen atom of the quinoline ring exhibits H-bonds with the key residues

F931. The 5,7-dimethylquinoline main core relatively imitated the hydrophobic contacts and π–π stacking featured by the VX-770 quinoline core, while the nitrogen atom of the bicyclic core of the potentiator **45** was correctly H-bonded to the F931 backbone. Hence, the potency profile shown for **45** (pEC_{50} = 6.00) was quite lower than that of VX-770 (pEC_{50} = 6.63) (Fig.2.2.6).

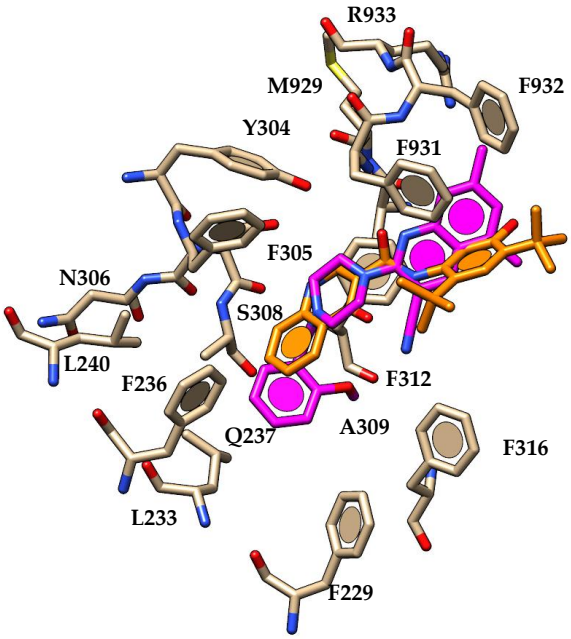

Fig.2.2.6. Selected docking poses of 45 (C atom: magenta) with VX-770 (C atom; orange) within hCFTR.

On the contrary, the isosteric substitution on the benzoyl group with a pyridine ring impaired the potency within the piperazine-containing 5,7-dimethyl-3-carbonitrile cyanoquinolines, missing the contacts mentioned above, as confirmed by the lower pEC_{50} of **48** (pEC_{50} = 5.13) and by inactive analogs **49-51**.

The significance of the methoxy benzoyl substituents, perhaps in terms of balanced hydrophobic-hydrophilic properties and of the related ligand positioning, is confirmed within the cyanoquinolines bearing the 1,2-ethylendiamine **33-35** (pEC_{50} = 5.22-5.63), being more **33-35** more potent than the unsubstituted benzoyl congener **39** (pEC_{50} = 5.00) and the dimethoxy benzoyl substituted analogs **40,41, 44** (pEC_{50} = 4.25-4.93).

The flexibility of the spacer of **34** allowed the benzoyl group to make one H-bond with R933; the nitrogen atom of the quinoline core was H-bonded to F931. This type of positioning ensures the same contacts for **45** and 34 at the CFTR protein, except for cation-π contacts between the benzoyl group of 34 and R933, determining a diminished potency for

potentiator. Interestingly, the substitution of the benzoyl moiety with the 2-carboxamide pyridine ring led to the optimized derivative **36** (pEC_{50} = 5.92), making one H-bond between the quinoline nitrogen atom and F931 and further contacts with Y304 and F305. The other pyridine-based analogs **37** and **38** (pEC_{50} = 4.87-5.00) exhibited a similar positioning even with a loss of potency.

The extension of the linker employing the introduction of the 1,3-propylendiammine chain allowed the yield of potentiators **51-53** (pEC_{50} = 4.55-5.33), decorated with a methoxybenzoyl ring which presented an adequate F508del-CFTR potentiator potency, whereas the related pyridine analogs **54-56** (pEC_{50} = 4.79-5.21) were in some way endowed with lower pEC_{50} values. Within these compounds, the docking mode of **53** (pEC_{50} = 5.30) was comparable with that described for **34** (pEC_{50} = 5.63), hence exhibits similar potency. Compound **53** was H-bonded to the R933 side chain while the quinoline nitrogen atom to F931. Several π–π stacking, including the Y304, F305, and F312, were detected by the quinoline mentioned above the core.

An additional series of F508del-CFTR potentiators that I considered comprises the tetrahydropyridoindole-based compounds (**57-69**; pEC_{50} = 4.52-5.69), that were endowed with lower pEC_{50} values than the GLPG analogs (**1-26**; pEC_{50} = 6.10-9.26) and with comparable potency to cyanoquinoline derivatives (**33-56**; pEC_{50} = 4.25-5.92).

Along with them, the benzyl-substituted derivatives **57-59** (pEC_{50} = 5.00-5.69) and **61-63** (pEC_{50} = 4.52-4.88) were more potent than **64-69** (pEC_{50} = 4.52), featuring benzoyl rings or other alkyl-based substituent onto the indole portion. Consequently, the related docking poses allowed the enlightenment of the main role of a quite flexible aromatic group tethered to the basic nitrogen atom as R1 substituent, which is the potentiator engaged in hydrophobic contacts and π–π stacking with F236, Y304, F305, A309.

Additionally, in the most promising compound **58**, its protonated nitrogen atom showed cation-π interaction with F931, having a key role in stabilizing the ligand at the CFTR channel, while the methoxy group in R3 was H-bonded to R933. Therefore, the 2,4-di-F derivatives **58** (pEC_{50} = 5.69) and **59** (pEC_{50} = 5.58) display similar docking poses and higher potency values than their mono-substituted analog **57** (pEC_{50} = 5.00) or the isostere **60** (pEC_{50} = 5.29), having a thiazole ring as a substitute of the benzyl ring (Fig.2.2.7). The studied positioning of the

analog **57** (pEC_{50} = 5.00) disclosed only one H-bond involving the methoxy group at the R1 substituent and R933 while no cation-π stackings were detected.

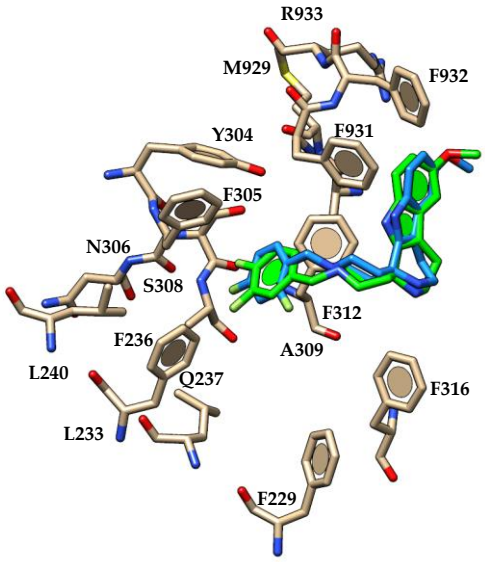

Fig.2.2.7. Selected docking pose of compound **58** (C atom; blue) and compound **59** (C atom; green) within hCFTR.

Eliminating any halogen atom from the benzyl moiety and also the methoxy group on the indole core led to the modest potentiator **61-63** (pEC_{50} = 4.79-4.88), perhaps for the limited number of hydrophobic contacts and polar interactions with the aforementioned key residues, especially lacking H-bonds with R933. The insertion of an additional H-bonding acceptor group as the carbonyl moiety in place of the benzyl group in compounds **65-67** (pEC_{50} = < 4.52) quite reduced the efficacy of the potentiators.

The compounds **64** and **67** maintained one H-bond with R933 using the methoxy group, but the R1 substituent was unable to exhibit cation-π contacts with F931.

As regard compound **64**, the cyclohexyl group in R1 impaired π-π stacking with the surrounding aromatic residues.

About the series of pyrazolo-quinolines **70-80** (pEC_{50} = 4.52-6.52), the presence of lipophilic and electron-withdrawing groups at positions 2 and 4 of the aromatic ring (R3 substituent) led to potent derivatives **74** (pEC_{50} = 5.61) and **78** (pEC_{50} = 5.76), by correctly increasing the hydrophobic contacts with the biological target.

Compound **74** was able to mimic the *tert*-butyl motifs decorating the terminal phenyl ring of VX-770 through its halogen atoms onto the benzoyl group.

In this way, many Van der Waals contacts were detected, stabilizing the ligand at the protein channel.

Interestingly, the two nitrogen atoms of the **74** tricyclic core demonstrated to be adequately superposed on the two oxygen atoms of the reference compound, being one of them H-bonded to the F931 backbone. Also, the primary amine group exhibited H-bonds with Y304 and S308 (Fig2.2.8).

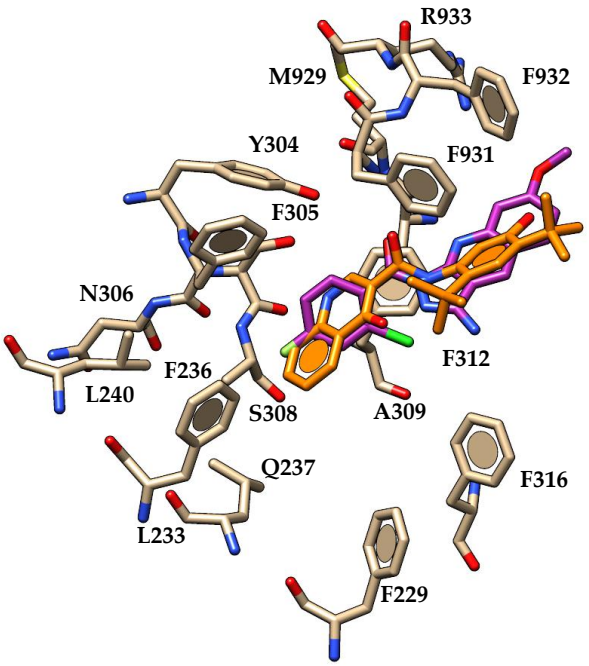

Fig.2.2.8. Selected docking pose of **74** (C atom; magenta) and VX-770 (C atom; orange) within hCFTR.

The compound **78** could mimic the carboxamide-substituted quinolone-based ring of VX-770 and, thanks to the primary amine group, detects H-bonds with S308 and M929. The pyrazole portion of the tricyclic core of **78** and the nitro group was H-bonded to F931 and R933, respectively. The π–π stackings were maintained, such as with F236, Y304, F305, and other ones with F312, while the cation-π contacts with R933 and Van der Waals interactions with A309, F312 were weaker or lacking.

These data agreed with the quite lower potency experienced by **78** (pEC_{50} = 5.61) if compared to VX-770 (pEC_{50} = 6.63).

Accordingly, **74** and **78** proved to be more potent than those analogs featuring polar groups or electron-donor moieties in R3 such as **71** (R3 = 4-pyridine; pEC_{50} = 4.52), **73** (R3 = 3,4,5-methoxyphenyl; pEC_{50} = 4.52), and **75** (R3 = 3-methyl 4-nitrophenyl; pEC_{50} = 4.52).

The consistency of these computational data is also in agreement with the higher potency values exhibited by compound **80** (pEC_{50} = 6.52), bearing a bulky, aromatic, and hydrophobic portion interacting with R933, a key residue for the potentiator binding, as well as the high number of interactions involving the R3 substituent and Y304, F305, A309, F312, F316.

The aminoarylthiazoles derivatives (AATs) represent the last examined series herein investigated. Specifically, I consider compounds **81**-**90** (pEC_{50} = 4.14-5.71), featuring F508del-CFTR potentiator ability, that our research group recently reported and discussed [164,165].

The insertion of a 4-substituted phenyl ring at position 4 of the thiazole ring or a bicyclic ring led to the most promising compounds (**82**, **89**-**90**; pEC_{50} = 4.56-5.71) to 3-substituted derivative **83** (pEC_{50} = 4.27).

Compound **82** (pEC_{50} = 4.56) oriented the 4-F-phenyl group in the proximity of the *tert*-butyl portion of VX-770, detecting the same hydrophobic contacts with F931 and F932.

The main thiazole core was a bioisostere of the VX-770 carboxamide function while the aminoaryl moiety of **82**, exhibiting the lipophilic thiomethyl substituent, overlapped onto the quinolone group of VX-770. This arrangement allowed the compound to involve Van der Waals contacts and π-π stacking with F236, F305, and F312. More interestingly, this type of positioning assures H-bond to the F931 backbone and Y304 sidechain through the thiazole nitrogen atom and the amine group, respectively.

A 4–CN group as a replacement for the 4-F substituent onto the terminal phenyl ring quite switched the docking mode maintaining π-π stacking with F931 and one H-bond with S308 through the amine group. This was in agreement with the lower potency of **81** (pEC_{50} = 4.46) in comparison to **82** (pEC_{50} = 4.56).

The benzoxazolone ring at position 4 of the thiazole ring led to the most potent AAT potentiator **84** (pEC_{50} = 5.19), characterized by the key H-bond with the R933 side chain and the oxygen atom of the carbamate portion.

This kind of positioning allowed the compound to involve a higher number of hydrophobic contacts, with CFTR being the nitrogen atom of the carbamate moiety H-bonded to F305. On the other hand, the thiazole ring interacts with the F931 backbone through its nitrogen atom while the thiomethyl group mimics the *tert*-butyl substituents onto the prototype VX-770 also involved in hydrophobic interactions with F931 and F932 (Fig 2.2.9)

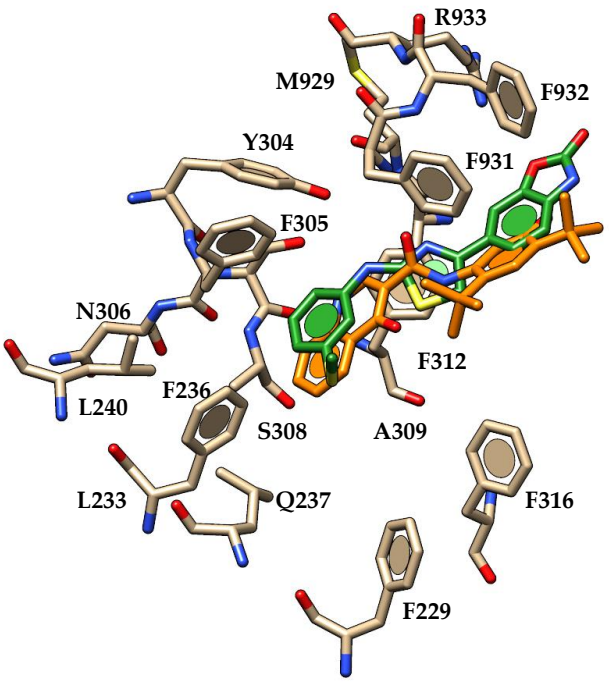

Fig.2.2.9 Selected docking poses of 84 (C atom; green) and VX-770 (C atom; orange) within hCFTR.

The most promising derivative **89** (pEC_{50} = 5.71) exhibited a comparable docking mode if compared to **84**, being endowed with higher hydrophobic contacts played by the indolinone moiety with respect to the benzoxazolone one of the congener **84**. This binding mode allowed mimicking the tert-butyl portion of VX-770 better.

The replacement of the phenyl ring at position 4 of the thiazole of **81-83** (pEC_{50} = 4.27-4.56) with a five-membered ring, such as **86-88** (pEC_{50} = 4.23-5.00) left unvaried the potentiator binding ability, which showed comparable docking mode and potency trend.

Among them, compound **86** (pEC_{50} = 5.00) experienced two H-bonds with F931 and Y304 thanks to the thiazole nitrogen atom and the amine group.

2.2.1 Discussion

A preliminary visual inspection of the X-ray crystallographic data reported by Liu et al. [21] suggested a high number of hydrophobic contacts and Van der Waals interactions and π–π stacking with residues F236, Y304, F305, S308, A309, and F312 together with H-bonds to S308 and F931. The quinolone moiety of VX-770 detected these interactions as well as the most promising series of potentiators previously discussed. This binding mode could allow the potentiator to assume an adequate arrangement within the channel crevice. The subsequent refined docking calculations highlight H-bonds' key role with Y304, F305, and R933 residues, detecting with the last residue not only H-bonds but also cation-π contacts. It is thought that the potentiator is stabilized within the protein cavity need of hydrophobic contacts or π–π stacking and additional polar interactions involving Y304, S308, and F305.

Mainly, H-bonds with F931, R933, S308, and Y304 led to derivatives exhibiting higher potency as CFTR potentiators, as illustrated for most of the GPLG1837 analogs (series **1**-**26**). The other series of potentiators presented many of these contacts showing a variable potency ability.

To validate the whole computational approach applied, I proceeded by choosing from the literature and evaluating *in silico* compounds **91**-**139** (see Appendix A12-A14); only five are modest CFTR potentiators while the other ones proved to be completely inactive.

These compounds have been examined through molecular docking calculations applying the same docking protocol previously discussed for the potentiators **1**-**90**.

Conformity to our docking calculations, some of the thiazoles **91**-**106** exhibited a comparable docking mode. Two H-bonds contacts characterize them; one H-bond involves one oxygen atom of the ester moiety and R933, while the second H-bond involves the oxygen of the carboxamide function and F931. Thiazoles **107**-**111** presented only two weak H-bonds with Y304 and F931, missing any contact with R933. For instance, the di-substitution at the R substituent with electron-withdrawing groups is supposed to impair the aromatic ring's ability to be involved in cation-π contacts with R933.

It is important to note that the most effective potentiators explored above featured at least two contacts with F931 and another one with S308 or Y304, and several H-bonds or cation-π contacts with R933. All of them were considered key points for the potentiator.

Regarding **91**-**106**, the examined poses were variable even if preserving these two interactions, except for the congeners **100** and **101**. Indeed, both of them were well stabilized at the biological target thanks to two H-bonds with R933 and two others with F931. Only 100 and 101 were considered putative potentiators on this foundation, being in good agreement with the biological assays reported in the literature.

The docking mode of **100** and **101** showed two H-bonds with R933 and F931 thanks to the ester moiety and the carboxamide and thiazole nitrogen atom. This kind of positioning allowed the compounds to be well attached at the binding site projecting the ester chain and the phenyl ring towards the hydrophobic crevice surrounded by F931, F932, and L233, F236, F305, respectively.

Consequently, the two hydrophobic cores partially imitated the quinolone ring and the *tert*-butyl substituent of VX-770, while the tertiary amide chain was involved in Van der Waals contacts with F931 and F305.

Compounds **112**-**139** were designed as hybrid derivatives of the F508del-CFTR corrector VX-809, showing comparable or higher potency ability. Only **127**, **128,** and **139** were endowed with a modest CFTR potentiator activity, while all other analogs are entirely inactive. Consequently, the docking poses obtained for **127** and **128** highlighted two H-bonds and cation-π contacts between the benzodioxole group and R933, one H-bond between the oxygen atom of the carboxamide moiety and F931, and an additional H-bond involving the *m*-OH-phenyl ring and F305. The predicted positioning of the hybrid **139** was adequately superposed on that of the reference VX-770, maintaining π–π stacking and Van der Waals contacts with Y304, F305, F236, F312, and L233, A309, respectively, thanks to the **139** quinoline moiety. Also, the two oxygen atoms of the benzodioxole ring guarantee H-bonds with R933.

2.2.2 Material and methods

The compounds were manually built by the 'MOE Builder' tool and then were parameterized with AM1 partial charges as calculation method, and the energy minimization was performed using the 'Energy Minimize Program' with MMFF94x forcefield and RMS (= root

mean square) equal to 0.0001 Kcal/mol/A^2 of the MOE compute module, to produce a single low-energy conformation for each ligand [158].

Molecular docking of all the explored compounds was performed within the X-ray structure of human CFTR in complex with the potentiator VX-770 (PDB code = 6O2P) and GLPG1837 (PDB code = 6O1V) [163], which were prepared through the 'Structure Preparation' program of the MOE software.

Docking calculations were performed thanks to the LeadIT 2.1.8 software suite (www.biosolveit.com). In particular, the FlexX scoring algorithm is employed by LeadIT 2.1.8, relying on binding free energy calculations considering the Gibbs-Helmholtz equation. The docking approach is centered on a spherical search space, defined detecting the binding site as a radius of 6 Å far from the co-crystallized ligand.

The docking algorithm is a state-of-the-art fragment docker: Ligands are divided into fragments. An initial fragment is placed into multiple places in the pocket – and scored using a very fast pre-scoring scheme. From the *n* solutions placed, the ligand is built up, fragment by fragment, and the intermediate solutions are scored against each other. The best-scored poses pass the process, and those are delivered to the user. The initial idea relates to the FlexX algorithm; many advances have been made over the years, such as the "Single Interaction Scan" (SIS) placement that finds solutions when there are few polar groups in a compound. The SIS algorithm uses virtual lines between protein and ligand interaction spots. The calculated docking poses were ranked by the score values of the lowest energy pose of the derivatives docked to the macromolecule. All compounds were refined and re-ranked by assessment with HYDE, belonging to the LeadIT 2.1.8 software [166].

CHAPTER 3: LIGAND BASED APPROACH

3.1. QSAR studies applied on correctors as F508del-CFTR modulators

In preceding work performed by our research group QSAR analyses on a dataset of sixty-three F508del-CFTR correctors featuring the thiazole, tetrahydropyridopyrimidines, and cyanoquinolines scaffolds have been described. This research allowed the discovery of eight descriptors describing the corrector ability range of the collected library, being five and three of them 2D and 3D descriptors. These included parameters correlated to atoms and bound counts (b_single, a_IC, and a_nH) and surface area descriptors (Vsurf_DD12 and Vsurf_W8). The connectivity-based descriptor chi1, the distance matrix parameter weinerPol, and the potential energy descriptor E_nb were also maintained[164].

These studies supported the design of branched scaffolds enriched with flexible substituents and quite polar moieties within overall limited and bulky conformations. Considering the prediction achieved with the model, several hybrids endowed with a promising CFTR rescue ability have been designed and synthesized.

During my Ph.D., I refine the previous QSAR model, including the chemical structure and the related corrector profile of the in-house hybrid correctors in the newly developed dataset. The optimized QSAR model aims to expand the SAR information of this potent series of CFTR modulators[148].

The utilized dataset consists of eighty compounds (**1**-**80**; see Appendix A1-A3), being compounds **1** (pEC_{50} = 5.59), the corrector VX-809, and derivatives **2**-**29,** the hybrids mentioned above. Compounds **30**-**80** relate to the tetrahydropyridopyrimidines and cyanoquinolines considered in the literature as F508del-CFTR correctors [167].

The new predictive mathematical model was calculated separating compounds **1**-**80** into a training set (**3**-**13**, **15**-**18**, **23**-**27**, **30**-**32**, **37**-**47**, **49**, **50**, **54**-**63**, **65**-**68**, **70**, **71**, **73**-**80**) to create the QSAR model, and into a test set containing twenty derivatives (**1**, **2**, **14**, **19**-**22**, **28**, **29**, **33**-**36**, **48**, **51**-**53**, **64**, **69**, **72**), in order to estimate the reliability of the mathematical relationship. Specifically, the obtained statistical tool was produced by using non-cross-validated PLS analysis to provide a cross validated r^2 (r^2_{cv}) = 0.80 a non-cross validated r^2 (r^2_{ncv}) = 0.84, a root mean square error (RMSE) = 0.333 and a test set r^2 (r^2_{pred}) = 0.78. The predicted and

experimental rescue ability for all the derivatives is listed as tables together with the collected descriptors, as shown in supplementary data (see Appendix A15-16).

To develop QSAR analyses, three hundred molecular descriptors (including 2D- and 3D-parameters) were analyzed using MOE software.

2D molecular descriptors are distributed in seven subsets that represent physical properties (2D-I), subdivided surface areas (2D-II), atom and bond counts (2D-III), connectivity-based descriptors (2D-IV), partial charges descriptors (2D-V), pharmacophore features descriptors (2D-VI) and the so-called Adjacency and Distance Matrix Descriptors (2D-VII).

3D-descriptors contain five groups, such as potential energy descriptors (3D-I), MOPAC descriptors (3D-II), Surface Area (3D-III), Volume and Shape Descriptors (3D-IV), and Conformation-Dependent Charge Descriptors (3D-V).

The statical method used to perform the studies is the same as our research group's previous work.

A limited cluster of descriptors was chosen utilizing the QSAR-Contingency module implemented in MOE. Firstly, the top-fifty best-ranked parameters were maintained based on the contingency scoring function. Then they were further filtered by re-iterative partial least square (PLS) analyses, involving only those parameters displaying the highest relative importance (RI) values.

Following this method, I identified six descriptors related to the collected library's rescue ability profile, mostly 3D descriptors (see Table3.1). Indeed, two descriptors drop in the 3D-I cluster, three in the 3D-V series, and only one in the 2D-VI. Descriptor E_nb was the only one also retained in the previously published QSAR model.

Descriptor	Type	Series	RI
E_nb	Value of the potential energy related to non-bonded terms	3D-I	1.000000
CASA$^+$	Positive charge weighted surface area, ASA+ times max {$q_i > 0$} [a]	3D-V	0.663223
ASA$^-$	Water accessible surface area of all atoms with negative partial charge	3D-V	0.3052252
E_ang	Angle bend potential energy	3D-I	0.2326607
CASA$^-$	Negative charge weighted surface area, ASA- times max {qi >0}	3D-V	0.229658
Vsa_pol	Approximation to the sum of VDW surface area (Å^2) of polar atoms	2D-VI	0.136024

Table.3.1. Selected descriptors and corresponding relative values (RI) based on the derived model.

The obtained model was developed, choosing the training set and test set compounds manually, taking into account the biological activity trend and structural variations.

All the 3D selected descriptors describe the correctors' polarity profile, lengthened along the molecular surface, considering the ligands' conformational disposition. Conversely, these characteristics also turn in specific and adequate prerequisites assisting the hydrophilic/hydrophobic balance onto the overall surface extent, as verified by the vsa_pol descriptor. This information is indicated for a suitable overall dimension and shape of the ligand, turning in favored branched and flexible substituents over rigid, planar, and much more extended groups. This data agrees with the whole need for a significant polarity profile to be solved along with a branched chemical structure.

Quantitatively, the corrector ability of the compounds examined is described by the following equation Eq. (1):

Eq. (1): pEC_{50} = 12.91882-0.10591 * E_nb -0.01931 * ASA-0.04699 * vsa_pol+0.00260 * CASA+0.00658 * CASA-0.02034 * E_ang

A representation of the high performance of the model is reported in Fig 3.1.2.

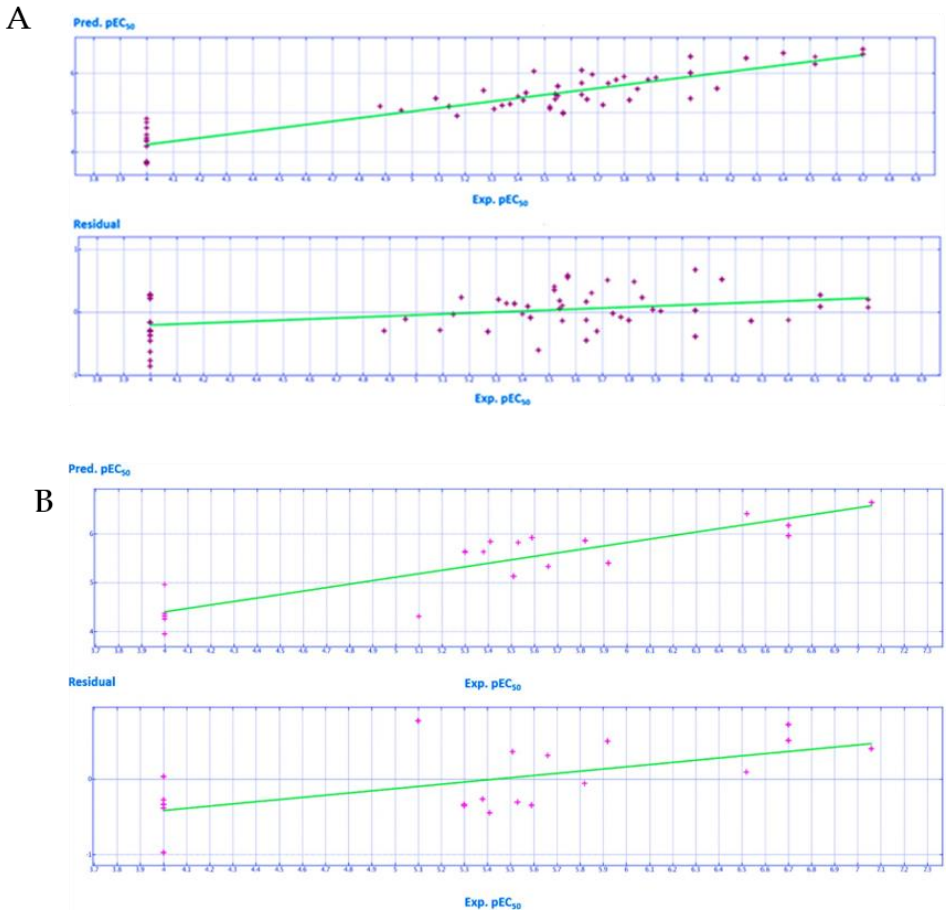

Fig.3.1.2 Schematic representation of the model's high performance when predicting modest to promising F508del-CFTR correctors (4.50 < pEC_{50} < 6.00), being the corresponding residual values near to zero. In (**A**) is represented the distribution of the predicted (Pred. pEC_{50}) and experimental (Exp. pEC_{50}) potency values of the training set compounds (violet crosses). The residual values have calculated the difference between the Exp.pEC_{50} and the Pred.pEC_{50}. In (**B**) is represented the distribution of the predicted (Pred.pEC_{50}) and experimental (Exp.pEC_{50}) potency values of the test set compounds (magenta crosses). Residual values are calculated as the difference between the Exp.pEC_{50} and the Pred.pEC_{50}.

Considering this information, E_nb and CASA+ are the most important molecular descriptors concerning the biological activity trend of the VX-809 hybrids, of the tetrahydropyridopyrimides, and the cyanoquinolines (Table 3.1), presenting RI values > 0.6. The E_nb mean value among the hybrid series changes from 35 to 40 (Kcal/mol) for the quiet and more promising correctors.

Rising in E_nb occurs with the introduction of a polar electron-donor group linked to the *meta* position of the phenyl ring rather than a bulky and hydrophobic group at the same position. In fact, the 5-methyl thiazole **9** (pEC_{50} = 5.80; E_nb = 37.62 Kcal/mol) presented a lower E_nb value than the congener *m*-OH-phenyl substituted **18** (pEC_{50} = 5.92; E_nb = 38.13 Kcal/mol). In addition, compound **18** experienced an elevated E_nb value than the *m*-Cl-phenyl substituted **8** (pEC_{50} = 5.64; E_nb = 37.86 Kcal/mol). Curiously, the ideal value regarding this descriptor (E_nb = 40 Kcal/mol) was exhibited by those hybrids presenting the ester moiety at the position 5 of the AAT. This was in accordance with the promising corrector ability of **5** (pEC_{50} = 6.05; E_nb = 39.97 Kcal/mol), **3** (pEC_{50} = 6.52; E_nb = 40.20 Kcal/mol) and **4** (pEC_{50} = 6.26; E_nb = 40.07 Kcal/mol) if compared to the non-substituted analogues **11** (pEC_{50} = 5.54; E_nb = 37.21 Kcal/mol), **12** (pEC_{50} = 5.31; E_nb = 37.43 Kcal/mol) and **13** (pEC_{50} = 5.09; E_nb = 37.21 Kcal/mol), respectively.

Conceivably, it is believed that deep changes of E_nb value occur in the presence of branched or flexible substituents tethered to the central scaffold of the corrector, leading to useful intra-molecular contacts as well as intra- hydrogen bonds and hydrophobic interactions. This type of conformation is experienced within the tetrahydropyridopyrimidines, presenting the most potent E_nb values spanning from 70 to 100 Kcal/mol, while the less active analogs experience E_nb higher than 100 Kcal/mol.

Tetrahydropyridopyrimidines with flexible chains in R2 in conjunction with H-bond acceptor functions (such as **45** and **50**; pEC_{50} =6.70) might be involved in intramolecular H bonds with the protonated nitrogen atom of the tetrahydropyridine ring, presenting proper levels in E_nb (**45**, E_nb = 84.29 Kcal/mol; **50**, E_nb = 74.34 Kcal/mol).

Conversely, more rigid tetrahydropyridopyrimidines with a piperazine ring linked to the main bicyclic core led to less promising derivatives displaying too high levels in the E_nb descriptor, over 100 Kcal/mol. This data is supported by the poor potency values of the piperazine-containing

38 (pEC_{50} = 4.00; E_nb = 153.96 Kcal/mol), **40**-**42** (pEC_{50} = 4.00; E_nb = 153.73- 158.42 Kcal/mol), **55**-**56** (pEC_{50} = 4.00; E_nb = 123.08- 132.29 Kcal/mol).

The most interesting cyanoquinolines show a E_nb value between 50 and 65 Kcal/mol, while the less potent analogs exhibit higher values of E_nb. According to these information, CQs featuring basic and flexible ethylene diamine spacer, such as **65**-**68** (pEC_{50} = 5.17-5.82; E_nb = 57.02 – 63.47 Kcal/mol) presented lower E_nb than the modestly active analogues bearing a propylene diamine spacer in R1, such as **73**-**74** (pEC_{50} = 4.88-5.52; E_nb = 52.39 – 54.52 Kcal/mol) and the poorly active piperazine-containing **75**-**80** pEC_{50} = 4.00; E_nb = 65.90 – 71.22 Kcal/mol).

Regarding $CASA^+$, the whole electropositive profile experienced by hybrids such as by cyanoquinolines was extremely comparable, disclosing a mean value for the most promising derivatives around 1100 $Å^2$. The introduction of an electro-donor moiety such as the ester function at the position 5 of the thiazole rises the CASA+ descriptor values, with an increase of the corrector ability of the compounds. Hence, **5** (pEC_{50} = 6.05; $CASA^+$ = 1154.36 $Å^2$), **3** (pEC_{50} = 6.52; $CASA^+$ = 1154.36 $Å^2$) and **4** (pEC_{50} = 6.26; $CASA^+$ = 1153.63 $Å^2$) are endowed with higher potency values than the analogues unsubstituted at the same position of the five-membered ring **11** (pEC_{50} = 5.54; $CASA^+$ = 728.87 $Å^2$), **12** (pEC_{50} = 5.31; $CASA^+$ = 708.34 $Å^2$) and **13** (pEC_{50} = 5.09; $CASA^+$ = 743.19 $Å^2$).

These results sustenance the high effectiveness of those hybrids bearing the hydroxyl group linked to the phenyl ring at the position 4 of the thiazole if compared with the chlorine substituted analogues (compare **16** (pEC_{50} = 5.74; $CASA^+$ = 890.95 $Å^2$), **17** (pEC_{50} = 5.64; $CASA^+$ = 893.51 $Å^2$), **25** (pEC_{50} = 5.89; $CASA^+$= 804.04 $Å^2$) and **18** (pEC_{50} = 5.92; $CASA^+$ = 966.20 $Å^2$) with **11** (pEC_{50} = 5.54; $CASA^+$ = 728.87 $Å^2$), **13** (pEC_{50} = 5.09; $CASA^+$ = 743.19 $Å^2$), **27** (pEC_{50} = 5.40; $CASA^+$ = 662.58 $Å^2$) and **8** (pEC_{50} = 5.64; $CASA^+$ = 791.71 $Å^2$))(Fig.3.1.3).

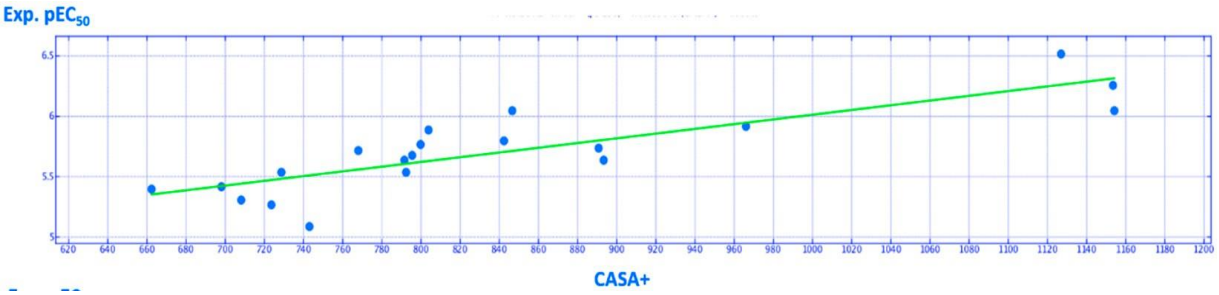

Fig.3.1.3. Distribution of the Experimental (Exp.pEC$_{50}$) potency values of the training set compounds based on the CASA+ descriptor (Å^2) of hybrid derivatives.

Regarding the cyanoquinolines series, the substitution onto the terminal aromatic ring with a methoxy- or dimethoxy- group allowed the increase of CASA$^+$ descriptor supplemented by a whole increase in terms of corrector ability. Similarly, the presence of benzamide moiety generates more promising compounds than the picolinamide or nicotinamide moieties. The reliability of this information is verified by the higher pEC$_{50}$ and by the CASA$^+$ descriptor profile when the methoxy-substituted **57–59** (pEC$_{50}$ = 4.96–5.66; CASA$^+$ = 911.40-923.78 Å^2) are compared to the unsubstituted heteroaryl-based analogues **60–62** (pEC$_{50}$ = 4.00–5.57; CASA$^+$ = 774.53–789.39 Å^2) and to the benzamide analogue **63** (pEC$_{50}$ = 4.00; CASA$^+$ = 709.99 Å^2). This information is maintained within the series of cyanoquinolines, presenting the dimethyl spacer and the diaminopropyl- and the piperazine-containing analogs. Indeed, the methoxy-substituted **71** (pEC$_{50}$ = 5.37; CASA$^+$ = 880.84 Å^2) was more potent than **74** (pEC$_{50}$ = 4.88; CASA$^+$ = 747.92 Å^2) (Fig.3.1.4).

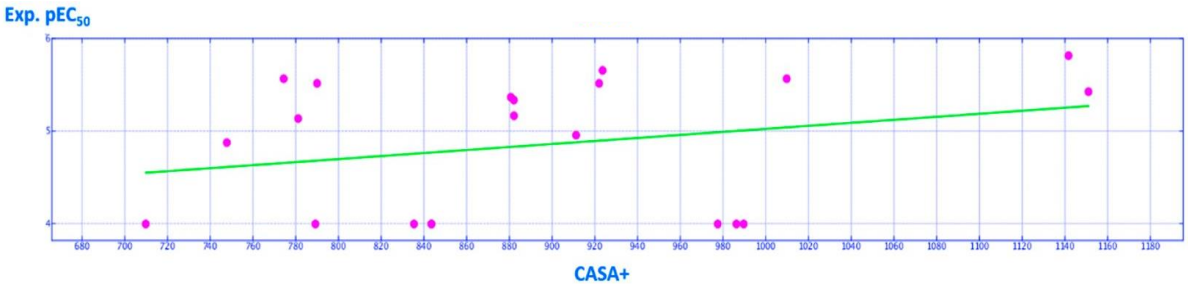

Fig.3.1.4. Distribution of the Experimental (Exp.pEC$_{50}$) potency values of the training set compounds based on the CASA+ descriptor (Å^2) of cyanoquinolines.

The most promising tetrahydropyridopyrimidines were characterized by a value of $CASA^+$ descriptor spanning from 1600 to 2300 $Å^2$, presenting the preponderance of the less potent (higher) values of this parameter. Conceivably, this evidence can be clarified based on the prominent polarity of this corrector series' main scaffold, being very enriched of nitrogen atoms and basic features.

Within them, the tetrahydropyridopyrimidines **50**, **51** (pEC_{50} = 6.70; $CASA^+$ = 1729.20 $Å^2$) exhibit adequate $CASA^+$ values thanks to their flexible basic chain in R2 as well as the methoxyphenyl-based analogue **45** (pEC_{50} = 6.70; $CASA^+$ = 2102.26 $Å^2$), also endowed with basic features (Fig.3.1.5).

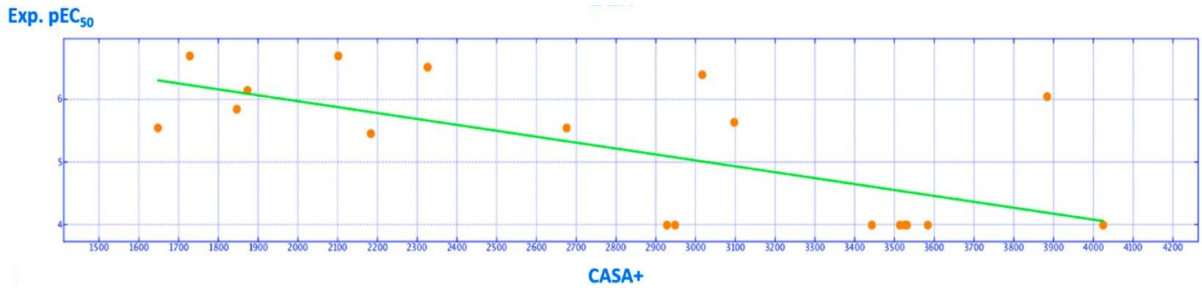

Fig.3.1.5 Distribution of the Experimental ($Exp.pEC_{50}$) potency values of the training set compounds based on the CASA+ descriptor ($Å^2$) tetrahydropyridopyrimidines.

3.1.2 Discussion

The information achieved by QSAR analyses agreed with those of docking results discussed in chapter 2, disclosing a consistent number of descriptors explaining the correctors' polarity profile. E_nb and CASA+ have been previously considered the most relevant parameters concerning the three CFTR modulators' series. Beyond these descriptors, the potency trend of hybrids was positively affected by increasing values of E_ang, in agreement with the whole promising potency of the ester-containing analogs, as well as by a balanced electro-negative profile.

These results were validated by the limited CASA- and ASA parameters exhibited by the most potent hybrids. Conversely, the pEC_{50} values of tetrahydropyridopyrimidines increased with these two descriptors, maybe because of the high polarity of the main core of this corrector series

featuring several nitrogen atoms and basic groups. Consequently, the vsa_pol descriptor was also positively correlated to this chemical series's corrector ability, supporting the need for a corrector shape endowed with a quite flexible and polar molecular surface to reach corrector behavior. Therefore, the most potent cyanoquinolines were accompanied by increasing values of the vsa_pol parameter.

3.1.3 Material and methods

QSAR studies were performed based on calculations of three hundred molecular descriptors, including 2D and 3D parameters, using MOE software. 2D molecular descriptors are identified as numerical properties that can be determined from the connection table representation of a molecule. 2D descriptors are not dependent on a molecule's conformation and are most proper for extensive database studies. They include descriptors associated with atom and bond counts, subdivided surface areas, physical properties, connectivity-based descriptors, pharmacophore feature descriptors, partial charges descriptors, and the Adjacency and Distance Matrix Descriptors. The 3D-descriptors comprise potential energy descriptors, MOPAC descriptors, Surface Area, Volume and Shape Descriptors, and Conformation Dependent Charge Descriptors.

Then, 302 molecular descriptors (2D and 3D) were calculated by MOE, and the resultant matrix was presented to the statistical analyses and quantitative structure-activity relationships (QSAR). Also, QuaSAR-Contingency was used for pruning molecular descriptors, while the QSAR analysis module of MOE software was utilized to create the final mathematical models.

To perform quantitative structure-activity relationship (QSAR) studies, sixty correctors were included in the training set for generating the model. The other ones into the test set for the validation of the model. The compounds were divided manually into the training and the test set to generate the mathematical model, based on representative criteria of the overall biological activity trend and structural variations. QSAR was done by employing various iterations of partial least-squares (PLS) multivariate analysis, taking into account the molecular descriptors as independent variables and corrector pEC_{50} values as dependent variables. For each iteration, the relative importance of every single descriptor in influencing corrector ability was calculated. Hence, the less important ones were discarded in the following PLS analysis until the final linear regression model generation. At every PLS, the Leave One Out method was utilized to verify the derived models' internal predictability.

The predictive ability of the derived model was evaluated for the test set compounds (expressed as r^2_{pred}) by using the following Equation (2):

$$r^2_{pred} = (SD - PRESS)/SD \quad (2)$$

SD is the sum of the squared deviations between the test set molecules' biological activities. The mean activity of the training set compounds, and PRESS, is the sum of the squared deviations between the observed and the test set compounds' predicted activities.

3.2 QSAR studies applied on F508del-CFTR potentiators

To explore the main features of the different potentiator abilities exhibited within the chemo-types **1-90**, I considered it interesting to proceed with a QSAR analysis. The derived QSAR model is supposed to deepen the SAR knowledge of this series of CFTR modulators[162].

Firstly, this study was administered based on different descriptors referring to 2D- and 3D-parameters (three hundred molecular descriptors), which were calculate thanks to the MOE software. As for the QSAR analysis performed on the corrector series previously discussed also in this case, the 2D molecular descriptors can be divided into seven sub-series, related to physical properties (2D-I), subdivided surface areas (2D-II), atom and bond counts (2D-III), connectivity-based descriptors (2D-IV), partial charges descriptors (2D-V), pharmacophore features descriptors (2D-VI) and the so-called Adjacency and Distance Matrix Descriptors (2D-VII). At the same time, 3D-descriptors are classified into five different sub-groups, including potential energy descriptors (3D-I), MOPAC descriptors (3D-II), Surface Area (3D-III), Volume and Shape Descriptors (3D-IV), and Conformation-Dependent Charge Descriptors (3D-V).

The dataset used to conduct the studies included seventy-five compounds (**1**,**3**,**4**,**6**-**12**,**22**-**41**, **43**-**48**, **51**-**69**, **71**-**90**) selected from the whole dataset, deleting the completely inactive compounds and those presenting a chiral carbon atom.

Thus, a final data matrix of 75 objects (compounds/ molecules) and 306 rows (molecular descriptors) was obtained.

The chemometric package PARVUS[168] was applied to check the constant predictors, dividing the data into training and test sets, removing the non-informative descriptors, and extracting

meaningful QSAR models to recognize the most important predictors accounting for the potentiator ability of the compounds in terms of pEC_{50} values.

Following this method, has been identified 20 relevant descriptors, five of them belong to the 2D subdivided surface area (Table 3.2.1; SlogP_VSA4, SlogP_VSA5, SlogP_VSA9, SMR_VSA2,SMR_VSA4) four to the 2D Adjacency and Distance Matrix Descriptors (Table 3.2.2; BCUT_SLOGP_1, BCUT_SMR_1, BCUT_SMR_2 BCUT_SMR_3) two to the 2D Partial Charge Descriptors (Table 3.2.1; PEOE_VSA+5, PEOE_VSA-6) one to the 2D Pharmacophore Feature Descriptors (Table 3.2.2; a_hyd), one to the Physical Properties (Table 3.2.2; logS) one to the 2D Atom Counts and Bond Counts (Table 3.2.2; b_1rotR). Regarding the selected 3D descriptors, four of them fall in the Surface Area, Volume, and Shape Descriptors (Table 3.2.3; vsurf_ID1, vsurf_ID7, vsurf_Wp2, vsurf_Wp3) while the other two were Conformation Dependent Charge Descriptors (Table3.2.39; dipoleY and ASA^{+}).

Descriptor	Type	Series	RI
SlogP_VSA4	Sum of n_i such that L_i is in (0.1,0.15]	2D-II	0.293739
SlogP_VSA5	Sum of n_i such that L_i is in (0.15,0.20]	2D-II	0.501133
SlogP_VSA9	Sum of n_i such that L_i is > 0.40	2D-II	0.686395
SMR_VSA2	Sum of n_i such that R_i is in (0.26,0.35]	2D-II	0.429419
SMR_VSA4	Sum of n_i such that R_i is in (0.39,0.44]	2D-II	0.234752
PEOE_VSA+5	Sum of n_i where q_i is in the range [0.25,0.30)	2D-V	0.053589
PEOE_VSA+6	Sum of n_i where q_i is less than -0.30	2D-V	0.461873

Table. 3.2.1 Selected 2D Subdivided Surface Area and Adjacency and Partial Charge descriptors and the corresponding relative importance values (RI) based on derived QSAR model.

Descriptor	Type	Series	RI
BCUT_SLOGP_1	The BCUT descriptors using atomic contribution to logP	2D-VII	0.578303
BCUT_SMR_1	The BCUT descriptors using atomic contribution to molar refractivity	2D-VII	0.500605
BCUT_SMR_2	The BCUT descriptors using atomic contribution to molar refractivity	2D-VII	0.029230
BCUT_SMR_3	The BCUT descriptors using atomic contribution to molar refractivity	2D-VII	0.720350
a_hyd	Number of hydrophobic atoms	2D-VI	0.101682
LogS	Log of the aqueos solubility (mol/L).	2D-I	0.950723
b_1rotR	Fraction of rotatable single bonds: number of rotatable bonds (b_1rotN) divided by number of bonds between heavy atoms (b_heavy)	2D-III	0.211130

Table.3.2.2. Selected 2D Adjacency and Distance Matrix Descriptors, Pharmacophore Feature Descriptors, Physical properties, and Atom Counts and Bound Counts descriptors and corresponding importance values (RI).

Descriptor	Type	Series	RI
vsurf_ID1	Hydrophobic integry moment	3D-III	0.119071
vsurf_ID7	Hydrophobic integry moment	3D-III	0.58227
vsurf_Wp2	Polar volume	3D-III	0.243649
vsurf_Wp3	Polar volume	3D-III	1.000000
dipoleY	The y component of the dipole moment	3D-V	0.492821
ASA+	Water accessibility surface area of all atoms with positive partial charge	3D-V	0.3096621

Table.3.2.3. Selected 3D Surface Area, Volume and Shape Descriptors and Conformation Dependent Charge descriptors and the related importance Values (RI).

All the chosen 3D descriptors are associated with the modulators' polarity profile, extended along the molecular surface area, considering the ligands' conformational disposition. Instead, all the 2D ones indicate balanced hydrophilic/hydrophobic properties onto the whole surface extent.

The final QSAR model was created, dividing the compounds into training and test sets applying the space-filling Kennard-Stone duplex design[169], the most prevalent algorithm for selecting a

subset sample with distribution as much as possible to the uniform distribution. As a result, sixty objects were picked for the training set, and 15 molecules were allocated to the test set (20% of the total molecules).

In details, the predictive model was calculated by including in the training set **1, 4, 7-10**, **12**, **22**, **23**, **25-30**, **31**, **33**, **34-37**, **39**, **41**, **43-48**, **51-54**, **56**, **58**, **60-65**, **67-69**, **71**, **73- 76**, **78-83**, **85-87**, **89,90**, which have been used to generate the QSAR model, and in the test set **3**, **6**, **11**, **24**, **32**, **38**, **40**, **55**, **57**, **59**, **66**, **72**, **77**, **84**, **88** in order to evaluate the reliability of the mathematical relationship. Specifically, the final model was generated by using non-cross-validated PLS analysis to give a cross validated r^2 (r^2_{cv}) = 0.74 a non-cross validated r^2 (r^2_{ncv}) = 0.90, root mean square error (RMSE) = 0.347, a test set r^2 (r^2_{pred}) = 0.86. The predicted and experimental rescue ability for all the derivatives are listed as tables together with the collected descriptors (A17, A18, A19, A20)

Quantitatively, the potentiator ability of the compounds is explained by the following equation Eq. (1):

Eq. (1): pEC_{50} = Potency = -2.51363 +1.87312 * BCUT_SLOGP_1 +1.58432 * BCUT_SMR_1 +0.09344 * BCUT_SMR_2 +1.48927 * BCUT_SMR_3 -1.39449 * b_1rotR -0.27817 * logS +0.25870 * dipoleY +0.01241 * a_hyd +0.00253 * ASA^+ +0.00205 * PEOE_VSA+5 -0.02622 * PEOE_VSA-6 +0.00522 * SlogP_VSA4 -0.00628 * SlogP_VSA5 +0.00393 * SlogP_VSA9 -0.00921 * SMR_VSA2 -0.00440 * SMR_VSA4 +0.13782 * vsurf_ID1 +0.41705 * vsurf_ID7 +0.00211 * vsurf_Wp2 +0.00957 * vsurf_Wp3

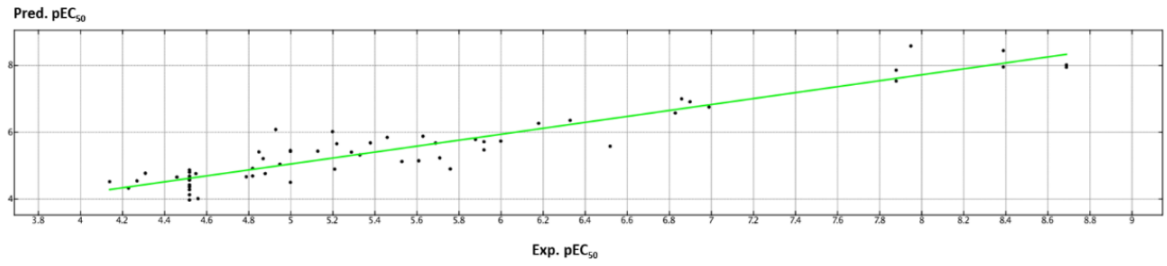

Fig.3.2.1. Representation of the developed model's high performance when predicting the potentiator ability of the in-house dataset (4.25 < pEC_{50} < 9.26). Representation of the predicted (Pred.pEC_{50}) and Experimental (Exp.pEC_{50}) potency values of the compounds (Black dots).

Considering these results, the existence of quite flat groups substituted with polar moieties and endowed with limited flexibility should be favored for much more linear and flexible groups. This type of information agrees with the need for a limited number of rotatable bonds and hydrophobic atoms, as suggested by the B_1rotR and a_hyd descriptors. Therefore, the calculated mean values of the B_1rotR descriptor within the most potent thienopyrans (**1**-**26**; B_1rotR_{mean} = 0,119343), and of the flat pyrazoloquinolines (**70**-**80**; B_1rotR_{mean} = 0.131342), were lower than those of cyanoquinolines (B_1rotR_{mean} = 0.182995), often displaying extended flexible chains (Table 3.2.4).

Indeed, the promising thienopyrans **19**, **22**-**24** (pEC_{50} = 8.52-8.69) featured branched moieties or small aromatic rings as R substituent as a substitute of a linear aliphatic chain, while the most potent pyrazoloquinoline **80** (pEC_{50} = 6.52) brings a thiophene-substituted quinoline as a planar group in R3. Concerning the less potent cyanoquinolines, the substitution of a piperazine spacer instead of diamino alkyl chain proved to be advantageous, as shown by **45**-**47** (pEC_{50} = 5.88-6.00) if compared to the diamino ethyl-based **33**-**35** (pEC_{50} = 5.22-5.63) and to the diamino propyl-containing **51**-**53** (pEC_{50} = 4.55-5.33). Taking into account, the ideal number of hydrophobic atoms should fall in a range spanning from 15 to 20 atoms. Higher values of this parameter might worsen the compounds' potency profile, as reported within the pyrazoloquinoline series displaying an a_hyd_{mean} value > 21.

Increasing values of the 3D descriptors Vsurf_ID7 and Vsurf_Wp3 turn in improved potency of the potentiators, favoring the key role of balanced polar and hydrophobic features at the molecular surface. It is possibly accompanied by differently substituted aromatic rings included in the potentiator's main structure, as the (at least) three quite co-planar aromatic rings of thienopyrans 1-26 pyrazoloquinolines **70**-**80** and AATs **81**-**90**.

These results were validated by the related mean values (Table 3.2.4) and according to the higher potency profile experienced by thienopyrans than all the other potentiators' classes. Conversely, the ideal value for the SlogP_VSA9 of at least 150 is predicted to be accompanied by pEC_{50} values > 7.00 M.

Potentiators	b_1rotR_{mean}	a_hyd_{mean}	$Vsurf\_Wp3_{mean}$	$Vsurf\_ID7_{mean}$	$SlogP\_VSA9_{mean}$	pEC_{50}
Thyenopyrans	0.11934	15.8667	183.5333	1.4341	178.6650	6.10-9.26
Cyanoquinolines	0.1830	19.0741	118.6481	1.1386	68.4367	4.25-6.00
Indole-based derivatives	0.0901	21.8461	117.8750	1.09374	26.9052	4.52-5.69
Pyrazoloquinolines	0.1313	17.1000	160.6875	0.9737	40.7683	4.52-6.53
Aminoaryl thiazoles	0.17156	17.5454	108.8875	0.98697	96.0631	4.14-5.71

Table 3.2.4. Mean values of the most important 3D descriptors and 2D descriptors were chosen as reference parameters within the different 2D subtypes.

Beyond these five descriptors, ASA+, logS, and BCUT_SMR3 summarized the overall role of balanced hydrophobic and polar properties displayed by all the potentiators herein investigated.

3.2.1 Material and methods

Quantitative Structure-Activity Relationships (QSAR) studies were completed based on calculations of three hundred molecular descriptors, including 2D- and 3D parameters, through MOE software. 2D molecular descriptors are identified as numerical properties computed from the connection table representation of a molecule. 2D descriptors are not dependent on a molecule's conformation and are most suitable for extensive database studies. They include descriptors correlated to physical properties, subdivided surface areas, atom and bond counts, connectivity-based descriptors, partial charges descriptors, pharmacophore features descriptors, and the so-called Adjacency and Distance Matrix Descriptors. The 3D-descriptors consist of potential energy descriptors, MOPAC descriptors, Surface Area, Volume and Shape Descriptors, and Conformation Dependent Charge Descriptors.

Then 306 molecular descriptors (2D and 3D) were calculated by MOE, and the resulting matrix was proposed to the statistical analyses and (QSAR) objects of the present work.

A final data matrix of 75 objects (compounds/ molecules) and 306 rows (molecular descriptors) was obtained. The chemometric package PARVUS[168] was applied to handle such information, particularly for inspecting the constant predictors, splitting the data into training and test sets, discarding the non-informative descriptors extracting meaningful QSAR models able to recognize the most important predictors accounting for potentiator pEC_{50} value.

Firstly, the CHECK module implemented in PARVUS was used to check the constancy of variables in five cancellation groups, and 283 molecular descriptors were retained after eliminating the constant predictors.

The space-filling Kennard-Stone duplex design[169] was used to split the data into representative training and test sets; this algorithm was applied using the first 10 principal components of the autoscaled data, considering the 90% of the total variance. Sixty objects were selected for the training set, and 15 molecules were assigned to the test set (20% of the whole molecules).

Iterative stepwise elimination PLS (ISEPLS) was applied, as a variable selection method, to evaluate the selected predictors' relevance concerning the possibility of predicting the response variable y (pEC_{50}). ISE is based on the importance of the predictors, defined as:

$$z_v = \frac{|b_v| s_v}{\sum_{v=1}^{V} |b_v| s_v}$$

where bv is the regression coefficient and sv the standard deviation of the descriptor v. In each elimination cycle, the descriptor with the minimum importance is removed. The model is computed again with the remaining predictors. The final model, with the maximum predictive ability in cross-validation, retained 20 relevant descriptors.

QSAR was completed by applying various iterations of partial least-squares (PLS) multivariate analysis through MOE software, considering the molecular descriptors as independent variables and corrector pEC_{50} values as the dependent variable. At each iteration, the relative importance of every descriptor in influencing corrector ability was calculated. Therefore, the less important ones were removed in the following PLS analysis until the final linear regression model generation. At

each PLS, the Leave One Out method was used to check the derived models' internal predictability.

The predictive ability of the derived model was evaluated for the test set compounds (expressed as r^2_{pred}) by using the following equation:

$$r^2_{pred} = (SD - PRESS)/SD$$

SD is the sum of the squared deviations between the test set molecules' biological activities. The mean activity of the training set compounds, and PRESS is the sum of the squared deviation between the observed and the test set compounds' predicted activities.

CHAPTER 4. DISCOVERY OF NEW CORRETTORS USING COMPUTATIONAL APPROACHES, CHEMICAL SYNTHESIS, AND BIOLOGICAL ASSAYS

Background

In the last years, to find new drugs for CF treatment, our research group reported the rational design, chemical synthesis, and biochemical characterization of a novel library of aminoarylthiazoles (AAT) and VX-809 hybrid derivatives showing interesting properties as F508del-CFTR correctors[1].

This type of substitution proved to be efficient as shown by the related analogs of VX-809 previously mentioned, such as the congeners ALK-809 and SUL-809[150], VX-661 (Tezacaftor), successfully evaluated on patients in combination with VX-770, or a library of compounds synthesized coupling 1-(2,2-difluorobenzo[d] [1,3]-dioxol-5-yl)cyclopropanecarboxylic acid with various amine monomers, as described by Wang et al. [170].

The in-house set of compounds has been called "hybrid compounds" since their structures were a "hybrid" between the AAT and the VX-809 scaffolds. Among them, several analogs have been identified featuring EC_{50} values in terms of CFTR rescue ability comprised between 0.09 and 0.2 mM, with compound **2a** being the most active (EC_{50} 0.087 mM; pEC_{50} = 7.06). These data were very useful for designing and discovering a new library of optimized hybrids, exhibiting ameliorated potency values (EC_{50} values spanning from 0.02 to 0.1 μM; pEC_{50} = 7.69-6.00) been obtained through the modification of some groups on the main core of the compounds.

In particular, the molecular docking studies performed on the CFTR NBD1 to explore the putative binding mode of the hybrid compounds, previously in-depth analyzed in chapter 2 of this thesis, permitted to explore better the structure-activity relationship (SAR) within the hybrid series and to identified novel chemical substitutions on the thiazole ring. The mathematical QSAR model obtained in the previous study helps select the most promising compounds to be synthesized[1].

The following synthetic strategies united with the compounds' biochemical evaluation and the subsequent biological evaluation F508del-CFTR correctors validated the effectiveness of the hybrid core in the search for novel potent CFTR modulators. All results have offered novel SAR

information on hybrids as correctors and led to the identification of molecules with a particular ability to rescue F508del-CFTR.

4.1 Rationale

Our research group's previous QSAR analyses promoted the design of branched scaffolds enriched with flexible substituents and quite polar moieties within overall limited and bulky conformations. This information led to the design and synthesis of several hybrids endowed with a promising CFTR rescue ability, with **2a** being the most potent.

The subsequent step included preliminary docking studies at the NBD1 domain to guide the rational design of new analogs of the compound **2a**. These calculations have been previously discussed in chapter 2 by exploring the putative docking mode of VX-809 and the two highly related analogs, ALK-809 and SUL-809, chosen as further reference compounds. Briefly, the two oxygen atoms of the VX-809 benzodioxole core detect two H-bonds with the K464 and T465 while the negatively charged carboxylic group and the carbamide moiety of the corrector are H-bonded to the backbone of E656 and N659, respectively. Concerning ALK-809 and SUL-809, both the two congeners were engaged in one H-bond between the (sulfon)amide moiety and the backbone of E656 being the two oxygen atoms of the benzodioxole near K464 and T465. In addition, the amide group on the main core of the derivatives was H-bonded to N659 while the aromatic rings and all the substituents were placed in proximity of G461, V603, A655, and N659 residues.

Concerning the docking calculations performed on hybrid compounds revealed that for all of them, the carboxamide moiety is involved in one H-bond with N659, while the two oxygen atoms of the benzodioxole ring were H-bonded to K464 and T465. The most probable docking mode of the most potent compound **2a** (EC_{50} 0.087 μM; pEC_{50} = 7.06) proved to agree with VX-809 (POS2) and SUL-809.

The carboxamide moiety and the benzodioxole ring of the hybrid simulate the binding mode of VX-809 and for the related congener SUL-809, showing the same contacts. Overall, the thiazole ring proved to be good bioisosteres of the pyridine, maintaining the previously mentioned interactions with the biological target. Notably, hydrophobic interactions exhibited by the benzoic group of VX-809 and by the sulfonamide moiety of SUL-809 are experienced by the two aromatic rings tethered to the **2a** thiazole core. In contrast, the benzoyl group's oxygen atom interacts with

the E656 side-chain, as reported for the two reference compounds. These findings allowed us to explore the role played by different substitutions on the benzoyl moiety of **2a** and to clarify: (i) the relevance of hydrophobic and polar contacts, especially with Y577, (ii) the possibility of substitutions on the carbonyl function with other H-bond acceptor moieties tethered adequately to the thiazole core.

The step forward is represented by the chemical synthesis and biological evaluation of **2a** analogs concentrating on variations of the benzoyl core (compounds **7a-7z**, **12a-12d**, **24a-24c**) (pEC_{50} = 4.86-7.76), whose potency profile in terms of CFTR rescue ability have been predicted using the QSAR model that has previously built before synthesis.

4.1.2 Synthesis of new F508del-CFTR modulators

During my second year of my Ph.D., I continue my studies to research new F508del-CFTR modulators at the Center of Excellence of Biomedical Research (CEBR), under the supervision of Professor Enrico Millo. In this context, I applied the previous knowledge derived from computational studies to guide the synthesis of a library of 33 new hybrid derivatives (pEC_{50} = 4.86-7.76). In particular I synthesize ten hybrids, within the aforementioned cited thirty-three compounds (**7e; 7o; 7s; 7v; 7w; 7x;** pEC_{50} = 4.86-6.88 and **12a-12b**; pEC_{50} = 5.59-5.89)[171].

For the synthesis of all the compounds has been applied a well-known synthetic route with appropriate modifications. To obtain the benzodioxole substituted portion has been used the cyclopropanation of active methylene compounds. The substituted aminoarylthiazoles are synthesized differently depending on the substituents at position 5 of the thiazole ring.

For the general structures of (2-amino-4-arylthiazol-5-yl) (aryl) methanone derivatives, a convergent synthesis was established (Scheme 4.1) according to the Wang protocol apporting minimum variations. To obtain a selective introduction of the substituent groups on the thiazole ring, a protected carbamothioyl amide was conjugated with substituted α-bromoketone. A mixture of 1- [4- (methoxy)phenyl]methanamine 1 and 4-(methoxy)benzaldehyde 2 was heated in refluxing methanol to obtain bis((4-(methoxy) phenyl)methyl)amine 3.

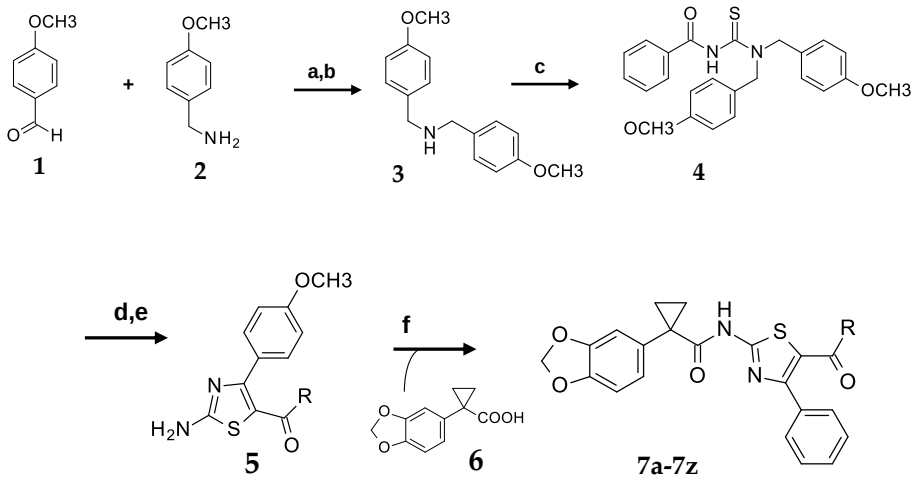

Scheme 4.1. **Reagents and conditions**: (a)methanol, reflux, 3h; (b)$NaBH_4$ 0°C to rt, 10h; (c) benzoylisothiocyanate, acetone, 0°C, 1h; (d) $RCOCH_2Br$, N,N-DMF, 85 °C, 3h; (e) TFA 80°C, 36h (f) HATU,DIPEA, N, N-DMF, 50 °C, 24h.

Protected carbamothioyl amide 4 was obtained by condensation of benzoylisothiocyanate and bis ((4-(methoxy) phenyl) methyl) amine 3 in high yield.

Condensation of protected carbamothioyl amide and α-haloketone followed by deprotection afforded the thiazolic derivatives 5, which were then further condensed with 1-(benzo[d] [1,3] dioxol-5-yl) cyclopropanecarboxylic acid 6 to produce the desired analogs **7a-7z**. This last synthetic step was reached by a 2-amino- thiazole reaction with the carboxylic group of cyclopropane carboxylic acid derivatives with uronium salt activation in anhydrous solvents.

A different synthetic route was applied for compound **12a** (Scheme 4.2). From ethyl 2-amino-4-arylthiazole-5-carboxylate 8, t-Boc protection at the aminic group was directed to minimize the thiazole ring's decarboxylation. To obtain the carboxamide derivative **10,** the appropriate 2- amino-thiazole-5-carboxylate 8 was treated with di-tert-butyl carbonate in the presence of 4-(N, N-dimethylamino)pyridine in tetrahydrofuran to produce the corresponding tert-butyl carbamate that upon basic hydrolysis afforded the acid **9**. Conversion of the carboxylic acid to its uronium salt using standard peptide coupling conditions and its subsequent treatment with aniline, in the presence of diisopropylethylamine in N,N-DMF gave the anilide derivative **10**. Further deprotection of the BOC-protecting group in trifluoroacetic acid afforded the aminothiazole **11**.

The final compound **12a** was obtained by condensation with the carboxylic group of cyclopropanecarboxylic acid derivative 6 as previously described.

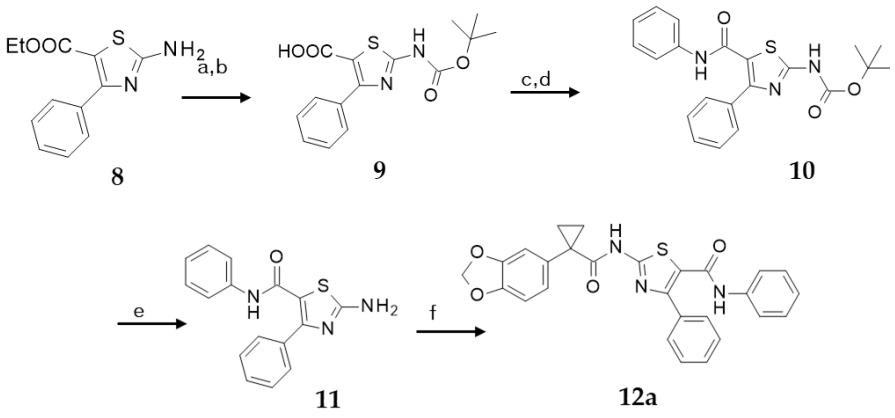

Scheme 4.2. Reagents and conditions: (a) Boc_2O, DMAP, THF, rt, 4h; (b) KOH 6 N, THF:EtOH = 1:15, 55 °C, 4h; (c) HATU, DIPEA, N, N-DMF, rt, 5 min; (d) $PhNH_2$, 40 °C, 2h; (e) TFA:DCM = 1:1, 0 °C, 4h; (f)6, HATU,DIPEA, N, N-DMF, 50 °C, 24h.

Another approach was used to prepare **12b**. N-(2-amino-4-(4- methoxyphenyl) thiazol-5-yl) benzamide was prepared, performing two-step synthesis starting from alfa-aminoacetophenone derivative **14** (Scheme 4.3). The starting reagent was prepared from 4- methoxyphenacyl bromide **13** following Delepine reaction (hexa- methylenetetramine in diethyl ether) as 4-methoxybenzoylmethylammonium chloride salt. Acylation of the amino functionality with benzoyl chloride advanced efficiently to provide N-(2-(4-methoxyphenyl)-2-oxoethyl) benzamide **15**. The low yield of this synthetic step is due to the difficulty of selectively monobromination of derivative **15** and isolating the respective unstable intermediate N-(1-Bromo 2-(4-methoxyphenyl)-2-oxoethyl) benzamide. But there was an increase in yield with the one-pot condensation of N-(2-(4-methoxyphenyl)-2-oxoethyl)benzamide with thiourea and iodine using triethylamine as catalyst under mild conditions [172]. The synthesis of amide derivatives of 2-aminothiazole was made by the condensation reaction of the 2-amino-thiazole with the carboxylic group of cyclopropanecarboxylic acid derivative 6 as previously described.

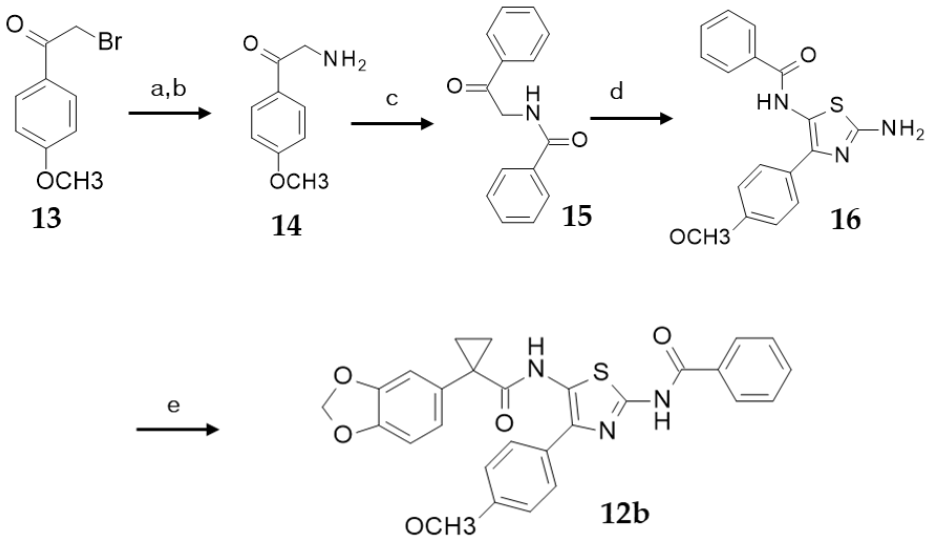

Scheme 4.3. **Reagents and conditions**: (a)hexamethylenetetramine, diethyl ether, rt, 2h; (b)HCl conc, EtOH, reflux, 3h; (c) C_6H_5COCl, $NaHCO_3$, THF, rt, 3h; (d)thiourea, I_2, EtOH, TEA, 80 °C, overnight; (e) HATU, DIPEA, N,N-DMF, 50 °C, 24h.

The synthesis of compounds **12c** and **12d** comprises a synthetic strategy hinged on a reaction between a substituted thiazole in position 5 and cyclopropanecarboxylic acid derivative. The functionalized thiazoles used for the substitution step were obtained, as shown in Scheme 44. Thiourea **17** was quantitatively activated as bis-thiazadiene **18** with an excess of N, N-dimethylformamide dimethylacetal in methanol. The thiazole ring was formed after the addition of the corresponding alfa-bromoketones **19a** and **19b** in THF. Intermediates **20a-20b** were deprotonated in situ, adding triethylamine. The second imine, used as a protecting group, was subsequently removed in situ with methylamine in water to form the expected products **21a** and **21b**. The final products **12c** and **12d** were obtained by condensation of the 2-amino-thiazole with the carboxylic group of cyclo- propanecarboxylic acid derivatives as previously described.

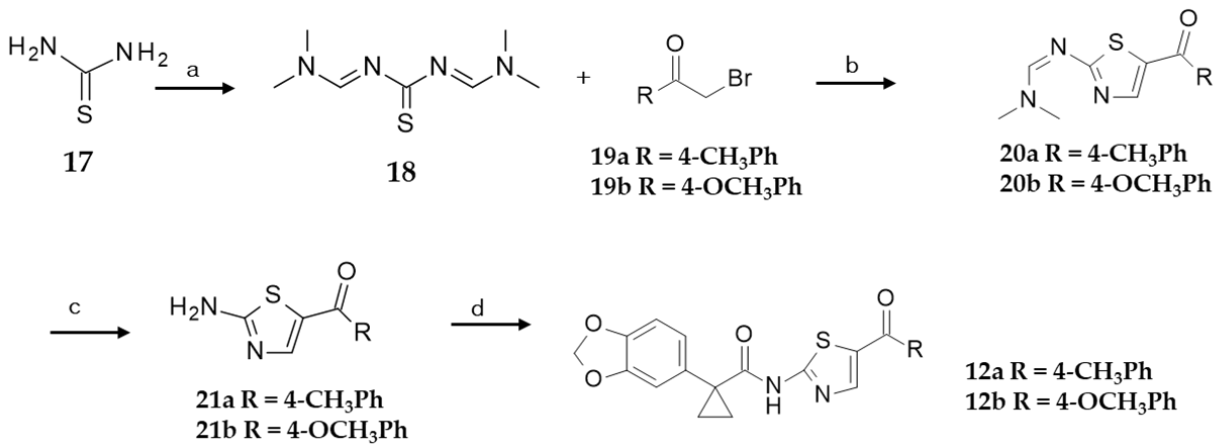

Scheme 4.4. **Reagents and conditions**: (a)N, N-Dymethyl formamide dimethyl acetate, DCM, reflux, 4h; (b)THF, rt to reflux, 18h; (c), 33% ac CH_3NH_2, THF, rt, 24h; (d) HATU, DIPEA, N,N-DMF, 50°C, 24 h.

To synthesize derivatives **24a, 24b, and 24c** have been applied the same synthetic route used in Scheme 4.1 but starting from aliphatic, heteroaromatic, and heterocycle haloketones **22a**, **22b 22c** (Scheme 4. 5).

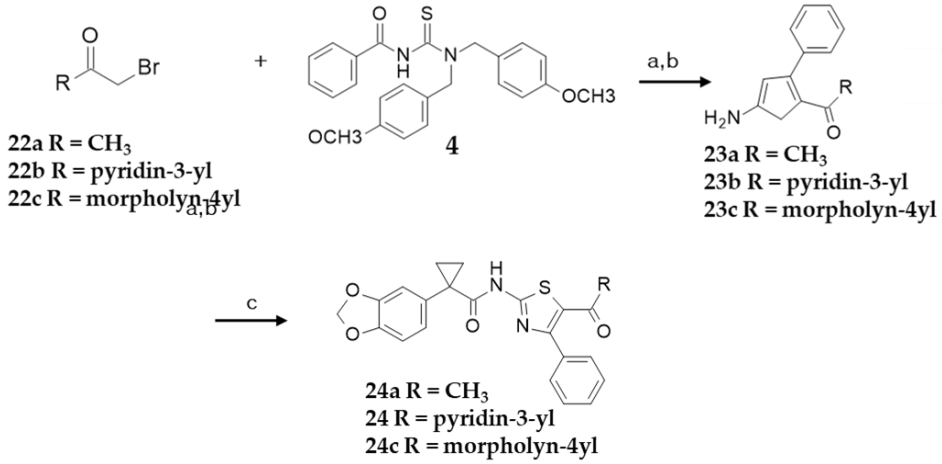

Scheme 4.5. Reagents and conditions: (a) N, N-DMF, 85 °C, 2 h; (b) TFA, 80 °C, 36 h; (c) 6, HATU, DIPEA, N,N-DMF, 50 °C, 18 h for 24a, 24 h for 24b and 24c.

4.1.3 Structure-activity relationship analysis of the new series of F508del-CFTR modulators

From the previous studies[1], in which the thiazolic ring was modified at different positions, our research group has identified that the most active compound **2a** (EC_{50} 0.087 μM; pEC_{50} = 7.06) was characterized by substitution at position 5 of the thiazole ring with benzoyl group and phenyl ring linked at the thiazole position 4. The substitution at position 5 of the thiazole ring is necessary for a good activity since the previous series's most active derivatives all contained a substituent at position 5. Indeed, the presence of a bulky substituent (benzoyl or ethyl acetate) at position 5 could be beneficial in increasing some pharmacokinetic characteristics, while the derivatives containing no substitution led to a reduction in corrector activity. First, removing the keto group present in the hit compound or substituting it with the amidic one led to a decrease in activity concerning the benzoyl analogs: compare **12a** (EC_{50} 1.26 μM; pEC_{50} = 5.89) and **12b** (EC_{50} 1.76 μM; pEC_{50} = 5.75) with **2a**.

For the comparative purpose, the phenyl ring at position 4 was kept intact. This substitution permitted the investigation of the substitutions at position 5 of the thiazole ring starting from the para position. Although several different electron-withdrawing groups were anchored at this position, such as a methylthio group **7a** (EC_{50} 0.10 μM; pEC_{50} = 8.00) or bromine **7b** (EC_{50} 0.53 μM; pEC_{50}= 6.27), only the first was tolerated and represented one of the most promising hybrids within this series. Regarding the compounds containing ester, carboxylic or amidic moieties, only the ethyl ester derivative **7c** maintains certain activity (EC_{50} =0.41 μM; pEC_{50} = 6.38) while the carboxylic derivative **7d** (EC_{50} = 7.31 μM; pEC_{50} = 5.13) led to a decrease in activity and finally the presence of the amidic group is very detrimental for activity.

To understand the para position's importance for F508del-CFTR rescue, electron-donating groups have been introduced in the same position.

The presence in this position of an alkyl amino group (**7f** (EC_{50}= 0.45 μM ; pEC_{50} = 6.34) or an alkyl moiety (**7g** (EC_{50}= 0.43 μM; pEC_{50} = 6.36) were not seen to improve the activity in a similar way the introduction of a methoxy group in **7h** not increase the activity (EC_{50} =0.45 μM; pEC_{50} = 6.34)). A comparable result was obtained also with a trifluoromethoxy group **7i** (EC_{50} = 0.36 μM; pEC_{50} = 6.44). Modifying the alkin chain's length to increase the hydrophobic portion led to derivative **7j** that present in substitution of the methyl group a propyl one that ameliorates the activity by about

five times (EC_{50} =0.017 μM; pEC_{50} = 7.76). Conversely, changing the propoxy group's position from para to meta position 7**k** (EC_{50}= 0.165 μM; pEC_{50} = 6.78) reduced the activity. This data suggest that there is a preference for hydrophobic groups. To further investigate this aspect has been used steric hindrance in the structures.

Subsequently, three different compounds were designed and built with a second aromatic ring like thiophene for **7l** (EC_{50} =1.06 μM; pEC_{50} = 5.97)) or phenyl for **7m** (EC_{50}= 0.07 μM; pEC_{50}= 7.15) or hetero aliphatic ring **7n** (EC_{50} =0.37 μM; pEC_{50} = 6.43). In this context, compound **7m** led to an increase in activity with an EC_{50} better than the reference compound 2a.

On the other hand, moving the methoxy group from the para **7h** to the ortho **7p** and the meta position **7q** led to a significant increase in activity (EC_{50} =0.14 μM; pEC_{50} = 6.85 and EC_{50}= 0.10 μM; pEC_{50} = 7.00).

Similar behavior was observed placing bromine in the meta position **7r** (EC_{50}= 0.18 μM; pEC_{50}= 6.74), which was revealed better than the para position. The bromine substitution with fluorine in the meta position caused increased potency in **7s** (EC_{50} =0.13 μM; pEC_{50} = 6.88).

Given the methoxy group's inclination for the meta/ortho substitution, two disubstituted analogs containing the methoxy group on the ortho position and the second one in the meta and para position, respectively (**7t** and **7u**), have been synthesized. notably, the 4-substitution wasn't well tolerated (EC_{50} =0.4 μM; pEC_{50} = 6.39), but the inclusion of a 3'-OCH_3 group afforded potent analogue (EC_{50}= 0.11 μM; pEC_{50} = 6.95).

Indeed, evaluating the molecules containing 3, 4-substituted benzoyl groups like **7v** (EC_{50} = 0.41 mM; pEC_{50} = 6.38 or **7w** (EC_{50}= 0.28 μM; pEC_{50} = 6.55), the substitution proved to be tolerated, especially with regard to the allyl moiety. Conversely, a high decline in activity was observed when one of these substituents was an amide group as in **7x** (EC_{50} = 13.7 μM; pEC_{50} = 4.86) and similarly with **7e.**

From the information furnished by this SAR, it was identified that an amide group was detrimental to activity.

All the compounds in the dataset contain at the 5 position only a benzoyl derivative. The insertion of a different keto group using aliphatic like methyl **24a**, heteroaromatic like pyridine **24b** and

heterocycle, morpholine in this case, **24c** in the same position proved that the only **24b** (EC_{50}= 0.79 μM; pEC_{50} = 6.10) had a certain activity while **24a** (EC_{50} =2.72 μM; pEC_{50} = 5.56) and overall **24c** (EC_{50}=8.5 μM ; pEC_{50} = 5.07) led to decreasing activity with respect to the progenitor (EC_{50} = 0.087 μM ; pEC_{50} = 7.06).

4.1.4 Biological assays

All designed compounds were then synthesized and tested to investigate the structure-activity relationships as correctors of F508del-CFTR.

The biological assays to test the compounds were performed at the U.O.C medical genetics at the Giannina Gaslini Institute in collaboration with Dr. Nicoletta Pedemonte.

This research group assayed the corrector's rescue ability F508del-CFTR using an electrophysiological technique: the transepithelial electrical resistance and potential difference measurements (TEER/PD). In this way, they proved the ability of the novel derivates to rescue F508del-CFTR on well-differentiated primary cultures of human bronchial epithelial cells from a CF patient homozygous for the F508del.

The two most potent derivatives, **7a** and **7m** have been tested. Epithelia were treated for 24 h with test compounds at different concentrations: **7a** (5-0.5-0.05 μM), **7m** (10 – 1-0.1 μM), VX-809 1 μM (as positive control), or vehicle alone (DMSO; negative control) and then assayed. Transepithelial electrical resistance was measured before and after stimulation with forskolin (20 μM) plus genistein (50 μM) to activate CFTR (Fig.4.1). Long-term treatment of CF primary epithelia with 7a and 7m significantly increased both CFTR-mediated conductance and equivalent short-circuit current.

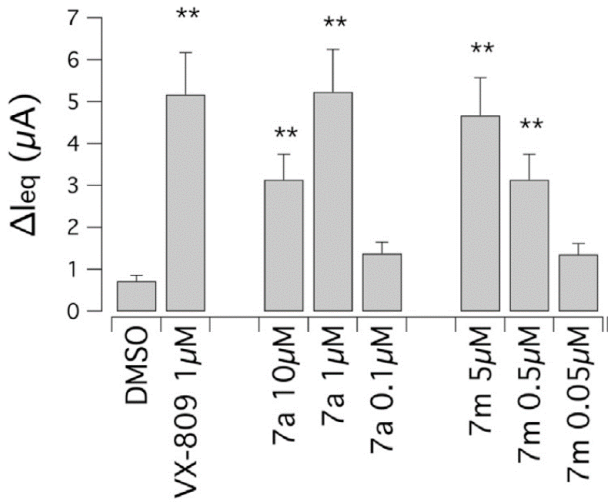

Fig.4.1. Bar graphs representing the delta between the values of electrical resistance measured before and after CFTR inhibition. Compounds 7a and 7m rescue F508del-CFTR activity in primary bronchial epithelia. In detail, the graph reports the equivalent short-circuit current (calculated from TEER/ PD measurements) in F508del/F508del bronchial epithelia, treated for 24 h with test compounds at the indicated concentration, or VX-809 (1 mM), or vehicle alone (DMSO).

Another assay used to analyze these compounds' structure-activity relationship is the YFP functional assay on F508del-CFTR CFBE41o- cells. This assay provides an incubation of 24 h at different concentrations to extrapolate the compounds' EC50 values as correctors of mutant CFTR. After incubation, the activity of F508del-CFTR in the plasma membrane was determined by measuring the rate of HS-YFP quenching caused by iodide influx. The activity was then compared to that of cells treated with vehicle alone (DMSO) or with the known corrector VX-809 (1 μM).

Then they evaluated the rescue of processing defect biochemically using the electrophoretic mobility of CFTR protein. In Western blots, CFTR protein is detected as two bands, named B and C. Band B corresponds to partially glycosylated CFTR residing in the ER, while band C is the mature CFTR that has passed through the Golgi. The prevalent form in cells expressing wild-type CFTR is band C. To evaluate the effect of hybrid compounds on CFTR electrophoretic mobility, they treat F508del-CFTR/HS-YFP expressing CFBE41o-cells with DMSO (vehicle alone) or test compounds **7m** and **7a** (0.5 μM) or **VX-809** (1 μM, as positive control). After an incubation of 24 h, cells were lysed, and lysates were subjected to SDS-PAGE followed by western blotting. Treatment of F508del-CFTR cells with corrector VX-809 significantly enhanced the expression of mature CFTR (band C), resulting in a change in the C band/B band ratio. Similarly, treatment with the compounds resulted in a significant increase in the C band/B band ratio, comparable to that obtained following treatment with VX-809 (Fig. 4.2).

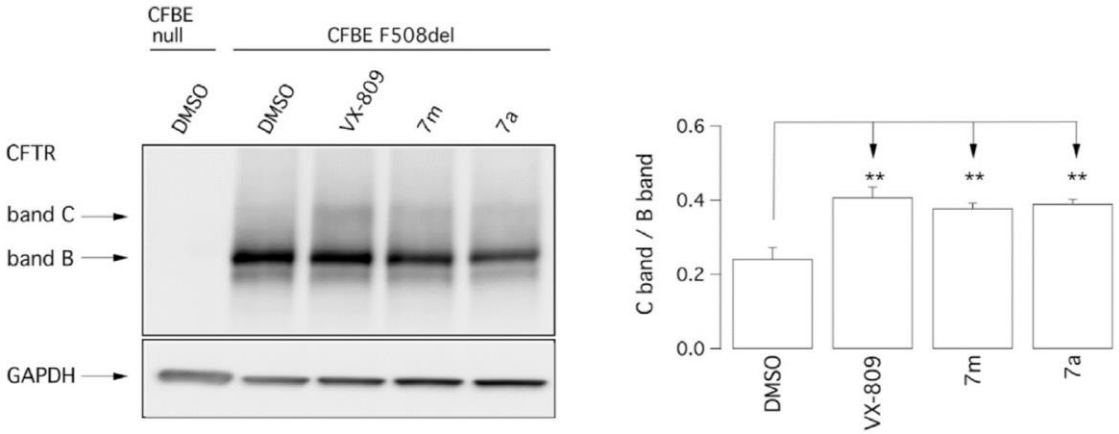

Fig.4.2. Biochemical analysis of the F508del-CFTR expression pattern. (*Left*) Electrophoretic mobility of F508del-CFTR in 2 different preparations of CFBE41o-cells, treated for 24 h with vehicle or test compounds (0.5 mM) or VX-809 (1 mM). Band C represents the complex-glycosylated; Band B represents the core-glycosylated forms of CFTR protein. (*Right*) The bar graph reports the densitometric analysis of band C/band B ratio normalized to GAPDH.

To characterize the biological activity of hybrid compounds, the compounds 7a, 7j, 7m were tested in combination with VX-809 and VX- 661 in CFBE41o-cells stably expressing F508del-CFTR using the YFP functional assay. Then, the cells were treated 24 h with single test compounds or their combinations and then assayed. No additive or synergistic effect was observed when combining **7a, 7j,** and **7m** with VX-809 or VX- 661, supporting the hypothesis that all these compounds possibly share the same binding site.

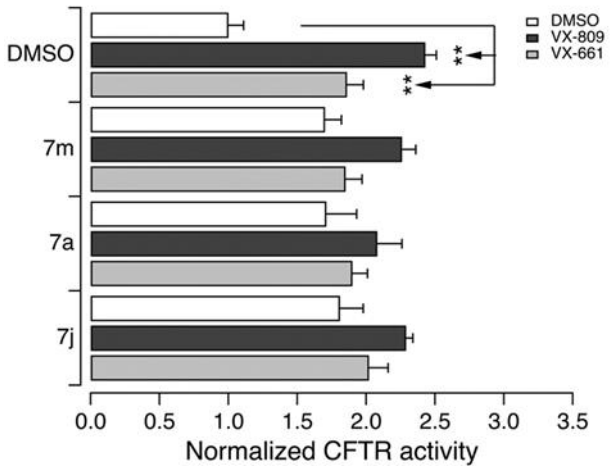

Fig.4.3. The F508del-CFTR activity was determined in CFBE41o− cells with the HS-YFP. Cells were treated with 7m (0.2 μM), 7a (1 μM), 7j (1 μM), VX-809 (1 μM), or VX-661 (10 μM), as single agents or as combinations.

CHAPTER 5. FINAL REMARKS

The rational design and study of useful modulators for CF treatment is tough due to the limited structural and experimental information on the complete F508del-CFTR protein. Furthermore, the mechanism of action of the F508del-modulators still needs to be clarified. In chapters 2 and 3 of this thesis, I wanted to emphasize how QSAR analysis is more predictive than the structure-based approach. The series of correctors allowed a very accurate prediction of their biological activity (expressed in terms of pEC_{50}) before their chemical synthesis.

Regarding potentiators, the available data of X-ray of wild-type CFTR in complex with the potentiators VX-770 and GLPG1837 guaranteed the reliable and feasible structure-based approach.

Conversely, the whole F508del-CFTR protein's limited experimental data quite impaired the reliability of the information coming from molecular docking approaches.

In this contest, experimental mutagenesis and molecular dynamics are urgently needed to clarify the modulators' putative mechanism of action.

The last chapter reported a new series of hybrids compounds, which their design has been helped by the computational studies mentioned above. Consequently, the second series of hybrids is synthesized from structural variations on the scaffold of the most active compound **2a**.

The following biological assays performed on all obtained compounds allowed us to verify the corrector ability as F508del-CFTR correctors and better explore their structure-activity relationships. Among these hybrids, the compounds **7j** and **7m** proved to be the most potent hybrids even if compared to the well-known corrector VX-809 (pEC_{50} = 5.59) and the compound 2a (pEC_{50} = 7.06).

Finally, the computational approaches applied during my Ph.D. years will continue with a new QSAR analysis that comprehended the new second hybrid compound series. This way permits our research group to design new reasonable structures to be synthesized and evaluated through biological assays. Furthermore, the structure of F508del-CFTR will be modeled to perform a structure-based study on the entire protein. Then, this model will be validated with known correctors. Regarding the synthesis of new aminothiazole hybrid derivatives, the most active compounds of the new library will be substituted in position 4 of the thiazole ring to study how

the substitution in 4 could affect the bioactivity of the molecules. Furthermore, the compounds will also be studied in combination with other correctors approved for Cystic Fibrosis, such as VX-445 and VX-661, and with the potentiator VX-770, to evaluate the best combination of drugs for CFTR protein rescue.

CHAPTER 6. EXPERIMENTAL SECTION

6.1 CHEMISTRY

Starting materials were purchased from Sigma Aldrich, Alfa Aesar, VWR, and Zentek. The analytical instrument used was Agilent 1260 high-performance liquid chromatography (HPLC). The analytical HPLC column was a Phenomenex C18 Luna.

The preparative HPLC was Agilent 1260 Infinity preparative HPLC and the column used for preparative chromatography was a Phenomenex C18 Luna. The analysis of the intermediates and the raw products was performed by liquid chromatography-electrospray mass spectrometry (HPLC-ESI-MS) using an Agilent 1100 series LC/MD ion trap instrument.

HRMS were performed using the Q Exactive Orbitrap instrument by Thermo Scientific.

The nuclear magnetic resonance (NMR) spectrometer was performed by Dr. Bruno Tasso at the Department of Pharmacy (DIFAR) at the University of Genoa, using a Varian Gemini 200 MHz. The proton spectra were acquired at 200 MHz, while carbon spectra were acquired at 50 MHz, at room temperature. Chemical shifts are reported in δ units (ppm) relative to TMS as an internal standard. Coupling constant (J) are reported in Hertz (Hz).

All the raw powders obtained were purified with preparative HPLC using the following gradient: from 0 to 5 min at 20% eluent B, then from 5 to 40 min to 100% eluent B, from 40 to 45 min at 100% of eluent B. eluant A was water with 0.1% formic acid (FOA) and eluent B was acetonitrile with 0.1% FOA. All analog submitted for testing were judged to be 95% or higher purity based on analytical HPLC/MS analysis. Compound purity was determined by integrating peak areas of the liquid chromatogram, monitored at 254 nm.

6.1.1 General procedure for the synthesis of the intermediate starting compound N-(bis(4-methoxybenzyl) carbamothioyl) benzamide for the synthesis of 7e- 7o-7s-7v-7w-7x derivatives.

A mixture of (4-methoxyphenyl) methanamine (535 μL, 4 mmol) and 4-(methoxy) benzaldehyde (595 μL, 4.8 mmol) in methanol (2 mL) was heated to reflux for 3 h, then cooled to T = 0 °C, $NaBH_4$ (228 mg, 6 mmol) was added portion-wise to the reaction. The resulting mixture was stirred at

room temperature for about 10 h. The solvent was removed under reduced pressure, and the residue was partitioned between ethyl acetate (EtOAc) and H_2O. The combined organic layers were washed with H_2O and then dried over anhydrous Na_2SO_4. After filtration, the solvent was removed in vacuum to afford bis [4-methoxyphenyl]methylamine (962 mg, 94%) as a colorless oil used in the next step without further purification. ESI-MS: m/z 258.0 $[M+H]^+$.

To a solution of benzoylisothiocyanate (140 µL, 1 mmol) in acetone (1 mL) cooled at T = 0 °C, bis [4-methoxyphenyl]methylamine (257 mg, 1 mmol) in acetone (1 mL) was added at this temperature and stirred for an additional 1 h. The mixture was concentrated under reduced pressure to afford N-(bis(4-methoxybenzyl) carbamothioyl)benzamide (398 mg, 95%) as yellow sticky oil, which was used in the next step without further purification. ESI-MS: m/z 421.0 $[M+H]^+$.

6.1.2 (7e): 4-(2-(1-(Benzo[d][1,3] dioxol-5-yl)cyclopropanecarboxamido)-4-phenylthiazole-5-carbonyl)-N-methilbenzamide

A solution of 4-(2-bromoacetyl)-N-methyl-benzamide methylbenzamide (128 mg, 0.5 mmol) and N-(bis(4-methoxybenzyl)carbamothioyl)-benzamide (210 mg, 0.5 mmol) in N, N-dimethylformamide (DMF) (3 mL) was stirred at T = 85 °C for 3h. After cooling to room temperature, the mixture was partitioned between EtOAc and H_2O. The organic layer was washed with brine and dried over anhydrous Na_2SO_4. After filtration, the solvent was removed in vacuum, and the residue was stirred in trifluoroacetic acid (TFA) (4 mL) at T = 80 °C for 24-36 h until complete deprotection. Most of TFA was removed under reduced pressure. The residue was then neutralized with $NaHCO_3$ 1N, and then extracted with EtOAc for 3 times. The combined organic layers were washed with brine and dried over anhydrous Na_2SO_4. After filtration, the solution was concentrated and further crystallized in acetonitrile to afford 4-(2-amino-4-phenylthiazole-5-carbonyl)-N-methylbenzamide (110 mg, 65%) as a brown oil. ESI-MS: m/z 337.09 $[M + H]^+$.

Benzo [1,3]dioxol-5-yl-cyclopropanecarboxylic acid (20.6 mg, 0.1 mmol) was resuspended in anhydrous DMF (1 mL); HATU (38 mg, 0.1 mmol) and DIPEA (35 µL, 0.2 mmol) were added. The reaction was vigorously stirred for 5 min and 4-(2-amino-4-phenylthiazole-5-carbonyl)-N-methylbenzamide (68 mg, 0.2 mmol) in anhydrous DMF (500 µL)was added. The reaction was kept at T= 50 °C until completeness (18-24 h) and then purified by preparative HPLC. The peak of interest was concentrated to obtain the title compound as brown oil with purity of >95% as determined by HPLC-MS (12 mg, 11%).

^{1}H NMR (200 MHz, DMSO-d6): δ 12.01 (s, 1H, broad, NH); 11.75 (s, broad, 1H, NH); 7.71e6.63 (m, 12H, arom); 6.03 (s, 2H OCH2O); 2.43 (s, 3H, CH3N); 1.72e1.46 (m, 2H, CH2, cyclopr); 1.42e1.11 (m,2H, CH2, cyclopr).

^{13}C NMR (50 MHz, DMSO-d6): δ 187.8, 172.3, 167.8, 154.1, 146.8, 146.3, 136.6, 131.8, 130.3, 129.3, 128.8, 128.1, 127.5, 123.2, 113.5, 110.2, 107.8, 100.6, 38.5, 30.3, 15.5.

HRMS (ESI) calculated for $C_{29}H_{24}N_3O_5S$:$[M + H]^+$ 526.14366; found 526.14343.

6.1.3 (7o) N-(5-([1,1'- Biphenyl] -3-carbonyl)-4-phenylthiazol-2-yl)-1-(benzo[d] [1,3] dioxol-5-yl)cyclopropanecarboxamide

A solution of 1-([1,1'-biphenyl]-3-yl)ethanone (196 mg, 1 mmol) was brominated with N-bromosuccinimide (NBS) providing [1,1'-biphenyl]-3-carbonyl bromide intermediate (202 mg, 73%). The purity was verified by HPLC-MS without further purification.

A solution of [1,1'-biphenyl]-3-carbonyl bromide (130 mg, 0.5 mmol) and N-(bis(4-methoxybenzyl)carbamothioyl)-benzamide (230 mg, 0.5 mmol) in N, N-dimethylformamide (DMF) (3 mL) was stirred at T = 85 °C for 3h. After cooling to room temperature, the mixture was partitioned between EtOAc and H_2O. The organic layer was washed with brine and dried over anhydrous Na_2SO_4. After filtration, the solvent was removed in vacuum and the residue was stirred in trifluoroacetic acid (TFA) (4 mL) at T = 80 °C for 24-36 h until complete deprotection. Most of the TFA was removed under reduced pressure. The residue was then neutralized with $NaHCO_3$ 1N, and then extracted with EtOAc for 3 times. The combined organic layers were washed with brine and dried over anhydrous Na_2SO_4. After filtration, the solution was concentrated and further crystallized in acetonitrile to afford [1,1'-biphenyl]-3-yl(2-amino-4-phenylthiazol-5-yl) methanone (60,5 mg, 34%) ESI-MS: m/z 357.1 $[M + H]^+$.

Benzo [1,3]dioxol-5-yl-cyclopropanecarboxylic acid (20.6 mg, 0.1 mmol) was resuspended in anhydrous DMF (1 mL); HATU (38 mg, 0.1 mmol) and DIPEA (35 μL, 0.2 mmol) were added. The reaction was vigorously stirred for 5 min and[1,1'-biphenyl]-3-yl(2-amino-4-phenylthiazol-5-yl) methanone (36 mg, 0.1 mmol) in anhydrous DMF (500 μL)was added. The reaction was kept at T= 50 °C until completeness (18-24 h) and then purified by preparative HPLC. The peak of interest was concentrated to obtain the title compound as pale yellow oil with purity of >95% as determined by HPLC-MS (12.5mg, 23%).

^{1}H NMR (200 MHz, DMSO-d6): δ 12.01 (s, 1H, broad, NH); 8.27e6.82 (m, 17H, arom); 6.04 (s, 2H OCH2O); 1.69e1.42 (m, 2H, CH2, cyclopr); 1.41e1.03 (m, 2H, CH2, cyclopr).

^{13}C NMR (50 MHz, DMSO-d6): δ 187.9, 171.8, 157.4, 153.3, 146.9, 146.3, 141.7, 137.8, 137.2, 131.3, 129.4, 128.8, 128.1, 127.5, 123.1, 110.2, 107.8, 100.6, 30.3, 15.6.

HRMS (ESI) calculated for $C_{33}H_{25}N_2O_4S$: $[M+H]^+$ 515.15349; found 545.15331.

6.1.4 (7s) 1-(Benzo[d] [1,3] dioxol-5-yl)-N-(5-(3-fluorobenzoyl)-4-phenylthiazol-2 yl)cyclopranecarboxamide

A solution of 2-Bromo-1-(3-fluorophenyl)ethan-1-one (108 mg, 0.5 mmol) and N-(bis(4-methoxybenzyl)carbamothioyl)-benzamide (210 mg, 0.5 mmol) in N, N-dimethylformamide (DMF) (3 mL) was stirred at T = 85 °C for 3h. After cooling to room temperature, the mixture was partitioned between EtOAc and H_2O. The organic layer was washed with brine and dried over anhydrous Na_2SO_4. After filtration, the solvent was removed in vacuum, and the residue was stirred in trifluoroacetic acid (TFA) (4 mL) at T = 80 °C for 24-36 h until complete deprotection. Most of the TFA was removed under reduced pressure. The residue was then neutralized with $NaHCO_3$ 1N, and then extracted with EtOAc for 3 times. The combined organic layers were washed with brine and dried over anhydrous Na_2SO_4. After filtration, the solution was concentrated and further crystallized in acetonitrile to afford (2-amino-4-phenyl-1,3-thiazol-5-yl)(3-fluorophenyl)methanone (90 mg, 60%) as a brown solid. ESI-MS: m/z 299.06 [M + H]+.

Benzo [1,3]dioxol-5-yl-cyclopropanecarboxylic acid (20.6 mg, 0.1 mmol) was resuspended in anhydrous DMF (1 mL); HATU (38 mg, 0.1 mmol) and DIPEA (35 µL, 0.2 mmol) were added. The reaction was vigorously stirred for 5 min and (2-amino-4-phenyl-5-yl)(3-fluorophenyl)methanone (30 mg, 0.2 mmol) in anhydrous DMF (500 µL)was added. The reaction was kept at T = 50 °C until completeness (18-24 h) and then purified by preparative HPLC. The peak of interest was concentrated to obtain the title compound as a white solid with a purity of >95% as determined by HPLC-MS (13 mg, 27%).

^{1}H NMR (200 MHz, DMSO-d6): δ 11.93 (s, 1H, broad, NH); 8.01e6.74 (m, 12H, arom); 6.05 (s, 2H OCH2O); 1.73e1.44 (m, 2H, CH2, cyclopr); 1.42e1.08 (m, 2H, CH2, cyclopr).

^{13}C NMR (50 MHz, DMSO-d6): δ 188.0, 171.5, 158.7, 156.2, 146.9, 146.3, 137.0, 133.4, 131.1, 129.7, 128.8, 128.2, 127.6, 123.2, 113.8, 110.2, 107.8, 100.6, 30.3, 15.5.

HRMS (ESI) calculated for $C_{27}H_{20}FN_2O_4S$: [M + H]+ 487.11277; found 487.11243.

6.1.5 (7v) 1-(Benzo[d][1,3] dioxol-5-yl)-N-(5-(3-chloro-4-methoxybenzoyl)-4-phenyltiazol-2yl)cyclopropanecarboxamide

A solution of 2-bromo-1-(3-chloro-4-methoxyphenyl)ethan-1-one (132 mg, 0.5 mmol) and N-(bis(4-methoxybenzyl)carbamothioyl)-benzamide (210 mg, 0.5 mmol) in N, N-dimethylformamide (DMF) (3 mL) was stirred at T = 85 °C for 3h. After cooling to room temperature, the mixture was partitioned between EtOAc and H_2O. The organic layer was washed with brine and dried over anhydrous Na_2SO_4. After filtration, the solvent was removed in vacuum and the residue was stirred in trifluoroacetic acid (TFA) (4 mL) at T = 80 °C for 24-36 h until complete deprotection. Most of the TFA was removed under reduced pressure. The residue was then neutralized with $NaHCO_3$ 1N, and then extracted with EtOAc for 3 times. The combined organic layers were washed with brine and dried over anhydrous Na_2SO_4. After filtration, the solution was concentrated and further crystallized in acetonitrile to afford (2-amino-4-phenyl-thiazol-5-yl)(3-chloro-4-methoxyphenyl)methanone (110 mg, 63%) as a brown solid. ESI-MS: m/z 345.04 [M + H]+.

Benzo [1,3]dioxol-5-yl-cyclopropanecarboxylic acid (20.6 mg, 0.1 mmol) was resuspended in anhydrous DMF (1 mL); HATU (38 mg, 0.1 mmol) and DIPEA (35 μL, 0.2 mmol) were added. The reaction was vigorously stirred for 5 min and (2-amino-4-phenyl-thiazol-5-yl)(3-chloro-4-methoxyphenyl)methanone (40 mg, 0.1 mmol) in anhydrous DMF (500 μL)was added. The reaction was kept at T= 50 °C until completeness (18-24 h) and then purified by preparative HPLC. The peak of interest was concentrated to obtain the title compound as a white solid with a purity of >95% as determined by HPLC-MS (14.5mg, 27%).

^{1}H NMR (200 MHz, DMSO-d6) δ 12.14 (s, 1H, NH); 8.03e6.75 (m,11H, arom); 6.06 (s, 2H,OCH2O); 3.77 (s, 3H, OCH3); 1.78e1.46 (m, 2H, CH2, cyclopr); 1.42e1.10 (m, 2H, CH2, cyclopr).

^{13}C NMR (50 MHz, DMSO-d6) δ 184.5, 171.5, 162.2, 156.8, 153.1, 146.8, 146.3, 140.5, 137.2,131.2,128.8, 128.2, 123.3, 118.1, 113.6,110.2, 107.7, 100.6, 55.3, 30.3, 15.6.

HRMS (ESI) calculated for $C_{28}H_{22}C_lN_2O_5S$: [M + H]+ 533.09379; found 533.09336.

6.1.6 (7w) N-(5-(3-allyl-4-hydroxybenzoyl)-4-phenylthiazol-2-yl)-1- (benzo[d][1,3]dioxol-5-yl) cyclopropanecarboxamide

A solution of 2-bromo-1-[4-hydroxy-3-(prop-2-en-1-yl)phenyl]ethan-1-one (128 mg, 0.5 mmol) and N-(bis(4-methoxybenzyl)carbamothioyl)-benzamide (210 mg, 0.5 mmol) in N, N-dimethylformamide (DMF) (3 mL) was stirred at T = 85 °C for 3h. After cooling to room temperature, the mixture was partitioned between EtOAc and H_2O. The organic layer was washed with brine and dried over anhydrous Na_2SO_4. After filtration, the solvent was removed in vacuum and the residue was stirred in trifluoroacetic acid (TFA) (4 mL) at T = 80 °C for 24-36 h until complete deprotection. Most of the TFA was removed under reduced pressure. The residue was then neutralized with $NaHCO_3$ 1N, and then extracted with EtOAc for 3 times. The combined organic layers were washed with brine and dried over anhydrous Na_2SO_4. After filtration, the solution was concentrated and further crystallized in acetonitrile to afford (3-allyl-4-hydroxyphenyl)(2-amino-4-phenylthiazol-5-yl)methanone (115 mg, 68%) as a brown solid. ESI-MS: m/z 345.04 [M + H]+.

Benzo [1,3]dioxol-5-yl-cyclopropanecarboxylic acid (20.6 mg, 0.1 mmol) was resuspended in anhydrous DMF (1 mL); HATU (38 mg, 0.1 mmol) and DIPEA (35 μL, 0.2 mmol) were added. The reaction was vigorously stirred for 5 min and (3-allyl-4-hydroxyphenyl)(2-amino-4-phenylthiazol-5-yl)methanone (34 mg, 0.1 mmol) in anhydrous DMF (500 μL)was added. The reaction was kept at T ¼ 50 °C until completeness (18-24 h) and then purified by preparative HPLC. The peak of interest was concentrated to obtain the title compound as brown solid with a purity of >95% as determined by HPLC-MS (10 mg, 19%).

^{1}H NMR (200 MHz, DMSO-d6) δ 12.02 (s, 1H, NH); 9.73 (s, 1H,OH); 7.88e6.72 (m, 11H, arom); 6.05 (s, 2H, OCH2O); 5.95e5.61 (m,1H, CH2CH]CH2); 4.92e4.68 (m, 2H, CH2CH]CH2); 3.18 (d, J ¼ 15.2, 2H, CH2CH]CH2); 1.77e1.43 (m, 2H, CH2, cyclopr);1.42e1.14 (m, 2H, CH2, cyclopr).

^{13}C NMR (50 MHz, DMSO-d6) δ 178.4, 170.5, 161.1, 156.2, 152.9,146.9, 146.3, 145.2, 136.9, 136.5, 131.2, 128.8, 128.3, 123.4, 114.2,110.2, 107.8, 100.6, 34.9, 30.3, 15.6.

HRMS (ESI) calculated for $C_{30}H_{25}N_2O_5S$: [M + H]+ 525.14841;found 525.14803.

6.1.7 (7z) 1-(Benzo[d][1,3dioxol-5-yl)-N-(5-(benzo[d][1, 3]dioxole-5- carbonyl)-4-phenylthiazol-2-yl) cyclopropanecarboxamide

A solution of 5-(bromoacetyl)-2-hydroxybenzamide (129 mg, 0.5 mmol) and N-(bis(4-methoxybenzyl)carbamothioyl)-benzamide (210 mg, 0.5 mmol) in N, N-dimethylformamide (DMF) (3 mL) was stirred at T = 85 °C for 3h. After cooling to room temperature, the mixture was partitioned between EtOAc and H_2O. The organic layer was washed with brine and dried over anhydrous Na_2SO_4. After filtration, the solvent was removed in vacuum and the residue was stirred in trifluoroacetic acid (TFA) (4 mL) at T = 80 °C for 24-36 h until complete deprotection. Most of the TFA was removed under reduced pressure. The residue was then neutralized with NaHCO3 1N, and then extracted with EtOAc for 3 times. The combined organic layers were washed with brine and dried over anhydrous Na_2SO_4. After filtration, the solution was concentrated and further crystallized in acetonitrile to afford 4-(2-amino-4-phenyl-1,3-thiazole-5-carbonyl)-2-hydroxybenzamide (90 mg, 53%) as a brown oil. ESI-MS: m/z 345.04 [M + H]+.

Benzo [1,3]dioxol-5-yl-cyclopropanecarboxylic acid (20.6 mg, 0.1 mmol) was resuspended in anhydrous DMF (1 mL); HATU (38 mg, 0.1 mmol) and DIPEA (35 μL, 0.2 mmol) were added. The reaction was vigorously stirred for 5 min and 4-(2-amino-4-phenyl-1,3-thiazole-5-carbonyl)-2-hydroxybenzamide (32.4 mg, 0.1 mmol) in anhydrous DMF (500 μL)was added. The reaction was kept at T = 50 °C until completeness (18-24 h) and then purified by preparative HPLC. The peak of interest was concentrated to obtain the title compound as brown oil with a purity of >95% as determined by HPLC-MS (15.5 mg, 30%).

^{1}H NMR (200 MHz, DMSO-d6) δ 12.08 (s, 1H, NH); 7.77e6.68 (m, 11H, arom); 6.07 (s, 2H, OCH2O); 6.03 (s, 2H, OCH2O); 1.64e1.41 (m, 2H, CH2, cyclopr); 1.41e1.00 (m, 2H, CH2, cyclopr).

^{13}C NMR (50 MHz, DMSO-d6) δ 178.8, 171.4, 159.3, 154.8, 151.5, 146.9, 146.3, 137.0, 131.2, 128.8, 128.1, 127.4, 123.2, 114.6, 110.3, 107.8, 100.6, 30.3, 15.4.

HRMS (ESI) calculated for $C_{28}H_{21}N_2O_6S$: [M + H]+ 513.11203; found 513.11187.

6.1.8 (12a) 2-(1-(Benzo[d][1,3]dioxol-5-yl)cyclopropanecarboxamido)- N,4-diphenylthiazole-5-carboxamide

A solution of ethyl 2-amino-4-phenylthiazole-5-carboxylate(248 mg, 1 mmol), di-tert-butyl carbonate (262 mg, 1.2 mmol) and catalytic 4-(N,N-dimethylamino) pyridine (8 mg, 0.07 mmol) in anhydrous THF (1 mL) was stirred for 4 h at room temperature. The mixture was concentrated under vacuum and after extraction with EtOAc (3 x 3 mL), washed with H2O (3 x 2 mL). The organic phases were dried over Na_2SO_4 and concentrated under vacuum. Crystallization in acetonitrile afford ethyl 2-((tert-butoxycarbonyl)amino)-4-phenylthiazole-5-carboxylate (170 mg, 49%) which was used in the next step without further purification. ESI-MS: m/z349.1 [M+H]+.

A solution of ethyl 2-((tert-butoxycarbonyl)amino)-4-phenylthiazole-5-carboxylate (170 mg, 0.49 mmol) in THF-EtOH(2.5 mL, 1:1.5) and 6 N aq KOH solution (1 mL) was heated at

T = 55 °C for 4 h. The solution was cooled to T = 0°C and acidified with conc. HCl to pH 1. The solution was then concentrated in vacuum, and after extraction with diethyl ether (3 x 3 mL), washed with H_2O (3 x 2 mL) and dried over anhydrous Na_2SO_4. After filtration, the solution was evaporated to obtain 2-[[(tert-butyloxy)carbonyl]-amino]-4-phenyl-1,3-thiazole-5-carboxylic acid (100 mg, 64%) as a brown solid. ESI-MS: m/z 321.1 [M+H]+.

The 2-[[(tert-butyloxy)carbonyl]-amino]-4-phenyl-1,3- thiazole-5-carboxylic acid (75 mg, 0.23 mmol) was resuspended in anhydrous DMF (1 mL), HATU (87 mg, 0.23 mmol) and DIPEA (40 μL, 0.23 mmol) were added. The reaction was vigorously stirred for 5 min and aniline (23 mL, 0.24 mmol) in anhydrous DMF (500 μL) was added. The reaction was kept at T = 40°C for 2 h. The solvent was removed under reduced pressure and the residue was partitioned between diethyl ether and water. The combined organic layers were washed with water (3 x 2 mL) and dried over anhydrous Na_2SO_4. After filtration, the solvent was removed in vacuum, and the residue was stirred in a mixture of TFA: DCM 1:1 (2 mL) at T = 0 °C until complete deprotection (4-5 h). Most of TFA was removed under reduced pressure. The residue was neutralized with NaHCO31 N and then extracted with EtOAc for 3 times. Crystallization in acetonitrile furnishes 2-amino-N,4-diphenylthiazole-5- carboxamide (30 mg, 44%). ESI-MS: m/z 296.1 [M+H]+.

Benzo [1,3]dioxol-5-yl-cyclopropanecarboxylic acid (20.5 mg,0.1 mmol) was resuspended in anhydrous DMF (1 mL); HATU (38 mg, 0.1 mmol) and DIPEA (18 μL, 0.1 mmol) were added. After 5 min, 2-amino-N, 4-diphenylthiazole-5-carboxamide (30 mg, 0.1 mmol) in anhydrous DMF (500 μL) was added. The reaction was kept at T = 50°C until completeness (about 24 h).

The mixture was concentrated under vacuum and after extraction with EtOAc (3 x 3 mL),washed with H_2O (3 x 2 mL). The organic phase was dried over Na_2SO_4, concentrated under reduced pressure and purified by preparative HPLC. The peak of interest was concentrated to obtain the title compound as white solid with purity of >95% as determined by HPLC-MS (10 mg, 21%).

^{1}H NMR (200 MHz, DMSO-d6): δ 12.08 (s, broad, 1H, NH); 10.63 (s, broad, 1H, NH); 7.79e6.75 (m, 13H, arom); 6.05 (s, 2H OCH2O);1.81e1.45 (m, 2H, CH2, cyclopr); 1.43e1.01 (m, 2H, CH2, cyclopr).

^{13}C NMR (50 MHz, DMSO-d6) δ 183.5, 165.5, 161.9, 151.0, 146.8, 146.3,137.9,137.0,129.2,128.9,128.7,128.0,127.5,121.6,116.0,110.8, 107.2, 101.2, 30.3, 15.6.

HRMS (ESI) calculated for $C_{27}H_{22}N_3O_4S$: [M + H]+ 484.13309; found 484.13277.

6.1.9 (12b) N-(2-(1-(Benzo[d][1,3]dioxol-5-yl) cyclopropanecarboxamido)-4-(4-methoxyphenyl)thiazol-5-yl) benzamide

To a stirred solution of 4-methoxyphenacyl bromide (229 mg, 1 mmol) in diethyl ether (2 mL) was added hexamethylenetetramine (140 mg, 1 mmol) all at once and the mixture was stirred for 2 h at room temperature. The resulting solid was centrifugated, washed with diethyl ether (2 mL), and dried under reduced pressure to afford the quaternary salt. To the compound, EtOH (2 mL) and conc. HCl (0.1 mL) were added and the mixture was refluxed for 3 h. After cooling to room temperature, the solid was centrifugated, washed with EtOH (3 x 2 mL), and dried under vacuum to afford pure 4-methoxy20amino-acetophenone hydrochloride in near quantitative yield. ESI-MS: m/z 202.6 [M+H]+.

$NaHCO_3$ (252 mg, 3 mmol) was added to a solution of 4-methoxy20amino-acetophenone hydrochloride (202 mg, 1 mmol) in anhydrous THF (2 mL) with stirring at room temperature. Benzoyl chloride (116 ml, 1 mmol) was added to the solution and stirred for about 3 h at room temperature. The solvent was removed under reduced pressure to leave a yellow oil. The product was extracted with dichloromethane (DCM) (3 x 3 mL) and washed with H_2O (3 x 2 mL). The

organic phase was dried over Na_2SO_4 and then concentrated under reduced pressure. Removal of the solvent produced the N-(2-(4-methoxyphenyl)-2-oxoethyl)benzamide as a white solid of sufficient purity to be used in the next step (202 mg, 75%). ESI-MS: m/z 269.1 [M+H]+.

N-(2-(4-methoxyphenyl)-2-oxoethyl)benzamide (107 mg, 0.4 mmol) and thiourea (30 mg, 0.4 mmol) were solved in EtOH at room temperature. To this solution I2 (101 mg, 0.4 mmol) and triethylamine (TEA) (11 ml, 0.2 mmol) were added. The reactions were stirred at T = 80°C overnight. The mixture was concentrated under vacuum and after extraction with EtOAc (3 x 3 mL), was washed with H_2O (3 x 2 mL). The organic layer was dried over anhydrous Na_2SO_4. After filtration, the solvent was removed in vacuum to obtain N-(2-amino-4-(4-methoxyphenyl)thiazol-5-yl) benzamide (40 mg, 31%). The thiazole was used without further purification. ESI-MS: m/z 325.1 [M+H]+.

Benzo [1,3]dioxol-5-yl-cyclopropanecarboxylic acid (25 mg, 0.12 mmol) was resuspended in anhydrous DMF (1 mL), HATU (45 mg, 0.12 mmol) and DIPEA (42 µL, 0.24 mmol) were added.

After 5 min, N-(2-amino-4-(4-methoxyphenyl)thiazol-5-yl)benzamide (40 mg, 0.12 mmol) in anhydrous DMF (500 µL) was added.

The reaction was kept at T = 50°C until completeness (about 24 h). The mixture was concentrated under vacuum and after extraction with EtOAc (3 x 3 mL), washed with H_2O (3 x 2 mL). The organic phase was dried over Na_2SO_4, concentrated under reduced pressure and purified by preparative HPLC. The peak of interest was concentrated to obtain the title compound as brown solid with a purity of >95% as determined by HPLC-MS (11 mg, 18%).

^{1}H NMR (200 MHz, DMSO-d6): δ 12.19 (s, broad, 1H, NH); 11.59 (s, broad, 1H, NH); 8.02e6.81 (m, 12H, arom); 6.04 (s, 2H OCH2O); 3.86 (s, 3H, OCH3); 1.78e1.44 (m, 2H, CH2, cyclopr); 1.41e1.08 (m, 2H, CH2, cyclopr).

^{13}C NMR (50 MHz, DMSO-d6) δ 180.8, 167.3, 160.5, 151.4, 146.9, 146.4, 137.8, 136.8, 129.2, 128.9, 128.1, 127.5, 121.7, 116.3, 110.8, 107.2, 101.2, 53.7, 30.3, 15.5.

HRMS (ESI) calculated for $C_{28}H_{24}N_3O_5S$: [M þ H]þ 514.14366; found 514.14359.

6.1.10 (12c) 1-(Benzo[d][1,3]dioxol-5-yl)-N-(5-(4-methylbenzoyl) thiazol-2-yl)cyclopropanecarboxamide

N,N-Dimethyl formamide dimethyl acetal (1036 mL, 7.8 mmol) was added to a suspension of thiourea (198 mg, 2.6 mmol) in DCM (2 mL). The mixture was heated at reflux for 4 h. The solvent was removed, and the residue was crystallized from diethyl ether to

obtain (1E, 10E)-N′,N′′-thiocarbonylbis (N,N-dimethylformimidamide) (400 mg, 83%). ESI-MS: m/z 187.1 (M + H) +.

(1E, 1′E)-N′,N′′-Thiocarbonylbis-(N,N-dimethylformimidamide (100 mg, 0.53 mmol) was suspended in THF (1 mL) and 2-bromo40-methylacetophenone (113 mg, 0.53 mmol) was added. The mixture was stirred at room temperature for 15 min and then TEA (147 mL,1.16 mmol) was added, and the mixture was heated at reflux for 18 h. The mixture was concentrated under vacuum and after extraction with EtOAc (3 x 3 mL), washed with H_2O (3 x 2 mL). The organic phase was dried over Na2SO4, concentrated under reduced pressure to obtain (Z)-N′-(5-(4-methylbenzoyl) thiazol-2-yl)-N,Ndimethylformimidamide(108 mg, 70%). ESI-MS: m/z 273.1(M + H) +.

A 33% (wt./wt.) aqueous methylamine (400 μL) was added to a solution of (Z)-N′-(5-(4-methylbenzoyl)thiazol-2-yl)-N,N-dimethylformimidamide (101 mg, 0,37 mmol) in THF (1 mL) and the mixture was stirred for 24 h at room temperature. The mixture was concentrated under vacuum and after extraction with EtOAc (3 x 3 mL), washed with H_2O (3 x 2 mL). The organic phase was dried over Na_2SO_4, concentrated under reduced pressure to obtain a pale yellow oil. Crystallization in acetonitrile furnishes (2-aminothiazol-5-yl) (p-tolyl)methanone (36 mg, 45%). ESI-MS: m/z 219.1 [M+H]+.

Benzo [1,3]dioxol-5-yl-cyclopropanecarboxylic acid (33 mg, 0.16 mmol) was resuspended in anhydrous DMF (1 mL), HATU (61 mg, 0.16 mmol) and DIPEA (56 μL, 0.16 mmol) were added. After 5 min, (2-aminothiazol-5-yl) (p-tolyl) methanone (35 mg, 0.16 mmol) in anhydrous DMF (500 μL) was added. The reaction was kept at T = 50 °C until completeness (about 24 h).

The mixture was concentrated under vacuum and after extraction with EtOAc (3 x 3 mL),washed with H_2O (3 x 2 mL). The organic phase was dried over Na_2SO_4, concentrated under reduced pressure and purified by preparative HPLC. The peak of interest was concentrated to obtain the title compound as pale yellow solid with purity of >95% as determined by HPLC-MS (32.4 mg, 50%).

^1H NMR (200 MHz, DMSO-d6): d 11.87 (s, broad, 1H, NH); 8.05 (s,1H, arom); 7.81e6.78 (m, 7H, arom); 6.04 (s, 2H OCH2O); 2.32 (s,3H, CH3); 1.81e1.42 (m, 2H, CH2, cyclopr); 1.41e1.00 (m, 2H, CH2,cyclopr).

^{13}C NMR (50 MHz, DMSO-d6) d 186.2, 173.6, 146.8, 146.3, 137.0,133.1, 129.6, 129.1, 121.3, 110.8, 107.2, 101.2, 30.3, 24.6, 15.5.

HRMS (ESI) calculated for $C_{22}H_{19}N_2O_4S$: [M + H]+ 407.10654; found 407.10608.

6.1.11 (12d) 1-(Benzo[d][1,3]dioxol-5-yl)-N-(5-(4-methoxybenzoyl) thiazol yl)cyclopropanecarboxamide

(1E, 1'E)-N',N''-Thiocarbonylbis-N,N-dimethylformimidamide (100 mg, 0.53 mmol) was suspended in DCM (1 mL) and 2-bromo- 40-methoxyacetophenone (121 mg, 0.53 mmol) was added. The mixture was stirred at room temperature for 15 min and then TEA (147 µL,1.16 mmol)was added. The mixture was heated at reflux for about 20 h. At the end of the reaction the solution was concentrated under vacuum and after extraction with EtOAc (3 x 3 mL), washed with H_2O (3 x 2 mL). The organic phase was dried over Na_2SO_4, concentrated under reduced pressure to obtain (Z)-N'-(5-(4-methoxybenzoyl) thiazol-2-yl)-N,N-dimethylformimidamide (108 mg, 70%).

ESI-MS: m/z 290.1 [M+H]+.

A 33% (wt./wt.) aqueous methylamine (600 µL) was added to a solution of (Z)-N'-(5-(4-methoxybenzoyl)thiazol-2-yl)-N,N-dimethylformimidamide (108 mg, 0.37 mmol) in THF (1 mL) and the mixture was stirred for 24 h at room temperature. The solution was then concentrated under vacuum and after extraction with EtOAc (3 x 3 mL), washed with H_2O (3 x 2 mL). The organic phase was dried over Na_2SO_4, concentrated under reduced pressure to obtain a yellow oil.

Crystallization in acetonitrile furnishes (2-aminothiazol-5-yl) (4-methoxyphenyl)methanone (46 mg, 53%). MS ESI-MS: m/z 235.1 [M+H]+.

Benzo [1,3]dioxol-5-yl-cyclopropanecarboxylic acid (39 mg, 0.19 mmol) was resuspended in anhydrous DMF (1 mL), HATU (72 mg, 0.19 mmol) and DIPEA (66 μL, 0.19 mmol) were added. After 5 min, (2-aminothiazol-5-yl) (4-methoxyphenyl)methanone (45 mg, 0.19 mmol) in anhydrous DMF (500 μL) was added. The reaction was kept at T = 50°C until completeness (about 36 h). The mixture was concentrated under vacuum and after extraction with EtOAc (3 x 3 mL),washed with H_2O (3 x 2 mL). The organic phase was dried over Na_2SO_4, concentrated under reduced pressure and purified by preparative HPLC. The peak of interest was concentrated to obtain the title compound as brown solid with purity of >95% as determined by HPLC-MS (26.6 mg, 33%).

^{1}H NMR (200 MHz, DMSO-d6): δ 11.87 (s, broad, 1H, NH); 8.08 (s,1H, arom); 7.79e6.81 (m, 7H, arom); 6.04 (s, 2H OCH2O); 3.89 (s,3H, CH3); 1.78e1.41 (m, 2H, CH2, cyclopr); 1.40e1.03 (m, 2H, CH2,cyclopr).

^{13}C NMR (50 MHz, DMSO-d6) δ 182.7, 171.9, 146.9, 146.3, 137.1,133.0, 129.7, 128.8, 121.4, 110.8, 107.2, 101.2, 55.9, 30.3, 15.5.

HRMS (ESI) calculated for $C_{22}H_{19}N_2O_5S$: [M + H]+ 423.10146; found 423.10098.

6.2 BIOLOGICAL ASSAYS

6.2.1. Cell culture

The bronchial epithelial cell line CFBE41o-with stable coexpression of F508del-CFTR and the halide-sensitive yellow fluorescent protein (HS-YFP) was cultured with MEM medium supplemented with 10% fetal calf serum, 2 mM L-glutamine, 100 U/mL penicillin, and 100 mg/mL streptomycin.

6.2.2. Fluorescence assay for CFTR activity

CFBE41o-cells with the expression of mutant CFTR and HS-YFP were plated on clear-bottom 96-well black microplates at a density of 50,000 cells/well and kept at 37°C in 5% CO2 for 24 h. For the corrector assay, CFBE41o-cells were treated for a further 24 h with compounds and/or VX-809 or VX-661. After treatment, the culture medium was removed and cells in each well were stimulated for 30 min at 37°C with 60 mL PBS (containing 137 mM NaCl, 2.7 mM KCl, 8.1 mM Na2HPO4, 1.5 mM KH2PO4, 1 mM CaCl2, and 0.5 mM MgCl2) plus forskolin (20 μM) and genistein (50 μM).

At the time of assay, microplates carrying CFBE41o-cells were transferred to a microplate reader. The plate reader was equipped with high-quality excitation and emission

filters for YFP. The assay consisted of a continuous 14 s fluorescence reading with 2 s before and 12 s after injection of an iodide containing solution (165 mL of a modified PBS containing I- instead of Cl-; final I- concentration in the well: 100 mM). To determine fluorescence quenching rate associated with I- influx, the final 10 s of data for each well were fitted with an exponential function to extrapolate the initial slope (dF/dt). Dose-response relationships from each experiment were fitted to calculate EC50, maximal effect, and Hill coefficient.

6.2.3. Transepithelial electrical resistance (TEER) evaluation

Primary bronchial epithelial cells obtained from one patient with CF (homozygous for F508del mutation) were seeded at high density on porous membranes for transepithelial

electrical resistance (TEER). To test putative correctors, compounds were added to the basolateral medium for 24 h at 37°C and 5% CO2 before measuring the TEER. Control epithelia were treated with vehicle alone (DMSO). TEER was measured in each well under basal conditions, after ENaC

inhibition with apical amiloride (10 μM), after CFTR stimulation with forskolin (10 μM) and genistein (50 μM) on both sides, and after CFTR inhibition with apical PPQ102 (30 μM).

6.2.4. Biochemical analysis of CFTR expression pattern

CFBE41o-cells stably expressing mutant CFTR and HS-YFP were grown to confluence on 60-mm diameter dishes and treated for 24 h with test compounds or vehicle alone. After 24 h, cells were lysed in RIPA buffer containing a complete protease inhibitor. Cell lysates were subjected to centrifugation at 12000 rpm at 4°C for 10min. Equal amounts of protein (10 mg) were separated onto gradient (4-15%), transferred to a nitrocellulose membrane, and analyzed by Western blotting. Proteins were detected using monoclonal anti-CFTR or mouse monoclonal anti-GAPDH followed by horseradish peroxidase (HRP)-conjugated anti-mouse IgG (Abcam), and subsequently visualized by chemiluminescence.

REFERENCES

1. Liessi, N. *et al.* Synthesis and biological evaluation of novel thiazole- VX-809 hybrid derivatives as F508del correctors by QSAR-based filtering tools. *Eur. J. Med. Chem.* (2018) doi:10.1016/j.ejmech.2017.12.030.

2. Rogan, M. P., Stoltz, D. A. & Hornick, D. B. Cystic fibrosis transmembrane conductance regulator intracellular processing, trafficking, and opportunities for mutation-specific treatment. *Chest* (2011) doi:10.1378/chest.10-2077.

3. Meng, X., Clews, J., Martin, E. R., Ciuta, A. D. & Ford, R. C. The structural basis of cystic fibrosis. *Biochem. Soc. Trans.* **46**, 1093–1098 (2018).

4. Bhatt, J. M. Treatment of pulmonary exacerbations in cystic fibrosis. *European Respiratory Review* (2013) doi:10.1183/09059180.00006512.

5. Bhatt, J. M. Treatment of pulmonary exacerbations in cystic fibrosis. *Eur. Respir. Rev.* **22**, 205–216 (2013).

6. Castellani, C. & Massie, J. Newborn screening and carrier screening for cystic fibrosis: Alternative or complementary. *European Respiratory Journal* (2014) doi:10.1183/09031936.00125613.

7. Fajac, I. & De Boeck, K. New horizons for cystic fibrosis treatment. *Pharmacology and Therapeutics* (2017) doi:10.1016/j.pharmthera.2016.11.009.

8. Cohen-Cymberknoh, M., Shoseyov, D. & Kerem, E. Managing cystic fibrosis: Strategies that increase life expectancy and improve quality of life. *American Journal of Respiratory and Critical Care Medicine* (2011) doi:10.1164/rccm.201009-1478CI.

9. MacKenzie, T. *et al.* Longevity of patients with cystic fibrosis in 2000 to 2010 and beyond: Survival analysis of the Cystic Fibrosis Foundation Patient Registry. *Ann. Intern. Med.* (2014) doi:10.7326/M13-0636.

10. ANDERSEN, D. H. CYSTIC FIBROSIS OF THE PANCREAS AND ITS RELATION

TO CELIAC DISEASE. *Am. J. Dis. Child.* (1938) doi:10.1001/archpedi.1938.01980140114013.

11. Farber, S., Shwachman, H. & Maddock, C. L. PANCREATIC FUNCTION AND DISEASE IN EARLY LIFE. I. PANCREATIC ENZYME ACTIVITY AND THE CELIAC SYNDROME 1. *J. Clin. Invest.* (1943) doi:10.1172/jci101456.

12. HOWARD, P. J. FAMILIAL CHARACTER OF FIBROCYSTIC DISEASE OF THE PANCREAS. *Arch. Pediatr. Adolesc. Med.* (1944) doi:10.1001/archpedi.1944.02020110031007.

13. ANDERSEN, D. H. & HODGES, R. G. Celiac syndrome; genetics of cystic fibrosis of the pancreas, with a consideration of etiology. *Am. J. Dis. Child.* (1946) doi:10.1001/archpedi.1946.02020300069004.

14. Farinha, C. M. CFTR and Cystic Fibrosis. in (2018). doi:10.1007/978-3-319-65494-2_1.

15. PM, Q. Chloride impermeability in cystic fibrosis. *Nature* **301**, 421–2 (1983).

16. Riordan, J. R. *et al.* Identification of the cystic fibrosis gene: Cloning and characterization of complementary DNA. *Science (80-.).* **245**, 1066–1073 (1989).

17. Kerem, B. S. *et al.* Identification of the cystic fibrosis gene: Genetic analysis. *Science (80-.).* (1989) doi:10.1126/science.2570460.

18. Cutting, G. R. Cystic fibrosis genetics: From molecular understanding to clinical application. *Nature Reviews Genetics* (2015) doi:10.1038/nrg3849.

19. Cunningham, G. F. *et al. Williams Obstetrics 25Th Edition*. *Mc Graw Hill Education* (2018).

20. Dodge, J. A. & Ryley, H. C. Screening for cystic fibrosis. *Arch. Dis. Child.* (1982) doi:10.1136/adc.57.10.774.

21. Durie, P. R. *et al.* Plasma immunoreactive pancreatic cationic trypsinogen in cystic

fibrosis: A sensitive indicator of exocrine pancreatic dysfunction. *Pediatr. Res.* (1981) doi:10.1203/00006450-198110000-00010.

22. Crossle, J. R., Elliot, R. B. & Smith, P. A. DRIED-BLOOD SPOT SCREENING FOR CYSTIC FIBROSIS IN THE NEWBORN. *Lancet* (1979) doi:10.1016/S0140-6736(79)90825-0.

23. Simpson, N. *et al.* The cost-effectiveness of neonatal screening for cystic fibrosis: An analysis of alternative scenarios using a decision model. *Cost Eff. Resour. Alloc.* (2005) doi:10.1186/1478-7547-3-8.

24. Quinton, P. M. Chloride impermeability in cystic fibrosis. *Nature* (1983) doi:10.1038/301421a0.

25. LeGrys, V. A., Yankaskas, J. R., Quittell, L. M., Marshall, B. C. & Mogayzel, P. J. Diagnostic Sweat Testing: The Cystic Fibrosis Foundation Guidelines. *Journal of Pediatrics* (2007) doi:10.1016/j.jpeds.2007.03.002.

26. Hammond, K. B., Turcios, N. L. & Gibson, L. E. Clinical evaluation of the macroduct sweat collection system and conductivity analyzer in the diagnosis of cystic fibrosis. *J. Pediatr.* (1994) doi:10.1016/S0022-3476(94)70314-0.

27. Moskowitz, S. M. *et al.* Clinical practice and genetic counseling for cystic fibrosis and CFTR-related disorders. *Genetics in Medicine* (2008) doi:10.1097/GIM.0b013e31818e55a2.

28. Therrell, B. L. *et al.* Current status of newborn screening worldwide: 2015. *Seminars in Perinatology* (2015) doi:10.1053/j.semperi.2015.03.002.

29. Wagener, J. S., Zemanick, E. T. & Sontag, M. K. Newborn screening for cystic fibrosis. *Current Opinion in Pediatrics* (2012) doi:10.1097/MOP.0b013e328353489a.

30. Legrys, V. A., McColley, S. A., Li, Z. & Farrell, P. M. The need for quality improvement in sweat testing infants after newborn screening for cystic fibrosis. *J.*

Pediatr. (2010) doi:10.1016/j.jpeds.2010.07.053.

31. Bagheri-Hanson, A., Nedwed, S., Rueckes-Nilges, C. & Naehrlich, L. Intestinal current measurement versus nasal potential difference measurements for diagnosis of cystic fibrosis: A case-control study. *BMC Pulm. Med.* (2014) doi:10.1186/1471-2466-14-156.

32. Bienvenu, T. & Nguyen-Khoa, T. Current and future diagnosis of cystic fibrosis: Performance and limitations. *Arch. Pediatr.* (2020) doi:10.1016/S0929-693X(20)30046-4.

33. Rosenstein, B. J. & Cutting, G. R. The diagnosis of cystic fibrosis: A consensus statement. *J. Pediatr.* (1998) doi:10.1016/S0022-3476(98)70344-0.

34. HOLLAND, I. B. INTRODUCTION TO BACTERIAL ABC PROTEINS. in *ABC Proteins* (2003). doi:10.1016/b978-012352551-2/50009-3.

35. Jordan, I. K., Kota, K. C., Cui, G., Thompson, C. H. & McCarty, N. A. Evolutionary and functional divergence between the cystic fibrosis transmembrane conductance regulator and related ATP-binding cassette transporters. *Proc. Natl. Acad. Sci. U. S. A.* (2008) doi:10.1073/pnas.0806306105.

36. Sheppard, D. N. & Welsh, M. J. Structure and function of the CFTR chloride channel. *Physiological Reviews* (1999) doi:10.1152/physrev.1999.79.1.S23.

37. Vergani, P., Lockless, S. W., Nairn, A. C. & Gadsby, D. C. CFTR channel opening by ATP-driven tight dimerization of its nucleotide-binding domains. *Nature* (2005) doi:10.1038/nature03313.

38. Saint-Criq, V. & Gray, M. A. Role of CFTR in epithelial physiology. *Cell. Mol. Life Sci.* **74**, 93–115 (2017).

39. Shamsuddin, A. K. M. & Quinton, P. M. Native small airways secrete bicarbonate. *Am. J. Respir. Cell Mol. Biol.* (2014) doi:10.1165/rcmb.2013-0418OC.

40. Stoltz, D. A., Meyerholz, D. K. & Welsh, M. J. Origins of Cystic Fibrosis Lung Disease. *N. Engl. J. Med.* (2015) doi:10.1056/nejmra1300109.

41. Liu, F., Zhang, Z., Csanády, L., Gadsby, D. C. & Chen, J. Molecular Structure of the Human CFTR Ion Channel. *Cell* **169**, 85-95.e8 (2017).

42. Dahan, D. *et al.* Regulation of the CFTR channel by phosphorylation. in *Pflugers Archiv European Journal of Physiology* (2001). doi:10.1007/s004240100652.

43. Moran, O. The gating of the CFTR channel. *Cell. Mol. Life Sci.* **74**, 85–92 (2017).

44. Hoelen, H. *et al.* The primary folding defect and rescue of δf508 CFTR emerge during translation of the mutant domain. *PLoS One* (2010) doi:10.1371/journal.pone.0015458.

45. Sadlish, H. & Skach, W. R. Biogenesis of CFTR and other polytopic membrane proteins: New roles for the ribosome-translocon complex. *Journal of Membrane Biology* (2004) doi:10.1007/s00232-004-0715-6.

46. Yang, Y., Janich, S., Cohn, J. A. & Wilson, J. M. The common variant of cystic fibrosis transmembrane conductance regulator is recognized by hsp70 and degraded in a pre-Golgi nonlysosomal compartment. *Proc. Natl. Acad. Sci. U. S. A.* **90**, 9480–9484 (1993).

47. Riordan, J. R. CFTR function and prospects for therapy. *Annual Review of Biochemistry* (2008) doi:10.1146/annurev.biochem.75.103004.142532.

48. Pind, S., Riordan, J. R. & Williams, D. B. Participation of the endoplasmic reticulum chaperone calnexin (p88, IP90) in the biogenesis of the cystic fibrosis transmembrane conductance regulator. *J. Biol. Chem.* (1994).

49. Cheung, J. C. & Deber, C. M. Misfolding of the cystic fibrosis transmembrane conductance regulator and disease. *Biochemistry* (2008) doi:10.1021/bi702209s.

50. Turnbull, E. L., Rosser, M. F. N. & Cyr, D. M. The role of the UPS in cystic fibrosis.

BMC Biochemistry (2007) doi:10.1186/1471-2091-8-S1-S11.

51. Welsh, M. J. & Smith, A. E. Molecular mechanisms of CFTR chloride channel dysfunction in cystic fibrosis. *Cell* (1993) doi:10.1016/0092-8674(93)90353-R.

52. Amaral, M. D. Novel personalized therapies for cystic fibrosis: Treating the basic defect in all patients. *J. Intern. Med.* (2015) doi:10.1111/joim.12314.

53. Veit, G. *et al.* From CFTR biology toward combinatorial pharmacotherapy: Expanded classification of cystic fibrosis mutations. *Mol. Biol. Cell* **27**, 424–433 (2016).

54. Boyle, M. P. & De Boeck, K. A new era in the treatment of cystic fibrosis: Correction of the underlying CFTR defect. *The Lancet Respiratory Medicine* (2013) doi:10.1016/S2213-2600(12)70057-7.

55. Zielenski, J. & Tsui, L. C. Cystic fibrosis: Genotypic and phenotypic variations. *Annual Review of Genetics* (1995) doi:10.1146/annurev.ge.29.120195.004021.

56. Sheppard, D. N. *et al.* Mutations in CFTR associated with mild-disease-form Cl- channels with altered pore properties. *Nature* (1993) doi:10.1038/362160a0.

57. Hämmerle, M. M., Aleksandrov, A. A. & Riordan, J. R. Disease-associated Mutations in the Extracytoplasmic Loops of Cystic Fibrosis Transmembrane Conductance Regulator Do Not Impede Biosynthetic Processing but Impair Chloride Channel Stability. *J. Biol. Chem.* (2001) doi:10.1074/jbc.M011017200.

58. Haardt, M., Benharouga, M., Lechardeur, D., Kartner, N. & Lukacs, G. L. C-terminal truncations destabilize the cystic fibrosis transmembrane conductance regulator without impairing its biogenesis. A novel class of mutation. *J. Biol. Chem.* **274**, 21873–21877 (1999).

59. Meng, X., Clews, J., Kargas, V., Wang, X. & Ford, R. C. The cystic fibrosis transmembrane conductance regulator (CFTR) and its stability. *Cellular and Molecular Life Sciences* (2017) doi:10.1007/s00018-016-2386-8.

60. Du, K., Sharma, M. & Lukacs, G. L. The ΔF508 cystic fibrosis mutation impairs domain-domain interactions and arrests post-translational folding of CFTR. *Nat. Struct. Mol. Biol.* (2005) doi:10.1038/nsmb882.

61. Qu, B.-H. & Thomas, P. J. Alteration of the Cystic Fibrosis Transmembrane Conductance Regulator Folding Pathway. *J. Biol. Chem.* (1996) doi:10.1074/jbc.271.13.7261.

62. Lukacs, G. L. & Verkman, A. S. CFTR: Folding, misfolding and correcting the ΔF508 conformational defect. *Trends in Molecular Medicine* (2012) doi:10.1016/j.molmed.2011.10.003.

63. Bompadre, S. G., Sohma, Y., Li, M. & Hwang, T. C. G551D and G1349D, two CF-associated mutations in the signature sequences of CFTR, exhibit distinct gating defects. *J. Gen. Physiol.* (2007) doi:10.1085/jgp.200609667.

64. Dérand, R., Bulteau-Pignoux, L. & Becq, F. Comparative pharmacology of the activity of wild-type and G551D mutated CFTR chloride channel: Effect of the benzimidazolone derivative NS004. *J. Membr. Biol.* (2003) doi:10.1007/s00232-003-2030-z.

65. Bompadre, S. G., Li, M. & Hwang, T. C. Mechanism of G551D-CFTR (cystic fibrosis transmembrane conductance regulator) potentiation by a high affinity ATP analog. *J. Biol. Chem.* (2008) doi:10.1074/jbc.M709417200.

66. Gibson, R. L., Burns, J. L. & Ramsey, B. W. Pathophysiology and Management of Pulmonary Infections in Cystic Fibrosis. *American Journal of Respiratory and Critical Care Medicine* (2003) doi:10.1164/rccm.200304-505SO.

67. Alton, E. W. F. W. *et al.* Genetic medicines for CF: Hype versus reality. *Pediatric Pulmonology* (2016) doi:10.1002/ppul.23543.

68. Griesenbach, U., Pytel, K. M. & Alton, E. W. F. W. Cystic Fibrosis Gene Therapy in

the UK and Elsewhere. *Hum. Gene Ther.* (2015) doi:10.1089/hum.2015.027.

69. Griesenbach, U. & Alton, E. W. F. W. Recent advances in understanding and managing cystic fibrosis transmembrane conductance regulator dysfunction. *F1000Prime Rep.* (2015) doi:10.12703/P7-64.

70. Wilschanski, M. & Kerem, E. New drugs for cystic fibrosis. *Expert Opinion on Investigational Drugs* (2011) doi:10.1517/13543784.2011.600304.

71. Ashlock, M. A. & Olson, E. R. Therapeutics development for cystic fibrosis: A successful model for a multisystem genetic disease. *Annu. Rev. Med.* (2011) doi:10.1146/annurev-med-061509-131034.

72. Cuthbert, A. W. New horizons in the treatment of cystic fibrosis. *British Journal of Pharmacology* (2011) doi:10.1111/j.1476-5381.2010.01137.x.

73. Lai, H. C. J. Classification of nutritional status in cystic fibrosis. *Current Opinion in Pulmonary Medicine* (2006) doi:10.1097/01.mcp.0000245709.66762.f9.

74. Zemel, B. S., Jawad, A. F., FitzSimmons, S. & Stallings, V. A. Longitudinal relationship among growth, nutritional status, and pulmonary function in children with cystic fibrosis: Analysis of the Cystic Fibrosis Foundation National CF Patient Registry. *J. Pediatr.* (2000) doi:10.1067/mpd.2000.107891.

75. Sheikh, S., Zemel, B. S., Stallings, V. A., Rubenstein, R. C. & Kelly, A. Body composition and pulmonary function in cystic fibrosis. *Front. Pediatr.* (2014) doi:10.3389/fped.2014.00033.

76. Van Sambeek, L., Cowley, E. S., Newman, D. K. & Kato, R. Sputum glucose and glycemic control in cystic fibrosis-related diabetes: A cross-sectional study. *PLoS One* (2015) doi:10.1371/journal.pone.0119938.

77. Lanng, S., Thorsteinsson, B., Nerup, J. & Koch, C. Diabetes mellitus in cystic fibrosis: Effect of insulin therapy on lung function and infections. *Acta Paediatr. Int. J.*

Paediatr. (1994) doi:10.1111/j.1651-2227.1994.tb13156.x.

78. Fuchs, H. J. *et al.* Effect of Aerosolized Recombinant Human DNase on Exacerbations of Respiratory Symptoms and on Pulmonary Function in Patients with Cystic Fibrosis. *N. Engl. J. Med.* (1994) doi:10.1056/nejm199409083311003.

79. Robert, G., Stevens, A. & Colin-Jones, D. Dornase alfa for cystic fibrosis. *BMJ* (1995) doi:10.1136/bmj.311.7008.813.

80. Amin, R. *et al.* The effect of dornase alfa on ventilation inhomogeneity in patients with cystic fibrosis. *Eur. Respir. J.* (2011) doi:10.1183/09031936.00072510.

81. Suresh Babu, K., Kastelik, J. & Morjaria, J. B. Role of long term antibiotics in chronic respiratory diseases. *Respiratory Medicine* (2013) doi:10.1016/j.rmed.2013.02.009.

82. Konstan, M. W., Byard, P. J., Hoppel, C. L. & Davis, P. B. Effect of High-Dose Ibuprofen in Patients with Cystic Fibrosis. *N. Engl. J. Med.* (1995) doi:10.1056/nejm199503303321303.

83. Elkins, M. R. *et al.* A Controlled Trial of Long-Term Inhaled Hypertonic Saline in Patients with Cystic Fibrosis. *N. Engl. J. Med.* (2006) doi:10.1056/nejmoa043900.

84. Ramsey, W. B., Pepe, M. S. & Quan, J. M. Intermittent administration of inhaled tobramycin in patients with cvstic fibrosis. *Pneumologie* (1999) doi:10.1056/nejm199901073400104.

85. Assael, B. M. *et al.* Inhaled aztreonam lysine vs. inhaled tobramycin in cystic fibrosis: A comparative efficacy trial. *J. Cyst. Fibros.* (2013) doi:10.1016/j.jcf.2012.07.006.

86. Edmondson, C. & Davies, J. C. Current and future treatment options for cystic fibrosis lung disease: Latest evidence and clinical implications. *Therapeutic Advances in Chronic Disease* (2016) doi:10.1177/2040622316641352.

87. Guimbellot, J., Sharma, J. & Rowe, S. M. Toward inclusive therapy with CFTR modulators: Progress and challenges. *Pediatric Pulmonology* (2017)

doi:10.1002/ppul.23773.

88. Merkert, S. *et al.* High-Throughput Screening for Modulators of CFTR Activity Based on Genetically Engineered Cystic Fibrosis Disease-Specific iPSCs. *Stem Cell Reports* **12**, 1389–1403 (2019).

89. Giuliano, K. A. *et al.* Use of a High-Throughput Phenotypic Screening Strategy to Identify Amplifiers, a Novel Pharmacological Class of Small Molecules That Exhibit Functional Synergy with Potentiators and Correctors. *SLAS Discov.* **23**, 111–121 (2018).

90. Clancy, J. P. *et al.* Results of a phase IIa study of VX-809, an investigational CFTR corrector compound, in subjects with cystic fibrosis homozygous for the F508del-CFTR mutation. *Thorax* (2012) doi:10.1136/thoraxjnl-2011-200393.

91. Pollock, N. L., Rimington, T. L. & Ford, R. C. Characterizing diverse orthologues of the cystic fibrosis transmembrane conductance regulator protein for structural studies. *Biochem. Soc. Trans.* (2015) doi:10.1042/BST20150081.

92. Lewis, H. A. *et al.* Structure of nucleotide-binding domain 1 of the cystic fibrosis transmembrane conductance regulator. *EMBO J.* (2004) doi:10.1038/sj.emboj.7600040.

93. Atwell, S. *et al.* Structures of a minimal human CFTR first nucleotide-binding domain as a monomer, head-to-tail homodimer, and pathogenic mutant. *Protein Eng. Des. Sel.* (2010) doi:10.1093/protein/gzq004.

94. Aller, S. G. *et al.* Structure of P-glycoprotein reveals a molecular basis for poly-specific drug binding. *Science (80-.).* (2009) doi:10.1126/science.1168750.

95. Dawson, R. J. P. & Locher, K. P. Structure of a bacterial multidrug ABC transporter. *Nature* (2006) doi:10.1038/nature05155.

96. Ward, A., Reyes, C. L., Yu, J., Roth, C. B. & Chang, G. Flexibility in the ABC transporter MsbA: Alternating access with a twist. *Proc. Natl. Acad. Sci. U. S. A.*

(2007) doi:10.1073/pnas.0709388104.

97. Mornon, J. P., Lehn, P. & Callebaut, I. Atomic model of human cystic fibrosis transmembrane conductance regulator: Membrane-spanning domains and coupling interfaces. *Cell. Mol. Life Sci.* **65**, 2594–2612 (2008).

98. Serohijos, A. W. R. *et al.* Phenylalanine-508 mediates a cytoplasmic-membrane domain contact in the CFTR 3D structure crucial to assembly and channel function. *Proc. Natl. Acad. Sci. U. S. A.* **105**, 3256–3261 (2008).

99. Dalton, J., Kalid, O., Schushan, M., Ben-Tal, N. & Villà-Freixa, J. New model of cystic fibrosis transmembrane conductance regulator proposes active channel-like conformation. *J. Chem. Inf. Model.* (2012) doi:10.1021/ci2005884.

100. Corradi, V., Vergani, P. & Tieleman, D. P. Cystic fibrosis transmembrane conductance regulator (CFTR):closedandopenstate channelmodels. *J. Biol. Chem.* (2015) doi:10.1074/jbc.M115.665125.

101. Zhang, Z. & Chen, J. Atomic Structure of the Cystic Fibrosis Transmembrane Conductance Regulator. *Cell* (2016) doi:10.1016/j.cell.2016.11.014.

102. Ford, B. CFTR structure: Lassoing cystic fibrosis. *Nature Structural and Molecular Biology* (2017) doi:10.1038/nsmb.3353.

103. Zhang, Z., Liu, F. & Chen, J. Conformational Changes of CFTR upon Phosphorylation and ATP Binding. *Cell* **170**, 483-491.e8 (2017).

104. Ehrhardt, A. *et al.* Channel gating regulation by the cystic fibrosis transmembrane conductance regulator (CFTR) first cytosolic loop. *J. Biol. Chem.* (2016) doi:10.1074/jbc.M115.704809.

105. McClure, M. L., Barnes, S., Brodsky, J. L. & Sorscher, E. J. Trafficking and function of the cystic fibrosis transmembrane conductance regulator: A complex network of posttranslational modifications. *American Journal of Physiology - Lung Cellular and*

Molecular Physiology (2016) doi:10.1152/ajplung.00431.2015.

106. Lopes-Pacheco, M. CFTR Modulators: The Changing Face of Cystic Fibrosis in the Era of Precision Medicine. *Frontiers in Pharmacology* (2020) doi:10.3389/fphar.2019.01662.

107. Quon, B. S. & Rowe, S. M. New and emerging targeted therapies for cystic fibrosis. *BMJ* **352**, 1–14 (2016).

108. Kleizen, B., Van Vlijmen, T., De Jonge, H. R. & Braakman, I. Folding of CFTR is predominantly cotranslational. *Mol. Cell* (2005) doi:10.1016/j.molcel.2005.09.007.

109. Cheng, S. H. *et al.* Defective intracellular transport and processing of CFTR is the molecular basis of most cystic fibrosis. *Cell* **63**, 827–834 (1990).

110. Mijnders, M., Kleizen, B. & Braakman, I. Correcting CFTR folding defects by small-molecule correctors to cure cystic fibrosis. *Current Opinion in Pharmacology* (2017) doi:10.1016/j.coph.2017.09.014.

111. H., H. *et al.* The primary folding defect and rescue of deltaf508 CFTR emerge during translation of the mutant domain. *PLoS ONE* (2010).

112. Lukacs, G. L. *et al.* Conformational maturation of CFTR but not its mutant counterpart (ΔF508) occurs in the endoplasmic reticulum and requires ATP. *EMBO J.* (1994) doi:10.1002/j.1460-2075.1994.tb06954.x.

113. Ward, C. L., Omura, S. & Kopito, R. R. Degradation of CFTR by the ubiquitin-proteasome pathway. *Cell* (1995) doi:10.1016/0092-8674(95)90240-6.

114. Balch, W. E., Roth, D. M. & Hutt, D. M. Emergent properties of proteostasis in managing cystic fibrosis. *Cold Spring Harb. Perspect. Biol.* **3**, 1–16 (2011).

115. Loo, T. W., Bartlett, M. C. & Clarke, D. M. Corrector VX-809 stabilizes the first transmembrane domain of CFTR. *Biochem. Pharmacol.* (2013) doi:10.1016/j.bcp.2013.06.028.

116. Bobadilla, J. L., Macek, M., Fine, J. P. & Farrell, P. M. Cystic fibrosis: A worldwide analysis of CFTR mutations - Correlation with incidence data and application to screening. *Hum. Mutat.* **19**, 575–606 (2002).

117. Okiyoneda, T. *et al.* Mechanism-based corrector combination restores ΔF508-CFTR folding and function. *Nat. Chem. Biol.* (2013) doi:10.1038/nchembio.1253.

118. Van Goor, F. *et al.* Correction of the F508del-CFTR protein processing defect in vitro by the investigational drug VX-809. *Proc. Natl. Acad. Sci. U. S. A.* **108**, 18843–18848 (2011).

119. Taylor-Cousar, J. L. *et al.* Tezacaftor–Ivacaftor in Patients with Cystic Fibrosis Homozygous for Phe508del. *N. Engl. J. Med.* (2017) doi:10.1056/nejmoa1709846.

120. van Koningsbruggen-Rietschel, S. Novel treatment modalities for cystic fibrosis. *Pneumologe* (2019) doi:10.1007/s10405-018-0220-8.

121. Davies, J. C. *et al.* VX-659–Tezacaftor–Ivacaftor in Patients with Cystic Fibrosis and One or Two Phe508del Alleles. *N. Engl. J. Med.* (2018) doi:10.1056/nejmoa1807119.

122. Van Goor, F. *et al.* Rescue of CF airway epithelial cell function in vitro by a CFTR potentiator, VX-770. *Proc. Natl. Acad. Sci. U. S. A.* **106**, 18825–18830 (2009).

123. Ramsey, B. W. *et al.* A CFTR Potentiator in Patients with Cystic Fibrosis and the G551D Mutation . *N. Engl. J. Med.* (2011) doi:10.1056/nejmoa1105185.

124. Bompadre, S. G. *et al.* CFTR gating I: Characterization of the ATP-dependent gating of a phosphorylation-independent CFTR channel (ΔR-CFTR). *J. Gen. Physiol.* (2005) doi:10.1085/jgp.200409227.

125. Sheppard, D. N., Bear, C. E. & de Jonge, H. R. Editorial overview: Respiratory: Transformational therapies for cystic fibrosis. *Current Opinion in Pharmacology* (2017) doi:10.1016/j.coph.2017.11.006.

126. Eckford, P. D. W., Li, C., Ramjeesingh, M. & Bear, C. E. Cystic fibrosis

transmembrane conductance regulator (CFTR) potentiator VX-770 (ivacaftor) opens the defective channel gate of mutant CFTR in a phosphorylationdependent but ATP-independent manner. *J. Biol. Chem.* **287**, 36639–36649 (2012).

127. Jih, K. Y. & Hwang, T. C. Vx-770 potentiates CFTR function by promoting decoupling between the gating cycle and ATP hydrolysis cycle. *Proc. Natl. Acad. Sci. U. S. A.* **110**, 4404–4409 (2013).

128. Flume, P. A. *et al.* Ivacaftor in subjects with cystic fibrosis who are homozygous for the F508del-CFTR mutation. *Chest* **142**, 718–724 (2012).

129. Ren, H. Y. *et al.* VX-809 corrects folding defects in cystic fibrosis transmembrane conductance regulator protein through action on membrane-spanning domain 1. *Mol. Biol. Cell* **24**, 3016–3024 (2013).

130. Clancy, J. P. Rapid therapeutic advances in CFTR modulator science. *Pediatr. Pulmonol.* **53**, S4–S11 (2018).

131. Wainwright, C. E. *et al.* Lumacaftor–Ivacaftor in Patients with Cystic Fibrosis Homozygous for Phe508del CFTR . *N. Engl. J. Med.* (2015) doi:10.1056/nejmoa1409547.

132. Talamo Guevara, M. & McColley, S. A. The safety of lumacaftor and ivacaftor for the treatment of cystic fibrosis. *Expert Opinion on Drug Safety* (2017) doi:10.1080/14740338.2017.1372419.

133. Rowe, S. M. *et al.* Tezacaftor–Ivacaftor in Residual-Function Heterozygotes with Cystic Fibrosis. *N. Engl. J. Med.* (2017) doi:10.1056/nejmoa1709847.

134. Kirby, T. Tezacaftor-ivacaftor is safe and efficacious in patients with cystic fibrosis with Phe508del mutations. *The Lancet. Respiratory medicine* (2018) doi:10.1016/S2213-2600(17)30439-3.

135. H., H. *et al.* Phase 3 efficacy and safety of the ELX/TEZ/ iva triple combination in

people with CF homozygous for the F508del mutation. *Pediatr. Pulmonol.* (2019).

136. Heijerman, H. G. M. *et al.* Efficacy and safety of the elexacaftor plus tezacaftor plus ivacaftor combination regimen in people with cystic fibrosis homozygous for the F508del mutation: a double-blind, randomised, phase 3 trial. *Lancet* (2019) doi:10.1016/S0140-6736(19)32597-8.

137. FDA approves new breakthrough therapy for cystic fibrosis. *Case Med. Res.* (2019) doi:10.31525/cmr-1fc997b.

138. Trimble, A. T. & Donaldson, S. H. Ivacaftor withdrawal syndrome in cystic fibrosis patients with the G551D mutation. *J. Cyst. Fibros.* **17**, e13–e16 (2018).

139. Fukuda, R. & Okiyoneda, T. Cystic fibrosis transmembrane conductance regulator (CFTR) ubiquitylation as a novel pharmaceutical target for cystic fibrosis. *Pharmaceuticals* **13**, (2020).

140. Lobo, M., Amaral, M. D. & Farinha, C. M. EPAC1 (exchange protein activated by cyclic amp) is a novel player in CFTR regulation by cyclic amp at the cell surface. *Pediatr. Pulmonol.* (2014).

141. Alshafie, W., Chappe, F. G., Li, M., Anini, Y. & Chappe, V. M. VIP regulates CFTR membrane expression and function in Calu-3 cells by increasing its interaction with NHERF1 and P-ERM in a VPAC1- and PKCε-dependent manner. *Am. J. Physiol. - Cell Physiol.* **307**, 107–119 (2014).

142. Zaman, K. *et al.* S-nitrosothiols increases cystic fibrosis transmembrane regulator expression and maturation in the cell surface. *Biochem. Biophys. Res. Commun.* (2014) doi:10.1016/j.bbrc.2013.12.130.

143. Donaldson, S. H. *et al.* Pharmacokinetics and safety of cavosonstat (N91115) in healthy and cystic fibrosis adults homozygous for F508DEL-CFTR. *J. Cyst. Fibros.* **16**, 371–379 (2017).

144. Pranke, I. *et al.* Factors influencing readthrough therapy for frequent cystic fibrosis premature termination codons. *ERJ Open Res.* **4**, 00080–02017 (2018).

145. Prayle, A., Watson, A., Fortnum, H. & Smyth, A. Side effects of aminoglycosides on the kidney, ear and balance in cystic fibrosis. *Thorax* **65**, 654–658 (2010).

146. Kerem, E. *et al.* Effectiveness of PTC124 treatment of cystic fibrosis caused by nonsense mutations: a prospective phase II trial. *Lancet* (2008) doi:10.1016/S0140-6736(08)61168-X.

147. Kym, P. R., Wang, X., Pizzonero, M. & Van der Plas, S. E. *Recent Progress in the Discovery and Development of Small-Molecule Modulators of CFTR*. *Progress in Medicinal Chemistry* vol. 57 (Elsevier B.V., 2018).

148. Righetti, G. *et al.* Molecular docking and QSAR studies as computational tools exploring the rescue ability of F508DEL CFTR correctors. *Int. J. Mol. Sci.* (2020) doi:10.3390/ijms21218084.

149. Rusnati, M. *et al.* Recent strategic advances in CFTR drug discovery: An overview. *Int. J. Mol. Sci.* **21**, (2020).

150. Sinha, C. *et al.* Capturing the Direct Binding of CFTR Correctors to CFTR by Using Click Chemistry. *ChemBioChem* (2015) doi:10.1002/cbic.201500123.

151. Odolczyk, N. *et al.* Discovery of novel potent ΔF508-CFTR correctors that target the nucleotide binding domain. *EMBO Mol. Med.* (2013) doi:10.1002/emmm.201302699.

152. Rusnati, M. *et al.* Speeding up the identification of cystic fibrosis transmembrane conductance regulator-targeted drugs: An approach based on bioinformatics strategies and surface plasmon resonance. *Molecules* **23**, (2018).

153. Zhang, Z., Liu, F. & Chen, J. Molecular structure of the ATP-bound, phosphorylated human CFTR. *Proc. Natl. Acad. Sci. U. S. A.* **115**, 12757–12762 (2018).

154. Hall, J. D. *et al.* Binding screen for cystic fibrosis transmembrane conductance

regulator correctors finds new chemical matter and yields insights into cystic fibrosis therapeutic strategy. *Protein Sci.* (2016) doi:10.1002/pro.2821.

155. Farinha, C. M. *et al.* Revertants, low temperature, and correctors reveal the mechanism of F508del-CFTR rescue by VX-809 and suggest multiple agents for full correction. *Chem. Biol.* (2013) doi:10.1016/j.chembiol.2013.06.004.

156. Chiaw, P. K., Wellhauser, L., Huan, L. J., Ramjeesingh, M. & Bear, C. E. A chemical corrector modifies the channel function of F508del-CFTR. *Mol. Pharmacol.* (2010) doi:10.1124/mol.110.065862.

157. Connett, G. J. Lumacaftor-ivacaftor in the treatment of cystic fibrosis: Design, development and place in therapy. *Drug Des. Devel. Ther.* **13**, 2405–2412 (2019).

158. MOE. (Molecular Operating Environment). *Scientific Computing & Instrumentation* (2009).

159. Edelsbrunner, H., Facello, M., Fu, P. & Liang, J. Measuring proteins and voids in proteins. in *Proceedings of the Annual Hawaii International Conference on System Sciences* (1995). doi:10.1109/HICSS.1995.375331.

160. Soga, S., Shirai, H., Koborv, M. & Hirayama, N. Use of amino acid composition to predict ligand-binding sites. *J. Chem. Inf. Model.* (2007) doi:10.1021/ci6002202.

161. Reulecke, I., Lange, G., Albrecht, J., Klein, R. & Rarey, M. Towards an integrated description of hydrogen bonding and dehydration: Decreasing false positives in virtual screening with the HYDE scoring function. *ChemMedChem* **3**, 885–897 (2008).

162. Righetti, G. *et al.* New Insights into the Binding Features of F508del CFTR Potentiators : A Molecular Docking , Pharmacophore Mapping and QSAR Analysis Approach. **2**,.

163. Liu, F. *et al.* Structural identification of a hotspot on CFTR for potentiation. *Science (80-.).* **364**, 1184–1188 (2019).

164. Pesce, E. *et al.* Synthesis and structure-activity relationship of aminoarylthiazole derivatives as correctors of the chloride transport defect in cystic fibrosis. *Eur. J. Med. Chem.* **99**, 14–35 (2015).

165. Liessi, N. *et al.* Synthesis and structure-activity relationship of aminoarylthiazole derivatives as potential potentiators of the chloride transport defect in cystic fibrosis. *Med. Chem. (Los. Angeles).* (2020) doi:10.2174/1573406416666200306114300.

166. Böhm, H. J. The computer program LUDI: A new method for the de novo design of enzyme inhibitors. *J. Comput. Aided. Mol. Des.* (1992) doi:10.1007/BF00124387.

167. Knapp, J. M. *et al.* Structure-activity relationships of cyanoquinolines with corrector-potentiator activity in Δf508 cystic fibrosis transmembrane conductance regulator protein. *J. Med. Chem.* (2012) doi:10.1021/jm201372q.

168. Vandeginste, B. PARVUS: An extendable package of programs for data exploration, classification and correlation, M. Forina, R. Leardi, C. Armanino and S. Lanteri, Elsevier, Amsterdam, 1988, Price: US $645 ISBN 0-444-43012-1. *J. Chemom.* (1990) doi:10.1002/cem.1180040210.

169. Kennard, R. W. & Stone, L. A. Computer Aided Design of Experiments. *Technometrics* (1969) doi:10.1080/00401706.1969.10490666.

170. Singh, A. K. *et al.* Discovery and characterization of ABBV/ GLPG-2222, a novel first generation CFTR corrector. *Pediatr. Pulmonol.* (2016).

171. Parodi, A. *et al.* Discovery of novel VX-809 hybrid derivatives as F508del-CFTR correctors by molecular modeling, chemical synthesis and biological assays. *Eur. J. Med. Chem.* (2020) doi:10.1016/j.ejmech.2020.112833.

172. Abedi-Jazini, Z., Safari, J., Zarnegar, Z. & Sadeghi, M. A Simple and Efficient Method for the Synthesis of 2-Aminothiazoles Under Mild Conditions. *Polycycl. Aromat. Compd.* (2018) doi:10.1080/10406638.2016.1200104.

LIST OF PUBBLICATIONS

1) **Righetti, G.**, Casale, M., Liessi, N., Tasso, B., Salis, A., Tonelli, M., Millo, E., Pedemonte, N., Fossa, P., & Cichero, E. (**2020**). Molecular Docking and QSAR Studies as Computational Tools Exploring the Rescue Ability of F508del CFTR Correctors. *International journal of molecular sciences*, 21(21), 8084. https://doi.org/10.3390/ijms21218084

2) Parodi, A., **Righetti, G.**, Pesce, E., Salis, A., Tasso, B., Urbinati, C., Tomati, V., Damonte, G., Rusnati, M., Pedemonte, N., Cichero, E., & Millo, E. (2020). Discovery of novel VX-809 hybrid derivatives as F508del-CFTR correctors by molecular modeling, chemical synthesis and biological assays. *European journal of medicinal chemistry*, *208*, 112833. https://doi.org/10.1016/j.ejmech.2020.112833.

3) **Righetti, G.,** Casale, M., Tonelli, M., Liessi, N., Fossa, P., Pedemonte, N., Millo, E., & Cichero, E. (2020). New Insights into the Binding Features of F508del CFTR Potentiators: A Molecular Docking, Pharmacophore Mapping and QSAR Analysis Approach. *Pharmaceuticals (Basel, Switzerland)*, *13*(12), E445. https://doi.org/10.3390/ph13120445

4) **Righetti, G.,** Tonelli, M., Fossa, P., & Cichero, E. (2020). Exploring the selectivity profile of sigma receptor ligands by molecular docking and pharmacophore analyses. *Medicinal chemistry (Shariqah (United Arab Emirates))*, 10.2174/1573406416666201106110611. Advance online publication. https://doi.org/10.2174/1573406416666201106110611.

APPENDIX

A1. Chemical structure and biological activity of the hybrids **2-29** as F508del-CFTR correctors.

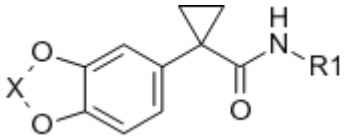

Cp.	X	R_1	pEC_{50}
2	$-CH_2$	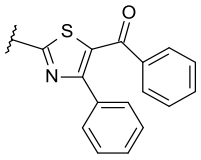	7.06
3	$-CH_2$	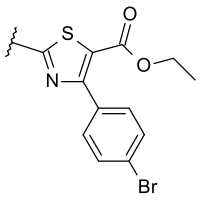	6.52
4	$-CH_2$	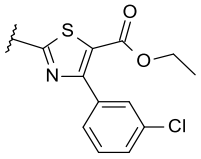	6.26
5	$-CH_2$	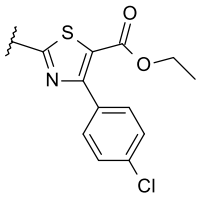	6.05
6	$-CH_2$	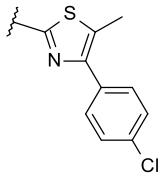	5.54

7	-CH_2	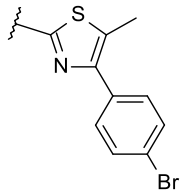	5.72
8	-CH_2	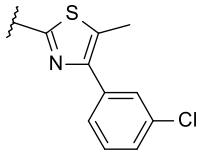	5.64
9	-CH_2	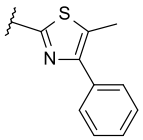	5.80
10	-CH_2	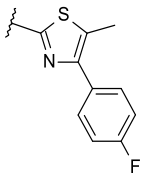	6.05
11	-CH_2	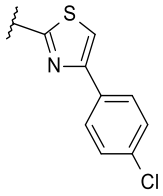	5.54
12	-CH_2	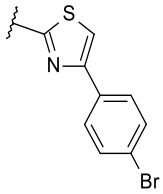	5.31
13	-CH_2	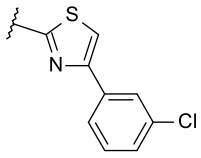	5.09
14	-CH_2	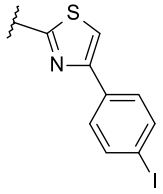	5.92

15	-CH_2	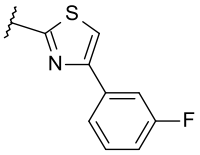	5.68
16	-CH_2	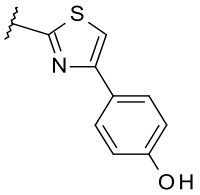	5.74
17	-CH_2	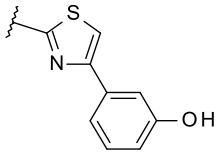	5.64
18	-CH_2	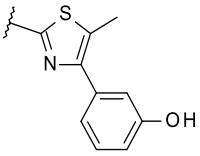	5.92
19	-CH_2	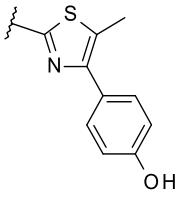	5.41
20	-CH_2	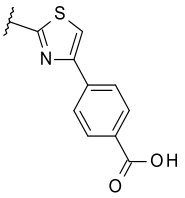	5.30
21	-CH_2	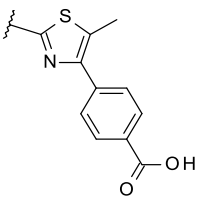	5.53

22	-CH_2	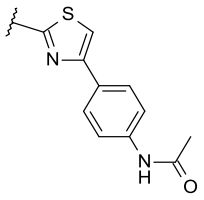	5.30
23	-CF_2	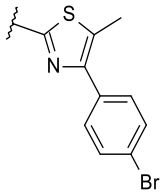	5.42
24	-CF_2	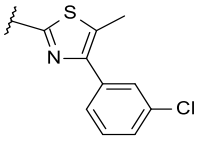	5.27
25	-CF_2	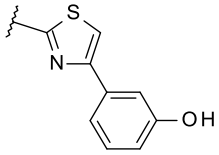	5.89
26	-CF_2	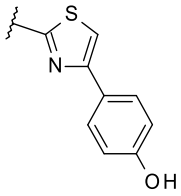	5.77
27	-CF_2	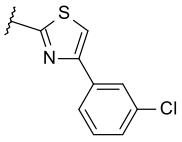	5.40
28	-CH_2	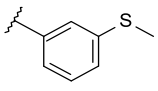	5.10
29	-CH_2	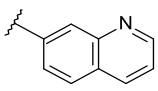	5.66

A2. Chemical structures and biological activity of the tetrahydropyridopyrimidines **30-56** as F508del-CFTR corrector.

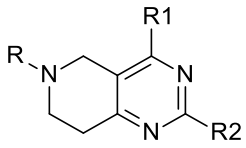

Cp.	R	R_1	R_2	pEC_{50}
30	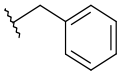	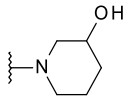	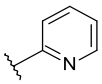	5.55
31	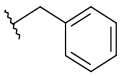	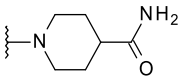	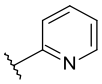	5.85
32	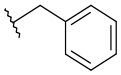	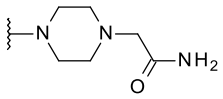	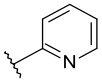	5.55
33	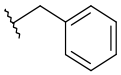	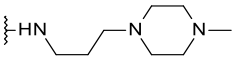	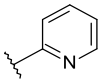	5.51
34	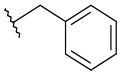	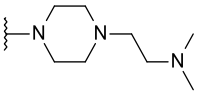	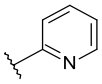	5.82
35	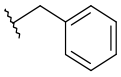	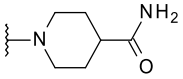	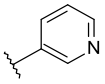	4.00
36	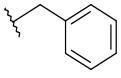	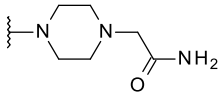	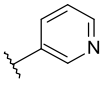	4.00
37	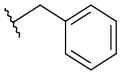	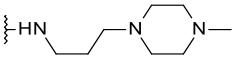	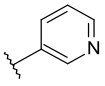	4.00

38	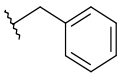	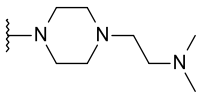	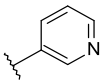	4.00
39	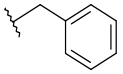	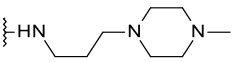	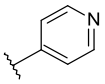	4.00
40	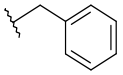	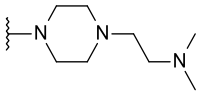	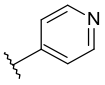	4.00
41	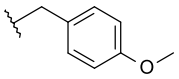	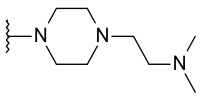	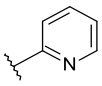	4.00
42	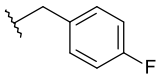	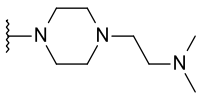	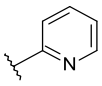	4.00
43	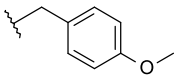	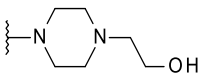	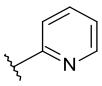	6.40
44	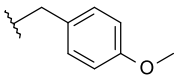	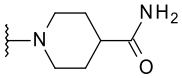	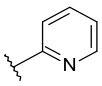	5.46
45	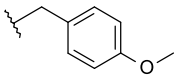	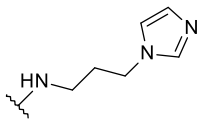	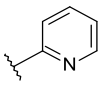	6.70
46	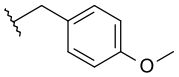	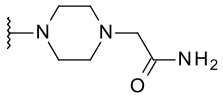	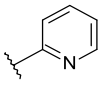	5.64
47	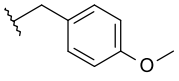	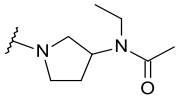	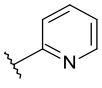	6.52

48	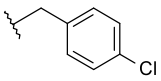	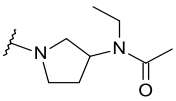	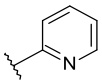	4.00
49	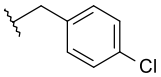	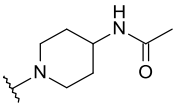	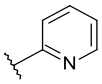	6.15
50	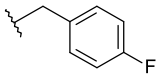	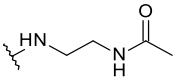	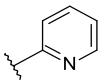	6.70
51	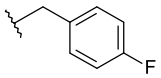	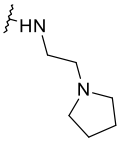	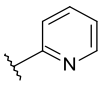	6.70
52	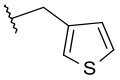	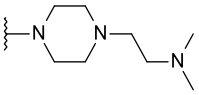	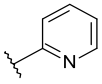	6.70
53	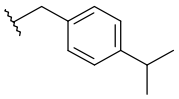	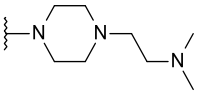	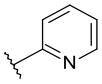	6.52
54	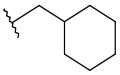	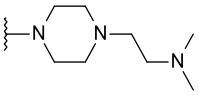	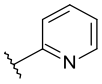	6.05
55	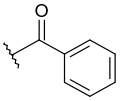	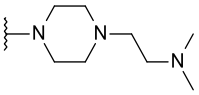	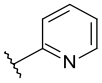	4.00
56	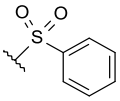	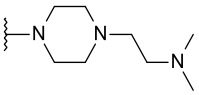	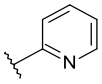	4.00

A3. Chemical structure and biological value of the cyanoquinolines **57-80** as F408del-CFTR correctors.

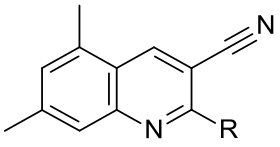

Cp.	R	pEC_{50}
57	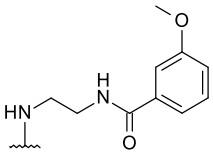	5.66
58	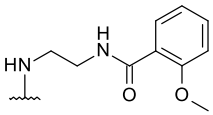	4.96
59	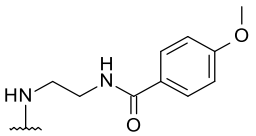	5.52
60	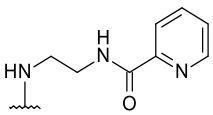	4.00
61	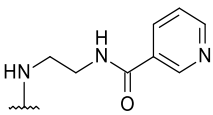	5.57
62	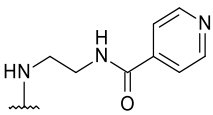	5.14
63	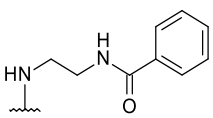	4.00

64	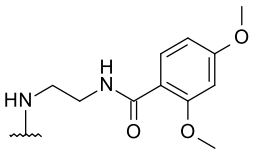	5.38
65	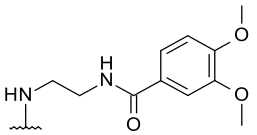	5.82
66	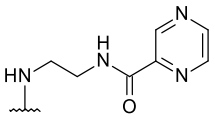	5.17
67	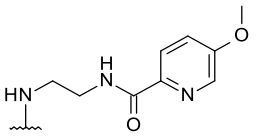	5.57
68	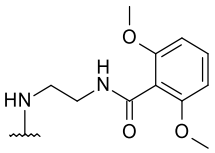	5.43
69	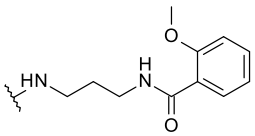	4.00
70	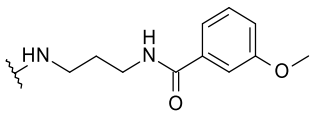	5.34
71	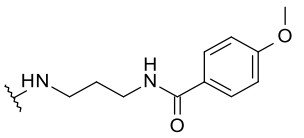	5.37
72	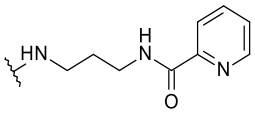	4.00

73	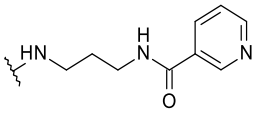	5.52
74	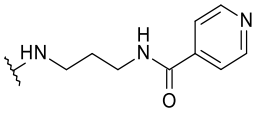	4.88
75	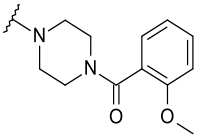	4.00
76	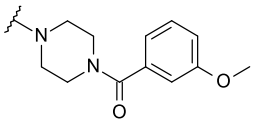	4.00
77	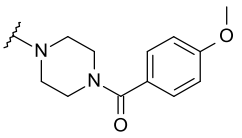	4.00
78	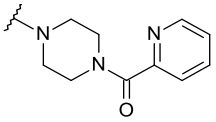	4.00
79	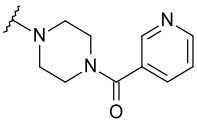	4.00
80	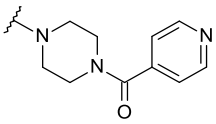	4.00

A4.Binding affinity values obtained by molecular docking studies of VX-809, ALK-809 and SUL-809.

hNBD1/(*CFTR*)-Corrector Complex (LeadIT)	**Binding Affinity Energy ΔG (kJ/mol)**		**Score**	
hNBD1/(*CFTR*)-**VX-809**	-23.0	*-25.0*	-21.5663	*-35.6469*
hNBD1/(*CFTR*)-**ALK-809**	-21.0	*-22.0*	-21.9843	*-31.4063*
hNBD1/(*CFTR*)-**SUL-809**	-24.0	*-22.0*	-24.5672	*-35.2638*

A5. Binding affinity values obtained by molecular docking studies of hybrids correctors.

hNBD1/(*CFTR*)-Corrector Complex (LeadIT)	**Binding Affinity Energy ΔG (kJ/mol)**		**Score**	
hNBD1/(*CFTR*)-**2**	-19.0	*-21.0*	-24.8888	*-28.4416*
hNBD1/(*CFTR*)-**3**	-18.0	*-16.0*	-24.3256	*-23.3950*
hNBD1/(*CFTR*)-**4**	-18.0	*-20.0*	-23.4393	*-23.2050*
hNBD1/(*CFTR*)-**5**	-19.0	*-21.0*	-24.4022	*-23.3299*

hNBD1/(*CFTR*)-**6**	-14.0	*-12.0*	-21.1282	*-23.0777*
hNBD1/(*CFTR*)-**7**	-10.0	*-13.0*	-21.3208	*-23.0264*
hNBD1/(*CFTR*)-**8**	-15.0	*-17.0*	-19.6742	*-23.5280*
hNBD1/(*CFTR*)-**9**	-16.0	*-18.0*	-19.2015	*-22.9820*
hNBD1/(*CFTR*)-**10**	-14.0	*-12.0*	-21.3407	*-22.7400*
hNBD1/(*CFTR*)-**11**	-14.0	*-16.0*	-22.1238	*-22.0175*
hNBD1/(*CFTR*)-**12**	-15.0	*-17.0*	-20.4414	*-21.9677*
hNBD1/(*CFTR*)-**13**	-14.0	*-12.0*	-21.5660	*-22.6050*
hNBD1/(*CFTR*)-**14**	-17.0	*-19.0*	-21.9788	*-22.3278*
hNBD1/(*CFTR*)-**15**	-16.0	*-14.0*	-21.4102	*-22.9320*
hNBD1/(*CFTR*)-**16**	-17.0	*-19.0*	-20.5806	*-24.5206*
hNBD1/(*CFTR*)-**17**	-14.0	*-16.0*	-19.8188	*-25.1833*
hNBD1/(*CFTR*)-**18**	-15.0	*-13.0*	-20.4794	*-25.7335*
hNBD1/(*CFTR*)-**19**	-12.0	*-10.0*	-20.1269	*-25.5958*
hNBD1/(*CFTR*)-**20**	-13.0	*-15.0*	-20.3380	*-34.2077*
hNBD1/(*CFTR*)-**21**	-16.0	*-18.0*	-19.6181	*-33.4221*
hNBD1/(*CFTR*)-**22**	-14.0	*-16.0*	-18.7362	*-30.3549*
hNBD1/(*CFTR*)-**23**	-14.0	*-12.0*	-17.4095	*-22.7536*
hNBD1/(*CFTR*)-**24**	-16.0	*-18.0*	-16.1613	*-23.1016*
hNBD1/(*CFTR*)-**25**	-10.0	*-12.0*	-22.8956	*-25.9998*

hNBD1/(*CFTR*)-**26**	-17.0	*-19.0*	-20.3272	*-25.7090*
hNBD1/(*CFTR*)-**27**	-16.0	*-17.0*	-20.0106	*-22.7284*
hNBD1/(*CFTR*)-**28**	-17.0	*-18.0*	-21.8150	*-20.3860*
hNBD1/(*CFTR*)-**29**	-16.0	*-15.0*	-23.5860	*-22.0357*

A6. Chemical structures and biological values of thienopyrazole derivatives **1-26** as F508del-CFTR potentiators.

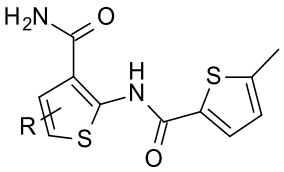

1-3

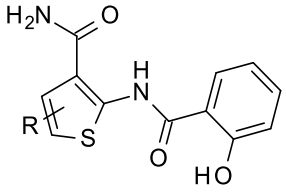

4-6

Cp.	**R**	**pEC$_{50}$**
1	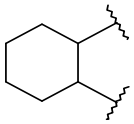	6.18
2	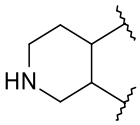	n.a
3	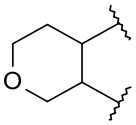	6.10

4	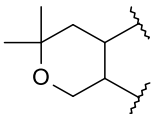	7.88
5	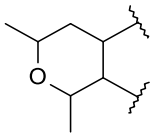	8.39
6	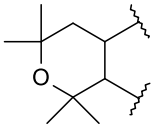	8.39

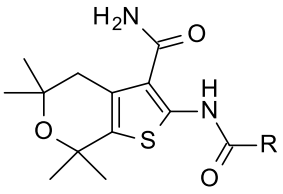

7-26

Cp.	R	pEC_{50}
7	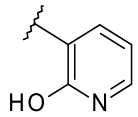	6.72
8	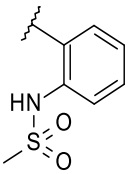	6.83
9	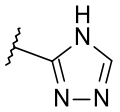	6.33

10	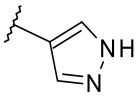	6.90
11	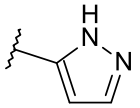	8.52
12	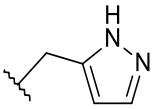	6.86
13	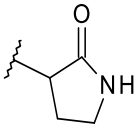	6.99
14	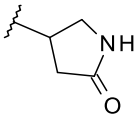	>10,000
15		7.63
16		7.79
17	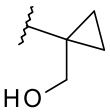	7.82
18	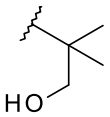	7.12
19	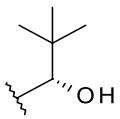	8.56
20	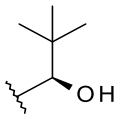	6.89

21	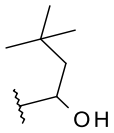	9.26
22	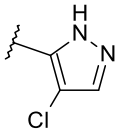	8.69
23	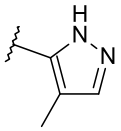	8.69
24	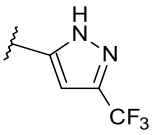	8.52
25	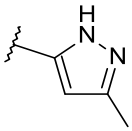	7.88
26	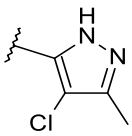	7.95

A7.Chemical structures and biological values of cyanoquinolines **27- 32** as F508del CFTR potentiators.

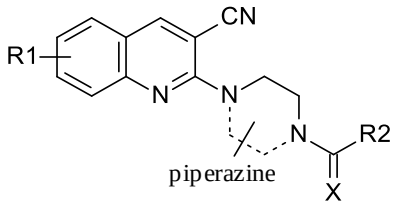

Cp.	Structure	pEC_{50}
27	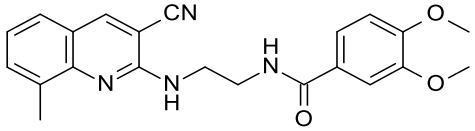	4.82
28	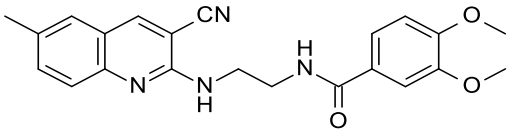	4.82
29	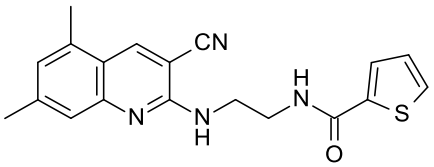	4.85
30	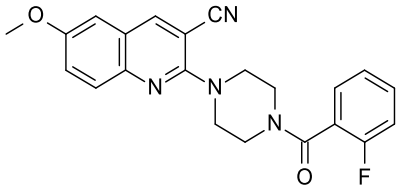	4.95

31	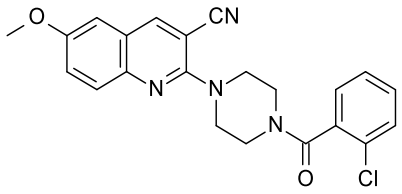	5.33
32	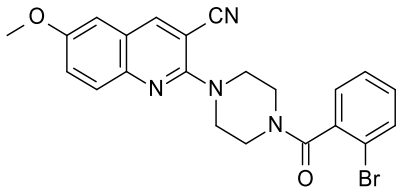	5.30

A8. Chemical structures and biological values of cyanoquinolines **33-56** as F508del CFTR potentiators.

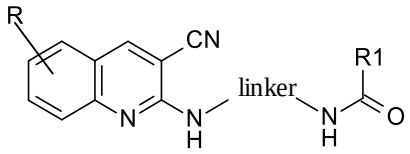

Cp.	Structure	pEC_{50}
33	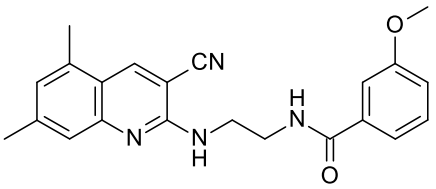	5.22
34	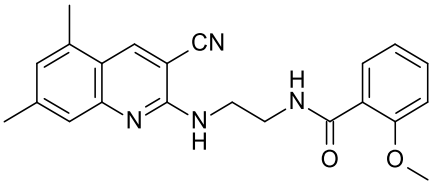	5.63
35	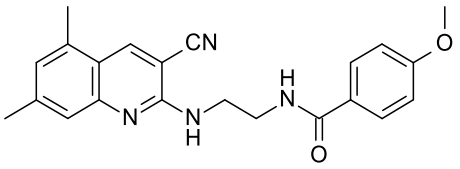	5.38
36	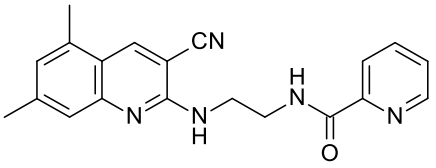	5.92
37	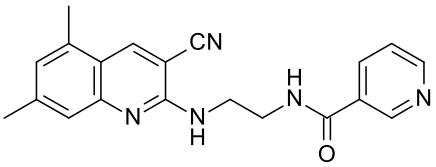	4.87
38	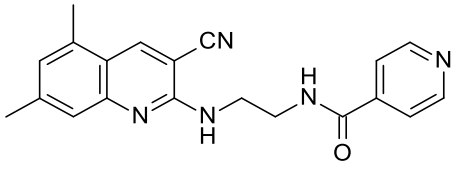	5.00

39	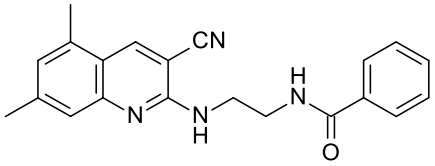	5.00
40	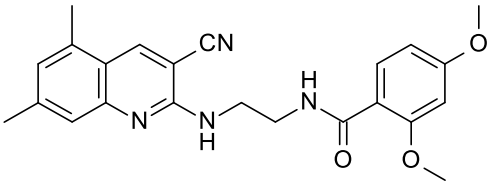	4.25
41	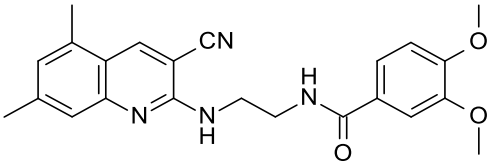	4.31
42	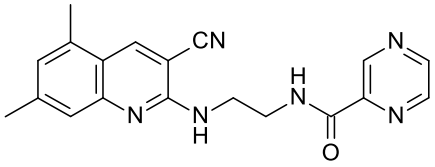	n.a
43	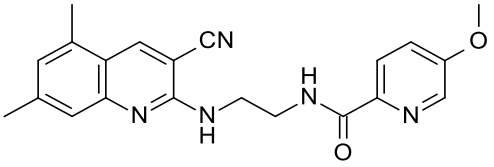	5.46
44	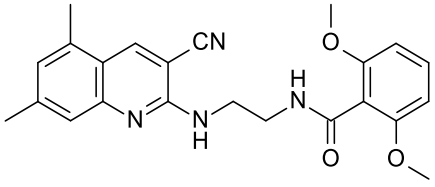	4.93
45	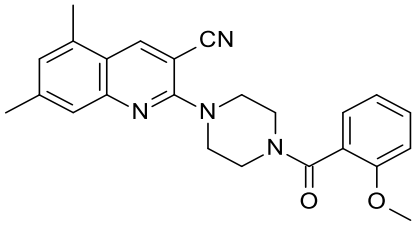	6.00

46	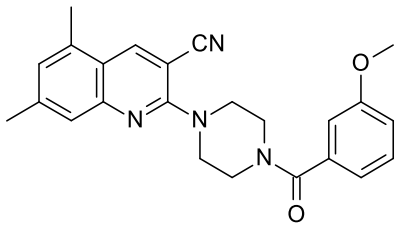	5.92
47	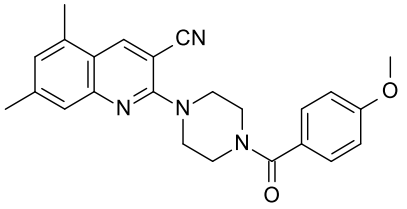	5.88
48	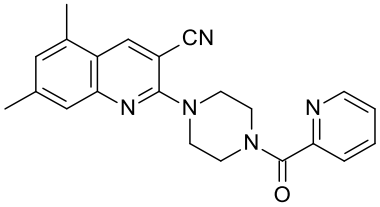	5.13
49	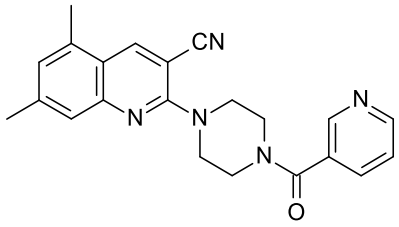	n.a
50	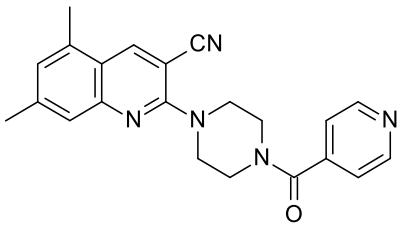	n.a
51	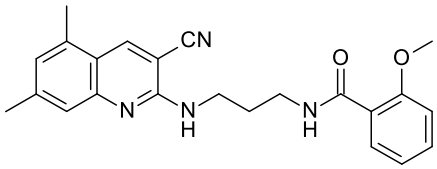	4.55

52	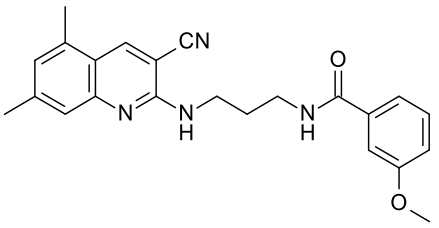	5.33
53	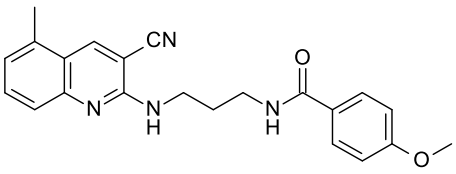	5.30
54	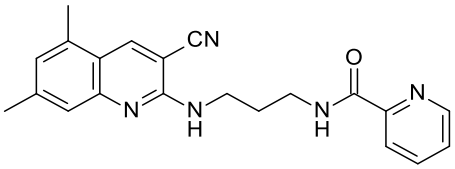	5.21
55	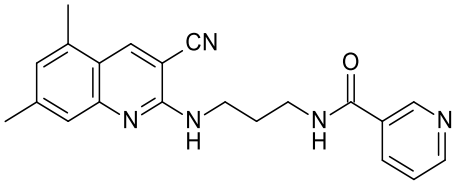	4.79
56	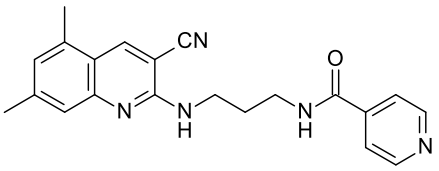	4.87

A9. Chemical structures and biological values of piperidine-pyridoindole analogs **57-69** as F508del CFTR potentiators.

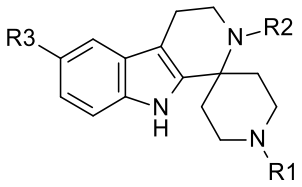

Cp.	R_1	R_2	R_3	pEC_{50}
57	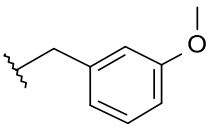	H	OMe	5.00
58	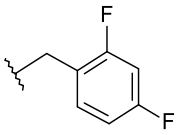	H	OMe	5.69
59	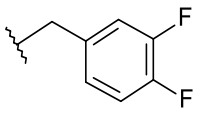	H	OMe	5.58
60	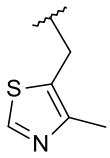	H	OMe	5.29
61	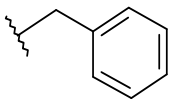	H	H	4.79
62	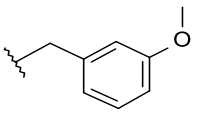	H	H	4.88
63	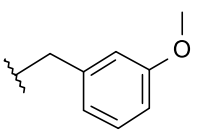	Me	H	< 4.52

64	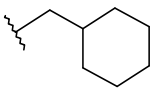	H	OMe	< 4.52
65	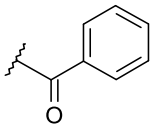	H	H	< 4.52
66	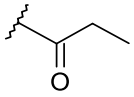	H	OMe	< 4.52
67	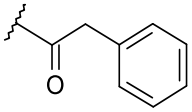	H	OMe	< 4.52
68	SO_2Me	H	OMe	< 4.52
69	Me	H	OMe	< 4.52

A10. Chemical structures and biological values of pyrazoloquinolines analogs **70-80** as F508del CFTR potentiators.

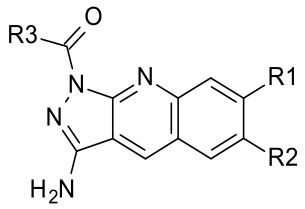

Cp.	R1	R2	R3	pEC50
70	OMe	H	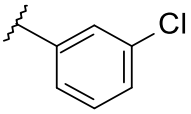	4.82
71	OMe	H	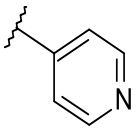	< 4.52
72	OMe	H	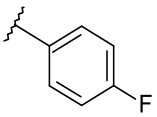	5.44
73	OMe	H	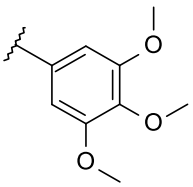	< 4.52
74	OMe	H	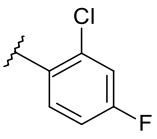	5.61
75	OMe	H	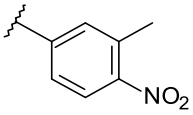	< 4.52

76	OMe	H	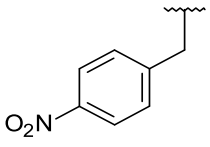	< 4.52
77	OMe	H	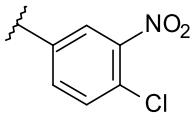	< 4.52
78	OMe	H	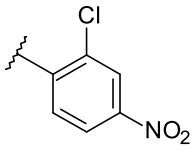	5.76
79	OMe	H	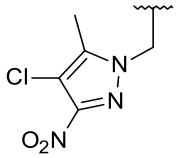	< 4.52
80	OMe	H	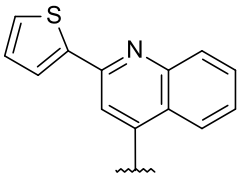	6.52

A11. Chemical structures and biological values of aminoarylthiazoles **81-90** as F508del CFTR potentiators.

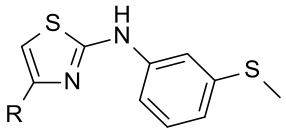

Cp.	R	pEC_{50}
81	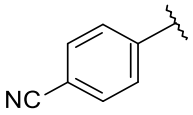	4.46
82	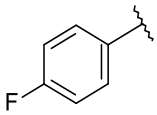	4.56
83	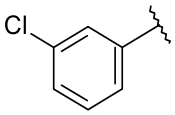	4.27
84	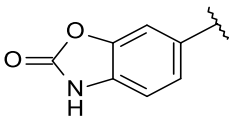	5.19
85	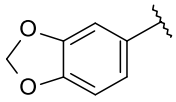	4.14
86	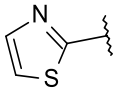	5.00
87	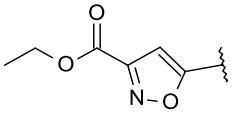	4.23
88	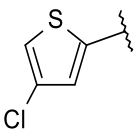	4.49

89	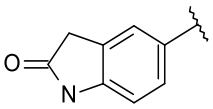	5.71
90	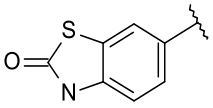	5.20

A12. Chemical structures of thiazole derivatives **91-106** as F508del-CFTR potentiators.

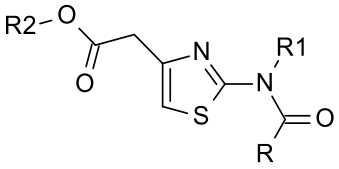

Cp.	**R**	**R_1**	**R_2**
91	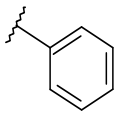	H	CH_2CH_3
92	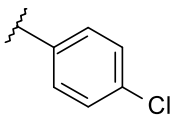	H	CH_2CH_3

93	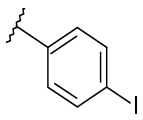	H	CH_2CH_3
94	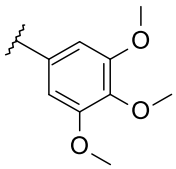	H	CH_2CH_3
95	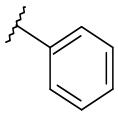	H	H
96	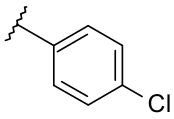	H	H
97	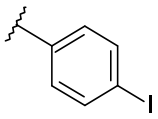	H	H
98	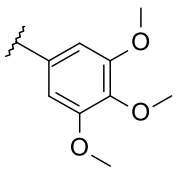	H	H
99	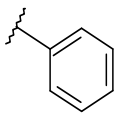	CH_2CH_3	CH_2CH_3
100	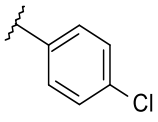	CH_2CH_3	CH_2CH_3

101	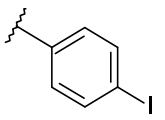	CH_2CH_3	CH_2CH_3
102	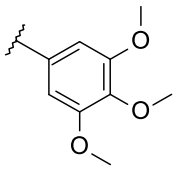	CH_2CH_3	CH_2CH_3
103	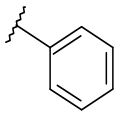	CH_2CH_3	H
104	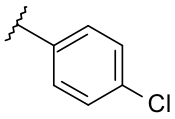	CH_2CH_3	H
105	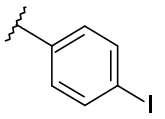	CH_2CH_3	H
106	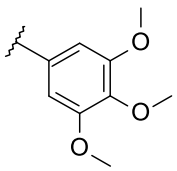	CH_2CH_3	H

A13. Chemical structures of aminoarylthiazoles derivatives **107-111.**

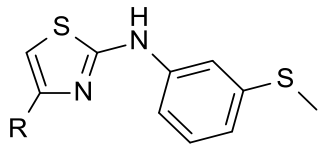

Cp.	R
107	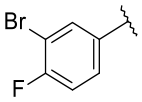
108	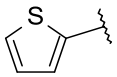
109	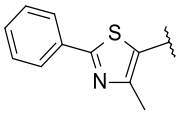
110	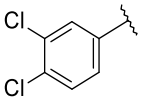
111	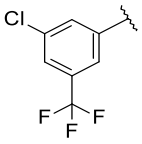

A14. Chemical structures of aminoarylthiazoles derivatives **112-139.**

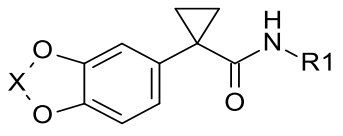

Cp.	X	R_1
112	-CH_2	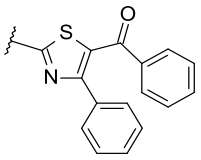
113	-CH_2	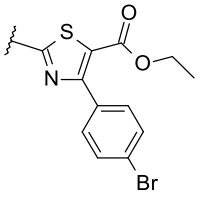
114	-CH_2	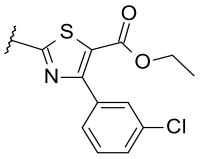
115	-CH_2	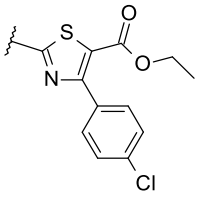
116	-CH_2	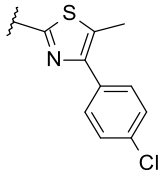
117	-CH_2	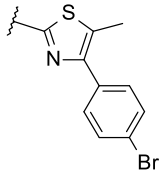

118	-CH_2	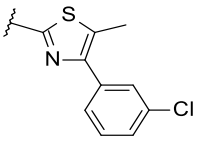
119	-CH_2	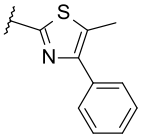
120	-CH_2	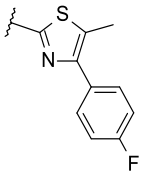
121	-CH_2	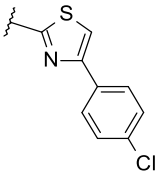
122	-CH_2	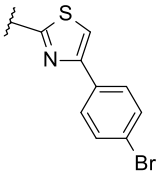
123	-CH_2	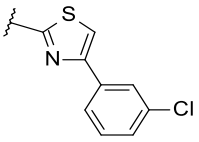
124	-CH_2	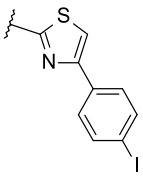
125	-CH_2	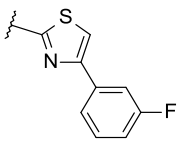

126	-CH_2	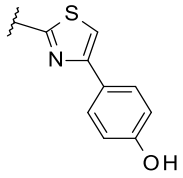
127	-CH_2	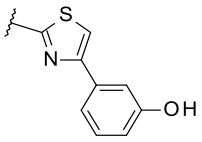
128	-CH_2	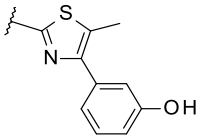
129	-CH_2	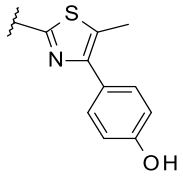
130	-CH_2	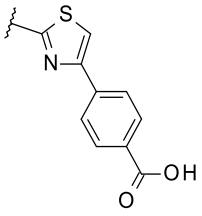
131	-CH_2	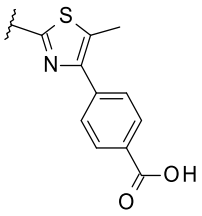
132	-CH_2	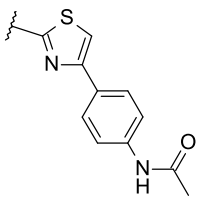

133	-CF_2	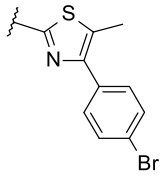
134	-CF_2	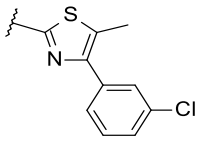
135	-CF_2	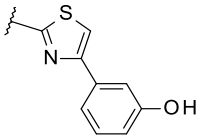
136	-CF_2	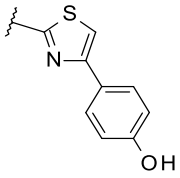
137	-CF_2	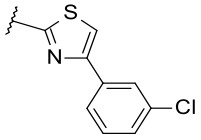
138	-CH_2	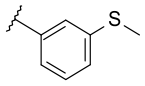
139	-CH_2	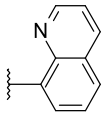

A15. Experimental (Exp.pEC_{50}) and predicted (Pred.pEC_{50}) values of the training set compounds according to the refined QSAR model.

Cp.	Exp. pEC_{50}	E_nb	ASA-	vsa_pol	CASA+	CASA-	E_ang	Pred. pEC_{50}	Residual
3	6.52	40.201546	311.06015	43.506508	1127.1584	786.98218	121.59032	6.24	0.2800
4	6.26	40.071484	295.21408	43.506508	1153.6713	754.27197	122.66916	6.39	-0.1316
5	6.05	39.974373	292.46686	43.506508	1154.363	746.96039	121.56782	6.43	-0.3811
6	5.54	37.910526	281.6275	29.939585	792.55768	580.71594	121.07256	5.47	0.0664
7	5.72	38.121964	305.53513	29.939585	768.17029	622.6806	121.0268	5.20	0.5169
8	5.64	37.865238	282.59271	29.939585	791.71173	582.98877	121.37415	5.47	0.1736
9	5.80	37.621845	236.54544	29.939585	842.57831	492.01453	121.02081	5.92	-0.1225
10	6.05	36.758995	252.77013	29.939585	846.78784	542.69745	122.49203	6.01	0.0352
11	5.54	37.211922	277.50491	29.939585	728.87549	562.22498	120.49342	5.35	0.1880
12	5.31	37.436359	298.69312	29.939585	708.33789	597.98364	120.47495	5.10	0.2088
13	5.09	37.212086	280.57724	29.939585	743.19354	569.01068	120.71957	5.37	-0.2798
15	5.68	35.795937	244.57336	29.939585	795.67621	516.53894	122.20341	5.98	-0.2962
16	5.74	37.433041	230.66957	43.506508	890.95435	525.00391	121.43837	5.75	-0.0125
17	5.64	37.343327	234.04518	43.506508	893.51337	533.62299	121.48071	5.76	-0.1192
18	5.92	38.131062	238.4789	43.506508	966.19189	552.31714	121.81725	5.90	0.0249
23	5.42	35.323212	381.84894	29.939585	698.24213	844.64984	120.17078	5.32	0.0989
24	5.27	35.113384	358.79428	29.939585	723.77502	802.6228	120.48874	5.57	-0.3021
25	5.89	34.822216	308.6485	43.506508	804.03973	757.4234	120.57159	5.84	0.0467
26	5.77	34.670029	308.59375	43.506508	799.9693	756.05463	120.56307	5.84	-0.0710
27	5.40	34.575485	355.2095	29.939585	662.57629	782.17133	119.65387	5.42	-0.0218
30	5.55	82.923752	171.84309	30.614649	1648.9868	370.83737	20.736029	5.68	-0.1298

31	5.85	82.42186	184.62444	48.35714	1847.3866	444.39102	22.800692	5.61	0.2405
32	5.55	106.46642	171.46677	48.35714	2676.562	455.58719	27.980944	5.44	0.1107
37	4.00	144.48102	122.29909	22.730305	3444.0505	287.52515	32.371471	4.37	-0.3663
38	4.00	153.96991	127.36039	17.047728	3526.8616	297.38651	36.52422	3.73	0.2738
39	4.00	147.62102	126.22911	22.730305	3584.5537	293.60892	32.575783	4.36	-0.3587
40	4.00	154.23276	123.18449	17.047728	3532.3589	284.55618	35.389881	3.73	0.2680
41	4.00	158.429	119.46897	19.551485	4025.5757	309.06622	38.373356	4.62	-0.6234
42	4.00	153.73146	153.67113	17.047728	3514.4336	374.03552	36.782146	3.71	0.2902
43	6.40	110.90891	133.17619	33.118404	3017.5261	351.71832	33.262741	6.52	-0.1196
44	5.46	87.505989	170.54222	50.860893	2184.323	448.35553	26.178873	6.06	-0.5979
45	6.70	84.29599	134.07512	30.916637	2102.2649	341.48932	57.236408	6.49	0.2082
46	5.64	111.44763	156.84193	50.860893	3098.0825	451.54794	31.014784	6.08	-0.4432
47	6.52	93.705719	173.39532	33.118404	2326.9932	451.52142	33.383991	6.42	0.0951
49	6.15	86.606331	225.05911	36.297226	1873.995	530.46436	21.122585	5.62	0.5286
50	6.70	74.338272	152.44916	41.979801	1729.2054	368.77454	21.081335	6.62	0.0827
54	6.05	148.64999	98.055092	17.047728	3884.696	228.27225	34.709503	5.37	0.6825
55	4.00	132.28711	164.27565	30.614649	2949.2405	432.04498	31.816795	4.15	-0.1528
56	4.00	123.07984	190.38725	49.064251	2928.6514	488.53369	46.862576	3.77	0.2313
57	5.66	55.075397	237.48724	50.860893	923.78021	500.8606	22.470055	5.35	0.3140
58	4.96	58.179813	234.20871	50.860893	911.40234	502.84613	22.384676	5.06	-0.1031
59	5.52	56.934811	234.43777	50.860893	922.17236	493.72595	22.341722	5.16	0.3606
60	4.00	54.783257	230.61339	54.039715	789.38843	457.07571	20.474987	4.76	-0.7638
61	5.57	51.930538	229.52635	54.039715	774.53314	448.72403	19.566298	5.01	0.5581
62	5.14	50.999371	214.56854	54.039715	781.28369	413.47357	20.403036	5.17	-0.0281

63	4.00	51.904221	252.33662	48.35714	709.98688	475.40222	19.385567	4.85	-0.8527
65	5.82	63.475273	226.01973	53.364651	1141.8444	538.83099	24.826355	5.33	0.4917
66	5.17	57.026089	191.64943	59.72229	882.32562	403.23041	19.090767	4.93	0.2428
67	5.57	60.584358	218.01747	56.543472	1009.9583	490.53931	24.855558	4.98	0.5911
68	5.43	62.59671	226.41823	53.364651	1151.2058	546.57361	23.791538	5.51	-0.0800
70	5.34	58.139511	219.83636	50.860893	882.26208	469.1308	15.243285	5.19	0.1472
71	5.37	57.90588	214.09308	50.860893	880.84534	456.23233	15.861175	5.23	0.1426
73	5.52	54.521137	204.4958	54.039715	790.16455	404.9017	12.876506	5.11	0.4106
74	4.88	52.395954	204.63695	54.039715	747.9267	399.45132	13.675772	5.17	-0.2899
75	4.00	71.220154	226.46532	39.495743	989.84216	478.97415	20.628365	4.45	-0.4482
76	4.00	71.40937	230.99619	39.495743	977.70166	479.77908	22.155819	4.28	-0.2833
77	4.00	71.750427	227.05901	39.495743	986.42834	470.92038	22.093498	4.29	-0.2889
78	4.00	70.656143	224.05431	42.674564	843.64532	437.12994	19.305321	3.78	0.2229
79	4.00	66.774406	216.00131	42.674564	835.51776	415.37051	20.192486	4.16	-0.1615
80	4.00	65.905418	207.23102	42.674564	843.74304	392.70279	19.777443	4.30	-0.3036

A16. Experimental (Exp.pEC_{50}) and predicted (Pred.pEC_{50}) values of the test set compounds according to the refined QSAR model.

Cp.	Exp. pEC_{50}	E_nb	ASA-	vsa_pol	CASA+	CASA-	E_ang	Pred. pEC_{50}	Residual
1	5.59	48.448597	381.67267	57.073425	725.31787	1243.8712	108.23756	5.93	-0.3400
2	7.06	53.35915	305.88519	43.506508	1120.5023	774.80719	121.30415	6.65	0.4051
14	5.92	37.931583	304.58237	29.939585	707.73633	608.5556	120.34983	5.41	0.5145
19	5.41	38.162426	238.59331	43.506508	953.86444	551.62775	121.88371	5.85	-0.4416
20	5.30	39.625359	255.47565	57.073425	1019.7084	648.90814	19.199339	5.63	-0.3321
21	5.53	40.260384	255.33957	57.073425	1096.9369	657.75476	19.016466	5.83	-0.3000
22	5.30	40.724495	233.93356	49.189083	1171.973	592.08582	18.133121	5.65	-0.3458
28	5.10	36.033928	246.28993	24.25701	585.13702	430.02222	106.14865	4.32	0.7800
29	5.66	48.590977	206.37631	29.939585	706.36316	397.68716	107.79346	5.34	0.3218
33	5.51	146.15053	133.94344	22.730305	3419.7056	318.91934	30.880795	5.14	0.3719
34	5.82	153.23914	136.87323	17.047728	3544.1233	323.7052	35.1539	5.87	-0.0456
35	4.00	82.230225	180.92363	48.35714	1837.0845	429.87457	25.189426	4.33	-0.3304
36	4.00	106.19363	165.49545	48.35714	2657.3655	434.75656	29.022572	4.38	-0.3754
48	4.00	89.662857	233.99181	30.614649	1898.8805	553.62463	30.238689	4.97	-0.9700
51	6.70	98.400475	154.97318	22.730305	2273.0305	328.85309	26.189623	5.97	0.7289
52	6.70	138.94405	110.62077	17.047728	3588.1072	261.39685	55.438435	6.18	0.5214
53	6.52	158.92085	142.09158	17.047728	3969.3804	352.67133	36.833698	6.42	0.0959
64	5.38	63.195755	223.05199	53.364651	1137.3612	529.30237	24.910639	5.64	-0.2592
69	4.00	61.174698	178.73625	50.860893	932.14954	388.21515	14.915898	4.27	-0.2692
72	4.00	54.135616	218.24225	54.039715	736.79474	438.01221	13.264742	3.96	0.0440

A17. Experimental (Exp.pEC_{50}) and predicted (Pred.pEC_{50}) values of the test set compounds according to the developed QSAR model. The selected 2D Subdivided Surface Area, Adjacency and Partial Charge descriptors and the 3D Surface Area, Volume and Shape Descriptor values have been reported.

Cp.	Exp. pEC_{50}	PEOE _VSA+5	PEOE_ VSA-6	SlogP _VSA4	SlogP _VSA5	SlogP _VSA9	SMR _VSA2	SMR _VSA4	vsurf_ ID1	Vsurf _ID7	vsurf_Wp2	vsurf_Wp3	Pred. pEC_{50}	Residual
3	6.10	12.949531	9.2917662	58.170788	18.868406	117.73722	0	51.837513	1.4823005	1.6377909	459.875	149.625	6.47	-0.3730
6	8.39	12.949531	9.2917662	58.170788	18.868406	230.11502	0	51.837513	1.0830811	1.896114	480.875	162.625	8.50	-0.1134
11	8.52	25.899061	9.2917662	58.210732	18.868406	165.51132	16.663008	51.837513	0.84125829	1.6844577	517.75	199.375	7.60	0.9194
24	8.52	25.899061	9.2917662	60.96748	18.868406	210.39166	24.422523	51.837513	1.641968	0.92884934	507.25	209	7.96	0.5565
32	5.30	12.949531	2.503756	30.233366	38.438972	53.52544	6.1794186	7.0450215	0.92542022	1.2124147	506.125	83.875	5.67	-0.3738
38	5.00	12.949531	0.13689101	36.604515	0	68.97995	18.01075	25.055773	1.0961233	0.84826136	502.25	132.5	4.92	0.0811
40	4.25	12.949531	5.1444035	36.604515	70.767738	79.466805	18.01075	25.055773	1.2389504	1.0051649	500.375	131.625	5.03	-0.7757
55	4.79	12.949531	0.13689101	36.604515	0	68.97995	18.01075	25.055773	0.69999182	0.85419071	525.75	125.625	5.08	-0.2927
57	5.00	0	5.2812943	9.1278973	89.636139	28.926434	34.79628	4.7171016	0.26172695	0.41990376	527.75	127.625	4.62	0.3786
59	5.58	0	2.7775381	9.1278973	54.252274	53.603233	53.038315	4.7171016	0.90120083	1.5566729	508.625	122	5.23	0.3450

66	4.52	0	2.7775381	5.9423227	54.252274	38.569443	34.7962 8	4.7171016	0.70693582	1.4608345	430	115.125	4.33	0.1878
72	5.44	12.949531	2.503756	27.047791	35.383869	22.531462	9.121018 4	11.333296	0.81351507	1.249822	484	147.25	4.96	0.4835
77	4.52	19.649082	2.503756	27.047791	35.383869	49.476738	50.93500 9	14.090043	0.6767658	0.7181255 8	540. 875	163	5.28	-0.7613
84	5.19	0	0	0	33.241909	98.617111	1.550733 9	47.978065	0.68520218	0.6181021 3	524. 25	138.625	5.12	0.0659
88	4.49	0	0	0	33.241909	137.18106	1.550733 9	25.383394	0.48546532	1.3971066	448. 5	96.375	5.60	-1.1057

A18. Experimental (Exp.pEC_{50}) and predicted (Pred.pEC_{50}) values of the test set compounds according to the developed QSAR model. The selected 2D Adjacency and Distance Matrix Descriptors, Pharmacophore Feature Descriptors, Physical Properties, Atom Counts and Bond Counts descriptors and the 3D Conformation Dependent Charge Descriptors values have been reported.

Cp.	Exp. pEC_{50}	BCUT_SLOGP_1	BCUT_SMR_1	BCUT_SMR_2	BCUT_SMR_3	b_1rotR	logS	dipoleY	a_hyd	ASA+	Pred. pEC_{50}	Residual
3	6.10	-0.33047944	-0.26404753	0.73366147	2.8013721	0.13043478	-4.14505	1.025835	14	349.56198	6.47	-0.3730
6	8.39	-0.17167728	-0.11908972	0.59196395	2.9551604	0.11111111	-5.4538898	1.0793978	18	416.81415	8.50	-0.1134
11	8.52	-0.2496783	-0.14757159	0.60403872	2.9551349	0.11538462	-3.9227901	1.0493044	15	352.38104	7.60	0.9194
24	8.52	-0.21303622	-0.1171928	0.5663017	2.9551418	0.1	-5.1322598	0.47866929	19	354.41968	7.96	0.5565
32	5.30	-0.47616071	-0.36629966	0.80957109	2.9251747	0.125	-5.6871099	0.31962168	20	390.99222	5.67	-0.3738
38	5.00	-0.53411287	-0.42294818	0.76985401	2.7408793	0.17857143	-4.0622401	0.090998821	17	314.42032	4.92	0.0811
40	4.25	-0.50695312	-0.33814892	0.72322482	2.7434282	0.21875	-5.4211402	-0.35460791	20	369.87402	5.03	-0.7757
55	4.79	-0.5048244	-0.41092402	0.74816161	2.7917297	0.20689656	-4.26401	0.043317597	18	341.32532	5.08	-0.2927
57	5.00	-0.50591195	-0.34110171	0.69058079	3.0343418	0.12121212	-4.0710001	-0.099414699	24	451.85364	4.62	0.3786
59	5.58	-0.50857282	-0.41164595	0.75098193	3.034306	0.090909094	-4.61058	-0.23075099	25	399.97519	5.23	0.3450
66	4.52	-0.50590354	-0.33911341	0.68981081	3.0312951	0.11111111	-2.6305399	-0.617037	18	383.77551	4.33	0.1878

72	5.44	-0.52836478	-0.46312457	0.81207639	2.5848756	0.10714286	-5.91992	-0.3858822	16	307.17242	4.96	0.4835
77	4.52	-0.50872862	-0.36945948	0.8581714	2.5899618	0.12903225	-7.1494598	-0.35955641	17	324.83478	5.28	-0.7613
84	5.19	-0.49309871	-0.45771432	0.93088794	2.6487799	0.14814815	-6.67063	-0.80477411	17	343.14407	5.12	0.0659
88	4.49	-0.34952211	-0.29147619	0.93386561	2.6100163	0.18181819	-6.24999	-0.531663	17	384.87665	5.60	-1.1057

A19. Experimental (Exp.pEC_{50}) and predicted (Pred.pEC_{50}) values of the training set compounds according to the developed QSAR model. The selected 2D Subdivided Surface Area, Adjacency and Partial Charge descriptors and the 3D Surface Area, Volume and Shape Descriptor values have been reported.

Cp.	Exp. pEC_{50}	PEOE _VSA+5	PEOE_ VSA-6	SlogP _VSA4	SlogP _VSA5	SlogP _VSA9	SMR _VSA2	SMR _VSA4	vsurf_ ID1	Vsurf _ID7	vsurf_Wp2	vsurf_Wp3	Pred. pEC_{50}	Residual
1	6.18	12.94953	6.788011	58.17079	37.73681	96.81097	0	51.83751	0.800828	0.493301	469.375	148.875	6.12	0.0584
4	7.88	12.94953	9.291766	58.17079	18.86841	184.3893	0	51.83751	1.128163	1.685388	472.75	159.25	7.32	0.5626
7	6.72	25.89906	17.05931	58.63956	18.86841	170.3259	0	51.83751	0.600447	1.687995	513.75	173.375	6.94	-0.2237
8	6.83	25.89906	14.97434	58.63956	50.55958	167.8393	0	70.57043	0.27258	0.752095	542.375	181.5	6.59	0.2433
9	6.33	25.89906	9.428658	57.7819	18.86841	165.5113	16.78553	51.83751	0.430511	1.366267	529.875	206.125	6.95	-0.6186
10	6.90	25.89906	9.291766	58.63956	18.86841	165.5113	16.66301	51.83751	0.565331	1.356548	523.75	197.875	7.36	-0.4613
12	6.86	12.94953	9.291766	34.34852	37.73681	165.5113	16.66301	51.83751	0.817541	1.646662	503.125	184.875	7.08	-0.2195
22	8.69	25.89906	9.291766	58.21073	18.86841	204.66	16.66301	51.83751	1.014075	1.970239	514.375	191.5	8.07	0.6208

23	8.69	25.89906	9.291766	61.39631	18.86841	198.8373	16.66301	51.83751	0.951192	1.522542	509.75	188.625	8.03	0.6621
25	7.88	25.89906	9.291766	60.96748	18.86841	198.8373	16.66301	51.83751	0.888762	1.297468	516.125	204.875	7.90	-0.0228
26	7.95	25.89906	9.291766	60.96748	18.86841	237.986	16.66301	51.83751	1.027718	1.585446	515.75	195.5	8.50	-0.5481

27	4.82	12.94953	5.144404	33.41894	70.76774	46.14079	18.01075	25.05577	0.653004	1.248182	516	123.125	4.31	0.5125
28	4.82	12.94953	5.144404	33.41894	70.76774	46.14079	18.01075	25.05577	0.731779	1.509997	521.875	128.875	4.60	0.2203
29	4.85	0	0.136891	34.77734	0	100.2576	18.01075	25.05577	0.610643	0.692451	504.125	136.875	5.18	-0.3335
33	5.22	12.94953	2.640647	36.60452	35.38387	74.22338	18.01075	25.05577	0.947415	1.384679	512.875	136.375	5.48	-0.2638
30	4.95	12.94953	2.503756	30.23337	35.38387	22.53146	12.24533	7.045022	1.173449	1.768574	473.5	80.375	5.12	-0.1726
31	5.53	12.94953	2.503756	30.23337	35.38387	46.71999	3.124314	7.045022	0.719132	1.033341	493.5	84.25	5.37	0.1581
34	5.63	12.94953	2.640647	36.60452	35.38387	74.22338	18.01075	25.05577	1.163676	1.649628	508.125	132.75	5.51	0.1183
35	5.38	12.94953	2.640647	36.60452	35.38387	74.22338	18.01075	25.05577	0.967555	0.913348	509.375	131.25	5.22	0.1587

36	5.92	12.94953	0.136891	36.17569	0	68.97995	18.01075	25.05577	0.899112	1.16417	507.5	132.75	5.14	0.7827
37	4.87	12.94953	0.136891	36.60452	0	68.97995	18.01075	25.05577	1.274256	1.278531	498.5	132.125	5.14	-0.2747
39	5.00	12.94953	0.136891	36.60452	0	68.97995	18.01075	25.05577	0.966741	0.86576	489.125	128.25	5.18	-0.1837
41	4.31	12.94953	5.144404	36.60452	70.76774	79.46681	18.01075	25.05577	1.189321	1.069763	440.75	118.125	4.62	-0.3131
43	5.46	12.94953	2.640647	36.17569	35.38387	74.22338	18.01075	25.05577	1.041974	1.364302	526.125	138.25	5.20	0.2614
44	4.93	12.94953	5.144404	36.60452	70.76774	79.46681	18.01075	25.05577	1.193353	1.539765	516.75	135.875	5.35	-0.4220
45	6.00	12.94953	2.503756	36.60452	35.38387	74.22338	3.124314	7.045022	0.906389	1.459584	485.25	93	5.77	0.2321
46	5.92	12.94953	2.503756	36.60452	35.38387	74.22338	3.124314	7.045022	0.900818	1.2158	486.375	92.625	5.72	0.1971
47	5.88	12.94953	2.503756	36.60452	35.38387	74.22338	3.124314	7.045022	0.933468	1.22687	495	89.875	5.64	0.2367
48	5.13	12.94953	0	36.17569	0	68.97995	3.124314	7.045022	0.752685	1.216956	484.75	92.375	5.55	-0.4168
51	4.55	12.94953	2.640647	36.60452	35.38387	74.22338	18.01075	25.05577	0.160016	0.717382	512.625	110.875	4.93	-0.3806
52	5.33	12.94953	2.640647	36.60452	35.38387	74.22338	18.01075	25.05577	0.558261	1.108011	522.75	128.75	5.41	-0.0813
53	5.30	12.94953	2.640647	36.60452	35.38387	74.22338	18.01075	25.05577	0.470551	0.787824	540.625	131.875	5.33	-0.0334
54	5.21	12.94953	0.136891	36.17569	0	68.97995	18.01075	25.05577	0.326577	0.776319	522.375	125.25	5.04	0.1700

56	4.87	12.94953	0.136891	36.60452	0	68.97995	18.01075	25.05577	0.701703	0.832017	529.125	126	5.01	-0.1352
58	5.69	0	2.777538	9.127897	54.25227	53.60323	53.03832	4.717102	1.188067	2.009089	510	122.5	5.47	0.2185
60	5.29	0	2.777538	10.05747	54.25227	88.28671	34.79628	4.717102	0.357714	0.54331	526	130	5.23	0.0564
61	4.79	0	0.273782	9.127897	18.86841	18.43958	34.79628	4.717102	0.498902	0.477126	490.375	113.875	4.76	0.0311
62	4.88	0	2.777538	9.127897	54.25227	23.68301	34.79628	4.717102	0.439908	0.629279	516.125	121.125	4.77	0.1099
63	4.52	0	2.640647	9.127897	87.14946	23.68301	16.78553	4.717102	0.393936	0.685366	484.125	86.75	4.57	-0.0495

64	4.52	0	2.777538	10.35312	54.25227	5.243428	39.20708	4.717102	0.212023	0.722736	482.75	118	4.94	-0.4189
65	4.52	12.94953	0.273782	32.99011	18.86841	0	34.79628	4.717102	0.848914	1.119773	480.375	119.375	4.92	-0.4048
67	4.52	0	2.777538	9.127897	73.12068	5.243428	34.79628	4.717102	0.449963	0.695605	527.5	128.375	4.48	0.0375
68	4.52	0	2.777538	5.942323	85.94345	5.243428	34.79628	4.717102	0.794642	2.366449	434.75	121	4.75	-0.2291
69	4.52	0	2.777538	5.942323	87.14946	5.243428	34.79628	4.717102	0.537017	1.531974	395.375	106.625	4.19	0.3275
71	4.52	12.94953	2.503756	27.04779	35.38387	7.571348	0	11.3333	0.701	0.923499	495.125	146.5	4.31	0.2087
73	4.52	12.94953	10.01502	27.04779	141.5355	23.30163	0	11.3333	0.73529	1.624358	534.25	161.25	4.79	-0.2698
74	5.61	12.94953	2.503756	27.04779	35.38387	61.68011	9.121018	11.3333	0.84081	1.107921	491.5	144.75	5.51	0.0977
75	4.52	19.64908	2.503756	30.23337	35.38387	43.65411	50.93501	14.09004	0.715313	0.807208	532.25	153.25	4.82	-0.3039
76	4.52	19.64908	2.503756	27.04779	54.25227	10.3281	50.93501	14.09004	0.61446	1.191052	581.875	166.875	4.63	-0.1123
78	5.76	19.64908	2.503756	27.04779	35.38387	49.47674	50.93501	14.09004	0.640504	0.81883	540.875	165.125	5.08	0.6800

79	4.52	12.94953	36.4348	26.61896	35.38387	100.8135	50.93501	13.66122	0.505315	0.708749	4.42	0.1031	4.42	0.1031
80	6.52	12.94953	2.503756	27.04779	35.38387	38.84904	0	20.16555	0.511739	0.588034	6.34	0.1828	6.34	0.1828
81	4.46	0	0	3.185575	33.24191	66.75472	1.550734	27.21057	0.739348	2.128536	4.86	-0.3981	4.86	-0.3981
82	4.56	0	0	0	33.24191	81.71484	10.67175	27.21057	0.286104	0.822712	4.13	0.4298	4.13	0.4298
83	4.27	0	0	0	33.24191	105.9034	1.550734	27.21057	0.587894	1.361566	4.84	-0.5710	4.84	-0.5710
85	4.14	0	5.007512	0	33.24191	77.24158	1.550734	27.21057	0.294075	0.617597	4.32	-0.1769	4.32	-0.1769
86	5.00	0	0	0	33.24191	98.03241	1.550734	24.95457	0.525247	1.002255	4.29	0.7073	4.29	0.7073
87	4.23	0	8.406116	26.61896	42.97603	100.0807	1.550734	29.47381	0.452959	0.437706	4.59	-0.3630	4.59	-0.3630
89	5.71	0	0.136891	3.185575	52.11031	69.51147	1.550734	47.97807	0.436705	0.886085	377.1368	0.3582	377.1368	0.3582
90	5.20	14.92559	0.136891	0	34.79264	125.5932	3.101468	47.97807	0.730122	0.597511	382.8594	-0.3414	382.8594	-0.3414

A20. Experimental (Exp.pEC_{50}) and predicted (Pred.pEC_{50}) values of the training set compounds according to the developed QSAR model. The selected 2D Adjacency and Distance Matrix Descriptors, Pharmacophore Feature Descriptors, Physical Properties, Atom Counts and Bond Counts descriptors and the 3D Conformation Dependent Charge Descriptors values have been reported.

Cp.	Exp. pEC_{50}	BCUT_SLOGP_1	BCUT_SMR_1	BCUT_SMR_2	BCUT_SMR_3	b_1rotR	logS	dipoleY	a_hyd	ASA+	Pred. pEC_{50}	Residual
1	6.18	-0.35568	-0.28266	0.798257	2.883142	0.130435	-4.78087	1.204581	15	371.5502	6.12	0.0584
4	7.88	-0.32796	-0.25849	0.652405	2.905984	0.12	-4.79947	1.044069	16	390.8534	7.32	0.5626
7	6.72	-0.35712	-0.26889	0.656855	2.955143	0.107143	-4.025	0.745493	16	382.3849	6.94	-0.2237
8	6.83	-0.34052	-0.25029	0.62132	2.955196	0.15625	-4.22493	1.129376	17	390.6831	6.59	0.2433
9	6.33	-0.34229	-0.26413	0.633213	2.955108	0.115385	-3.76415	0.740564	12	340.8268	6.95	-0.6186
10	6.90	-0.24732	-0.14753	0.604097	2.955141	0.115385	-3.76987	0.922183	15	354.6852	7.36	-0.4613
12	6.86	-0.25409	-0.13852	0.544934	2.955387	0.148148	-3.98426	0.652829	16	374.0897	7.08	-0.2195
22	8.69	-0.24278	-0.14413	0.618789	2.955143	0.111111	-4.65708	0.762706	16	386.3489	8.07	0.6208
23	8.69	-0.12432	-0.0424	0.496516	2.95516	0.111111	-4.08326	0.870343	16	369.6105	8.03	0.6621

25	7.88	-0.21336	-0.11747	0.566128	2.955142	0.111111	-4.23618	0.861456	16	389.3108	7.90	-0.0228
26	7.95	-0.19151	-0.06593	0.597892	2.95515	0.107143	-4.97047	0.794395	17	413.9033	8.50	-0.5481
27	4.82	-0.54106	-0.41293	0.753114	2.741984	0.225806	-4.63377	-0.6466	19	352.3749	4.31	0.5125
28	4.82	-0.57448	-0.41224	0.756553	2.741531	0.225806	-4.94722	-0.54837	19	373.7593	4.60	0.2203
29	4.85	-0.47238	-0.41315	0.724984	2.741931	0.185185	-5.12705	-0.83096	17	348.8117	5.18	-0.3335
33	5.22	-0.51784	-0.38127	0.74058	2.741941	0.2	-5.37076	0.008091	19	368.5545	5.48	-0.2638
30	4.95	-0.51287	-0.423	0.763975	2.924864	0.125	-4.8917	0.258115	20	329.1659	5.12	-0.1726

31	5.53	-0.47932	-0.38118	0.7931	2.925107	0.125	-5.33101	0.229203	20	374.0451	5.37	0.1581
34	5.63	-0.50703	-0.40016	0.750418	2.742956	0.2	-5.37076	-0.19278	19	365.1611	5.51	0.1183
35	5.38	-0.51276	-0.37429	0.73428	2.741745	0.2	-5.37076	-0.11834	19	368.825	5.22	0.1587
36	5.92	-0.47947	-0.40816	0.738283	2.739221	0.178571	-4.21516	-0.32604	17	333.2777	5.14	0.7827

37	4.87	-0.50561	-0.41076	0.752206	2.740608	0.178571	-4.06224	-0.05267	17	314.3405	5.14	-0.2747
39	5.00	-0.53808	-0.43228	0.76661	2.741382	0.178571	-5.32038	-0.11748	18	336.9756	5.18	-0.1837
41	4.31	-0.50842	-0.323	0.720619	2.742418	0.21875	-5.42114	0.140607	20	244.9699	4.62	-0.3131
43	5.46	-0.48756	-0.34619	0.715961	2.739452	0.2	-4.26554	-0.41474	18	364.4208	5.20	0.2614

44	4.93	-0.47628	-0.35879	0.734753	2.744759	0.21875	-5.42114	-0.54154	20	391.6472	5.35	-0.4220
45	6.00	-0.45021	-0.3566	0.742185	2.92537	0.121212	-5.54456	-0.63642	21	390.8438	5.77	0.2321
46	5.92	-0.47322	-0.34009	0.724696	2.925081	0.121212	-5.54456	-0.33508	21	390.7534	5.72	0.1971
47	5.88	-0.50543	-0.33309	0.725162	2.925036	0.121212	-5.54456	-0.50312	21	395.551	5.64	0.2367
48	5.13	-0.43985	-0.34697	0.726749	2.924191	0.096774	-4.38896	-0.57797	19	354.7831	5.55	-0.4168
51	4.55	-0.50608	-0.40037	0.747983	2.792774	0.225806	-5.57253	-0.28617	20	389.7123	4.93	-0.3806
52	5.33	-0.5166	-0.38144	0.737511	2.7923	0.225806	-5.57253	-0.04607	20	389.6762	5.41	-0.0813

53	5.30	-0.51268	-0.37444	0.730729	2.792214	0.225806	-5.57253	-0.13285	20	391.6064	5.33	-0.0334
54	5.21	-0.47884	-0.40832	0.735546	2.790994	0.206897	-4.41693	-0.20078	18	350.9011	5.04	0.1700
56	4.87	-0.53307	-0.42304	0.765963	2.791864	0.206897	-4.26401	0.021417	18	340.02	5.01	-0.1352
58	5.69	-0.50701	-0.412	0.750792	3.034299	0.090909	-4.61058	-0.22471	25	398.6733	5.47	0.2185
60	5.29	-0.39696	-0.27355	0.776773	3.034615	0.096774	-3.35656	-0.37939	22	429.9749	5.23	0.0564
61	4.79	-0.50193	-0.43781	0.787634	3.034265	0.068966	-3.97024	-0.10717	22	402.551	4.76	0.0311
62	4.88	-0.48485	-0.41943	0.745826	3.034298	0.096774	-4.02062	-0.1516	23	428.7566	4.77	0.1099
63	4.52	-0.44583	-0.36277	0.718034	3.047983	0.09375	-4.15157	-0.22446	24	429.1572	4.57	-0.0495
64	4.52	-0.49038	-0.37638	0.700285	3.061642	0.096774	-4.42709	-0.11681	23	488.7885	4.94	-0.4189
65	4.52	-0.53808	-0.4561	0.823608	3.028354	0.066667	-4.13893	-0.51908	21	367.1241	4.92	-0.4048
67	4.52	-0.52735	-0.43351	0.783545	3.03069	0.121212	-4.25078	-0.57581	23	414.729	4.48	0.0375
68	4.52	-0.44858	-0.27355	0.67972	3.058267	0.074074	-2.23887	0.122182	17	351.7489	4.75	-0.2291

69	4.52	-0.3969	-0.27356	0.67976	3.030895	0.041667	-2.25272	-0.17549	17	362.3517	4.19	0.3275

71	4.52	-0.53808	-0.49986	0.854311	2.582083	0.111111	-4.3668	-0.30719	14	300.6806	4.31	0.2087
73	4.52	-0.54843	-0.34375	0.705257	2.61022	0.181818	-5.77608	-0.46157	18	380.1791	4.79	-0.2698
74	5.61	-0.49763	-0.41475	0.867923	2.587962	0.103448	-6.65421	-0.27854	17	335.5798	5.51	0.0977
75	4.52	-0.5085	-0.3597	0.719454	2.606652	0.129032	-6.57564	-1.07103	17	298.6164	4.82	-0.3039
76	4.52	-0.53808	-0.45456	0.854311	2.643398	0.16129	-6.47664	-1.6727	17	322.3822	4.63	-0.1123
78	5.76	-0.5087	-0.40627	0.92341	2.591069	0.129032	-7.14946	-1.06612	17	314.7956	5.08	0.6800
79	4.52	-0.5071	-0.34196	0.717573	2.653562	0.15625	-6.1306	-0.849	15	341.0613	4.42	0.1031
80	6.52	-0.50761	-0.43667	0.885183	2.606634	0.105263	-8.23121	-0.67945	23	378.4928	6.34	0.1828
81	4.46	-0.52308	-0.46709	0.905181	2.609082	0.166667	-6.24408	-1.06445	17	304.207	4.86	-0.3981
82	4.56	-0.49315	-0.45805	0.909364	2.608691	0.173913	-6.18813	-0.7946	18	321.3681	4.13	0.4298

83	4.27	-0.49295	-0.45743	0.936491	2.609314	0.17391 3	-6.62744	-0.54232	18	305.224 7	4.84	-0.5710

85	4.14	-0.49312	-0.45774	0.909421	2.633948	0.153846	-5.84825	-0.54119	17	371.2936	4.32	-0.1769
86	5.00	-0.47654	-0.40829	0.92898	2.606236	0.190476	-5.02206	-0.49993	15	329.1525	4.29	0.7073
87	4.23	-0.34205	-0.28855	0.920589	2.609608	0.230769	-5.37016	-0.6221	15	400.5386	4.59	-0.3630
89	5.71	-0.51372	-0.37607	0.913362	2.750752	0.148148	-6.27911	-0.7058	18	377.1368	377.1368	0.3582
90	5.20	-0.4931	-0.45771	0.93233	2.697315	0.148148	-6.72573	-0.83967	18	382.8594	382.8594	-0.3414